The Philosophical Magazine

FIRST PUBLISHED IN 1798

A Journal of Theoretical Experimental and Applied Physics

Vol. 6 April 1961 No. 64
Eighth Series

25s. 0d., plus postage
Annual Subscription £13 10s. 0d., payable in advance

Printed and Published by
TAYLOR & FRANCIS LTD
RED LION COURT, FLEET STREET, LONDON, E.C.4

THE PHILOSOPHICAL MAGAZINE

Authors wishing to submit papers for publication in the Journal should send manuscripts directly to the Publishers.

Manuscripts should be typed in *double* spacing on one side of quarto (8×10 in.) paper, and authors are urged to aim at absolute clarity of meaning and an attractive presentation of their texts.

References should be listed at the end in alphabetical order of authors and should be cited in the text in terms of author's name and date. Diagrams should normally be in Indian ink on white card, with lettering in soft pencil, the captions being typed on a separate sheet.

A leaflet giving detailed instructions to authors on the preparation of papers is available on request from the Publishers.

Authors are entitled to receive 25 offprints of a paper in the Journal free of charge, and additional offprints can be obtained from the Publishers.

The *Philosophical Magazine* and its companion journal, *Advances in Physics*, will accept papers for publication in experimental and theoretical physics. The *Philosophical Magazine* publishes contributions describing new results, letters to the editor and book reviews. *Advances in Physics* publishes articles surveying the present state of knowledge in any branch of the science in which recent progress has been made. The editors welcome contributions from overseas as well as from the United Kingdom, and papers may be published in English, French and German.

Theory of the Self-diffusion Coefficient in Cubic Metals†

By G. M. Pound‡
Metallurgy Department, The University of Sheffield
and W. R. Bitler and H. W. Paxton
Metals Research Laboratory, Carnegie Institute of Technology, Pittsburgh 13, Pennsylvania

[Received in revised form August 16, 1960]

Abstract

The kinetics of diffusion in cubic metals is treated in terms of statistical mechanics from the point of view of absolute rate theory. An approximate description of the activated state leads to the conclusion that in the two degrees of freedom orthogonal to the jump direction only the lower vibrational energy levels are occupied. This circumstance gives rise to a negative contribution to the experimental entropy of activation for diffusion in solids which is negligible for the vacancy mechanism but very appreciable for the ring mechanism. It is suggested that a low D_0, perhaps of the order of 10^{-4} cm^2/sec, is an experimental criterion for the 4-atom ring mechanism and that the self-diffusion in pure chromium and uranium (b.c.c.) may occur by this mechanism. Further, a low Arrhenius frequency factor is predicted for all thermally activated processes in solids which require simultaneous jump of n atoms, e.g. in certain movements of dislocation loops.

§ 1. Introduction

Zener (1951, 1952), Wert and Zener (1949) and Wert (1950) have considered the diffusion of both interstitial and substitutional atoms in cubic alloys in terms of absolute rate theory. They conclude that the diffusion coefficient appropriate for use with the activity-gradient formulation (Hollomon *et al.* 1948) of Fick's first law is given by

$$D=\alpha a^2\nu \exp(\Delta S/k)\exp(-\Delta H/kT) \quad . \quad . \quad . \quad . \quad (1)$$

where a is the lattice parameter, ν is the Einstein vibrational frequency of lattice-site atoms, and ΔS and ΔH are the entropy and enthalpy of activation, respectively. The temperature-independent factors are usually grouped together to express

$$D_0=\alpha a^2\nu \exp(\Delta S/k). \quad . \quad . \quad . \quad . \quad . \quad . \quad . \quad (2)$$

The numerical factor α is determined by the geometry of the atomic jumps.

† Communicated by the Authors.
‡ Now at Metals Research Laboratory, Carnegie Institute of Technology, Pittsburgh 13, Pennsylvania, U.S.A.

Ignoring correlation coefficients, it is defined by

$$(\tfrac{1}{6})Zl^2 = \alpha a^2 \quad . \quad . \quad . \quad . \quad . \quad . \quad . \quad . \quad (3)$$

in which Z is the number of jump paths of length l. For diffusion of substitutional atoms by the vacancy mechanism, α is unity in both b.c.c. and f.c.c. lattices.

ΔH is difficult to calculate and is usually determined experimentally from the slope of an Arrhenius plot. The ΔS, which may be determined experimentally from the Arrhenius intercept, is presumed to be somewhat more susceptible to theoretical approaches. Zener (1951) invoked the thermodynamic relationship

$$\Delta S = -(\partial \Delta G/\partial T)_p \quad . \quad . \quad . \quad . \quad . \quad . \quad . \quad (4)$$

and evaluated the derivative on the assumption that elastic shear strain is the only temperature-dependent contribution to the Gibbs free energy of activation ΔG_m for motion. The resulting expression is

$$\Delta S_m = -\lambda \Delta H_m d(\mu/\mu_0)/dT \quad . \quad . \quad . \quad . \quad . \quad . \quad (5)$$

where μ is the measured elastic shear modulus and

$$\lambda = (\Delta G_0{}^e/\Delta G_0)_m = (\Delta H_0{}^e/\Delta H_0)_m = (\Delta H^e/\Delta H)_m \quad . \quad . \quad . \quad (6)$$

in which the superscript e refers to the elastic contribution and the subscript 0 to absolute zero of temperature. Thus, in view of the negative temperature coefficients of elastic moduli, it was suggested that entropies of activation for diffusion might always be positive. However, as pointed out by Huntington *et al.* (1955), the above treatment neglects dilatation of the activated species. This contribution to ΔS may be large and of either sign. Accordingly, the possibility of a negative entropy of activation in diffusion is not excluded by thermodynamic arguments. Nevertheless, most experimental values of ΔS for self-diffusion in cubic metals are positive and range from 4 to 14 e.u. (Zener 1951), and, with the exception of tungsten, the observed D_0's are of the order of unity.

Zener (1950) calculated that the potential energy of activation for the ring mechanism is a minimum for four atoms in the case of copper (f.c.c.). Thus it was conceived that diffusion might occur by the rotation of 4-membered rings. However, the estimates (Huntington and Seitz 1949, Zener 1950, LeClaire 1953 a, b, Huntington 1953, Fumi 1955) of the potential energies of activation for the various mechanisms of diffusion in f.c.c. lattices indicate that the vacancy mechanism is favoured. Also, the Kirkendall marker shift, which demonstrates the presence of the vacancy mechanism, has been found in many f.c.c. substitutional solid solutions.

The calculation of the potential energy of activation for ring diffusion in b.c.c. lattices has not been made, but it is considered (LeClaire 1953 a, b) that the ring mechanism might be favoured in some of the less closely packed lattices. Although Kirkendall shifts have been shown to accompany chemical diffusion in b.c.c. solid solutions, e.g. beta brass

(Landergren *et al.* 1956), titanium–molybdenum (Shewmon and Bechtold 1955), potassium–rubidium (Yang *et al.* 1958), uranium–molybdenum (Adda and Philibert 1958) and iron–chromium (Paxton *et al.* 1959b), it should be borne in mind that these measurements were conducted on fairly concentrated alloys, and it is possible that the ring mechanism might be operative for self-diffusion of the solvent atoms in more dilute solutions.

Zener (1951) evaluated α for 4-atom ring rotation and found that it is two for f.c.c. and six for b.c.c. lattices. Also he inferred that the elastic strain contribution to the entropy of activation should be positive and probably of the same order of magnitude as that for diffusion by the vacancy mechanism. Thus he concluded that the apparent entropy of activation

$$\Delta S_{\text{app}} = k \ln (D_0/a^2\nu) \quad . \quad . \quad . \quad . \quad . \quad . \quad . \quad (7)$$

for diffusion by the 4-atom ring mechanism should be positive and perhaps larger than that for the vacancy mechanism.

From a somewhat more fundamental point of view, Huntington and co-workers (1955) considered the entropy of ring formation in terms of changes in vibrational frequency upon activation, neglecting the partition functions of the atoms in the directions for rotation. For copper (f.c.c.), they calculated the entropy of formation of an activated 4-atom ring to be -4 e.u., in contrast to $+2$ e.u. for the activated species in diffusion by the vacancy mechanism. Significantly, they found the effect of Debye coupling to be negligible. However, this evaluation of the entropy of activation assumes that the energy levels of an activated atom in the two degrees of freedom orthogonal to the jump direction are those of an oscillator which is stationary with respect to the reaction coordinate. In the following discussion we will refer to these as the normal vibrational energy levels of the activated atom at its saddle-point position. One notes that these are not the levels of the atom in its lattice-site position, which are somewhat lower and more closely spaced.

§ 2. An Alternative Description of the Activated State

The present authors note that the above assumption may not be appropriate for evaluation of the partition function of the activated species in diffusion in solids. The difficulty is that the time of existence of the activated atom at the saddle point is so brief that a precise description of the energy states is incompatible with the quantum-mechanical uncertainty principle (Hirschfelder and Wigner 1939). More succinctly, the transition state cannot be defined because the curvature of the potential energy surface is too great to satisfy the condition

$$(h/2\pi)(K/m)^{1/2} \ll kT \quad . \quad . \quad . \quad . \quad . \quad . \quad . \quad (8)$$

where K is the 'spring constant' and m atomic mass. This difficulty might be obviated by considering the moving atom as a non-localized

particle in a periodic potential. In treating the problem of a particle in a sinusoidal potential, Slater (1952) showed that for energies less than the height ϵ of the potential barrier the solution may be approximated by that of a localized linear oscillator without appreciable error. Significantly he found that the levels for energies slightly greater than ϵ are not at all those of a freely translating particle as assumed for the degree of freedom in the reaction coordinate of standard absolute rate theory (Glasstone *et al.* 1941). In fact, a forbidden gap is present and only when the energies are appreciably greater than ϵ may the assumption of a freely translating particle be invoked. Unfortunately, the results of the Slater treatment are in a form which is not readily amenable to application in absolute rate theory. One notes that an exact treatment would involve a wave-mechanical approach, not just for one particle as carried out by Slater (1952), but for all the degrees of freedom of all atoms in terms of a normal-mode description of cooperative motion.

From the above discussion it would appear difficult to provide a direct, quantitative description of the true activated species for diffusion in solids. Accordingly, an alternative treatment is proposed in which the concentration of activated species is evaluated by calculating the equilibrium number of those reactant species which are in states favourable for reaction and assuming this to be equal to the actual number of activated species. In other words, a Boltzmann distribution is used to calculate the concentration of species in known vibrational states which are only incrementally removed from the true activated state at the saddle point. Actually, this is similar to Rice's (1958) treatment, except that here the difficult normal-mode description of cooperative motion of atoms is not employed.

One next considers the most appropriate formulation of the partition functions to be used in determining the Boltzmann distribution. The treatment of Vineyard (1957) or Rice (1958) in which the cooperative motion of the jumping atom and its neighbours is depicted by a normal-mode description would be more exact, particularly for low temperatures. However, for high temperatures where the long wavelengths are less important, it is considered that the Einstein formulation of the lattice dynamics in terms of independent oscillators should be satisfactory. Also, the Vineyard–Rice treatment is not readily amenable to numerical evaluation. Accordingly, due to its simplicity and applicability at the high experimental temperatures, the Einstein formulation of vibrational partition functions will be used in the present analysis.

2.1. *Self-diffusion by the Vacancy Mechanism*

If $\Delta G^0_{\mathrm{vac}}$ is the Gibbs free energy of formation of a vacancy, the probability of its existence at a given lattice site is

$$p_1 = \exp(-\Delta G^0_{\mathrm{vac}}/kT). \quad \ldots\ldots \quad (9)$$

Similarly, the probability that the j neighbouring atoms are in states

corresponding to the saddle-point configuration is

$$p_2 = \exp(-\Delta G^0_{con}/kT). \quad . \quad . \quad . \quad . \quad . \quad . \quad (10)$$

The probability that an adjacent atom has sufficient vibrational energy in the given x direction to surmount the saddle point for motion to the vacant site is

$$p_3 = \sum_{E_i=\epsilon}^{\infty} \exp(-E_i/kT)/f_v \cong \exp(-\epsilon/kT) \quad . \quad . \quad . \quad (11)$$

where ϵ is the height of the potential energy barrier and f_v is the Einstein partition function for vibration in the one degree of freedom.

The compound probability $p_1p_2p_3$ is not sufficient to express the likelihood that the atom is only incrementally removed from its saddle-point state, because the actual motion of the atom may be in a direction other than that leading to the vacancy. In this case, the energy levels of the activated species would be appreciably elevated. Thus the predominant reaction path is the axis between vacancy and jumping atom. The condition for the atom to be moving along this reaction path, i.e. in exactly the right direction, is that it have almost no vibrational energy in the two orthogonal directions. The probability that an atom has the least possible vibrational energy, i.e. the zero-point energy $\epsilon_0 = h\nu/2$, in one of its orthogonal degrees of freedom is $1/f_v$, and the probability of zero-point energy in both of its orthogonal degrees of freedom is $1/f_v^2$†. However, depending on the mode of interaction with its neighbours near the saddle point, the atom may be permitted some small vibrational energy in the orthogonal directions and still make the jump. That is, if the orthogonal vibrational energy is sufficiently small, the energy levels of the activated species will not be appreciably elevated. This critical orthogonal vibrational energy is difficult to evaluate, but one presumes that it is smaller in hard lattices than in soft ones where a misdirected jumping atom may push aside its saddle-point neighbours. Accordingly, for the case of very hard lattices (high Debye θ) only, the probability of motion in the reaction path is

$$p_d = 1/f_v^2 = \exp(-\Delta G_d/kT). \quad . \quad . \quad . \quad . \quad . \quad (12)$$

This term does not arise in treatments of diffusion by standard absolute rate theory which assume normal vibrational energy levels for the activated atom in the degrees of freedom orthogonal to the jump direction. Retaining the concept of vibrational energy levels, the presence of this factor suggests that these levels are much higher for the activated species than has been supposed (Huntington *et al.* 1955) and hence only the lower ones are occupied. In other words, high orthogonal vibrational frequencies of the activated atom are implied. This view is consistent with the idea that a proper wave-mechanical approach to the problem would yield high and widely spaced energy levels for the activated species. In this paper the term activated species is not restricted to a description of atoms that are in free translation over a potential energy barrier, as

† In order to simplify the notation, the zero-point energy is taken as the zero datum of energy in evaluating the partition functions.

it usually is in standard absolute rate theory. Rather it refers to all species which are crossing the barrier when the system is close to thermodynamic equilibrium. In this connection, one notes that the solid system in which diffusion is occurring under usual experimental conditions is quite close to its thermodynamic equilibrium state.

The probability that the atom has sufficient vibrational energy to surmount the potential energy barrier and motion in the right direction (i.e. that it is only incrementally removed from its saddle-point state) in lattices of high θ_D is

$$p = p_1 p_2 p_3 p_d = \exp\left[-(\Delta G^0_{\text{vac}} + \Delta G^0_{\text{con}} + \epsilon)/kT\right] 1/f_v^2. \qquad (13)$$

Assuming that p is the probability of occurrence of activated species and recognizing that the transmission frequency† is, by this model, the Einstein vibrational frequency ν, the actual atomic jump frequency becomes

$$\Gamma = \nu p. \qquad (14)$$

The diffusion coefficient is obtained from the standard expression for three-dimensional random walk as

$$D = (\tfrac{1}{6}) Z l^2 \Gamma = \alpha a^2 \nu \exp\left[-(\Delta G^0_{\text{vac}} + \Delta G^0_{\text{con}} + \epsilon)/kT\right] 1/f_v^2 \qquad (15)$$

for diffusion by the vacancy mechanism in hard cubic lattices. Upon differentiating the logarithm of eqn. (15) with respect to the reciprocal of absolute temperature, it emerges that the experimental enthalpy of activation is

$$\Delta H = \Delta H^0_{\text{vac}} + \Delta H^0_{\text{con}} + \epsilon + 2k[d \ln f_v / d(1/T)]. \qquad (16)$$

From eqns. (1), (15) and (16), the experimental entropy of activation is given by

$$\Delta S = \Delta S^0_{\text{vac}} + \Delta S^0_{\text{con}} - 2k[\ln f_v + (d \ln f_v / d \ln T)]. \qquad (17)$$

In view of the fact that only the terms containing f_v arose from the requirement for motion in the right direction, it is clear that the probability for such motion contributes the following quantities to the enthalpy and entropy of activation:

$$\Delta H_d = 2k[d \ln f_v / d(1/T)], \qquad (18)$$

$$\Delta S_d = -2k[\ln f_v + (d \ln f_v / d \ln T)]. \qquad (19)$$

Alternatively, eqns. (18) and (19) may be obtained directly from eqn. (12).

In general, ΔH_d and ΔS_d are negative contributions, and they are readily estimated on the present assumption of independent oscillators. The Einstein vibrational partition function for one degree of freedom is

$$f_v = \sum_{v=0}^{\infty} \exp\left[-v h\nu/kT\right] = \left[1 - \exp\left(-h\nu/kT\right)\right]^{-1}, \qquad (20)$$

† The transmission coefficient is assumed to be unity.

and at high temperatures where $kT > h\nu$, $f_v \cong kT/h\nu = T/\theta_D$. Subject to this approximation, eqns. (18) and (19) become

$$\Delta H_d = -2kT \quad . \quad . \quad . \quad . \quad . \quad . \quad . \quad . \quad . \quad (21)$$

$$\Delta S_d = -2k[1 + \ln(T/\theta_D)]. \quad . \quad . \quad . \quad . \quad . \quad . \quad (22)$$

At the usual high experimental temperatures ($\cong 1000°K$) for self-diffusion in solid metals, $f_v \cong T/\theta_D$ is often about 3. Accordingly, in a typical case of self-diffusion by the vacancy mechanism in cubic metals of high Debye θ,

$$\Delta H_d \cong -4000 \text{ cal/mole and } \Delta S_d \cong -8 \text{ e.u.}$$

One notes that the sign and orders of magnitude of these contributions are consistent with our physical model of the diffusion process; they represent the losses in energy and entropy occasioned by the inaction of two degrees of freedom. Thus the contributions from the probability of correct direction of vibrational motion to the enthalpy and entropy of activation are not very large in the case of the vacancy mechanism where only one atom undergoes net movement.

2.2. *Self-diffusion by the Ring Mechanism*

Analogously to the treatment outlined above, it is readily shown that the expression for the coefficient of diffusion by the n-atom ring mechanism in hard cubic lattices is

$$D = \alpha a^2 \nu \exp[-(\Delta G^0_{con} + n\epsilon)/kT] 1/f_v^{2n} \quad . \quad . \quad . \quad (23)$$

in which the probability of correct direction of motion for the n atoms is identified as

$$p_d = 1/f_v^{2n} = \exp(-\Delta G_d/kT). \quad . \quad . \quad . \quad . \quad . \quad (24)$$

Also, the analogues of eqns. (18) and (19) for the contributions of p_d to the enthalpy and entropy of activation are

$$\Delta H_d = 2nk[d \ln f_v/d(1/T)] \quad . \quad . \quad . \quad . \quad . \quad (25)$$

and

$$\Delta S_d = -2nk[\ln f_v + (d \ln f_v/d \ln T)]. \quad . \quad . \quad . \quad . \quad (26)$$

Again, invoking the approximation that $f_v \cong T/\theta_D$,

$$\Delta H_d = -2nkT \quad . \quad . \quad . \quad . \quad . \quad . \quad . \quad . \quad (27)$$

and

$$\Delta S_d = -2nk[1 + \ln(T/\theta_D)] \quad . \quad . \quad . \quad . \quad . \quad (28)$$

Accordingly, for the interesting case of self-diffusion by the 4-atom ring mechanism in cubic metals of high θ_D in a typical situation where

$$T \cong 1000°K \text{ and } T/\theta_D \cong 3,$$

$$\Delta H_d \cong -16\,000 \text{ cal/mole and } \Delta S_d \cong -32 \text{ e.u.}$$

Thus, the probability of correct direction of vibrational motion, which has a relatively small effect in diffusive processes involving jump of only one atom, becomes very important in processes involving simultaneous jump of several atoms. This circumstance arises from the compounding of probabilities for correct direction of vibrational motion for all of the n atoms. As discussed in the section on self-diffusion by the vacancy mechanism, the requirement of correct direction of atomic motion may be viewed, from a more fundamental standpoint, as signifying high vibrational energy levels for the activated atom in the two degrees of freedom perpendicular to the direction of jump.

It is obvious that $\exp(\Delta S_d/k)$ is by no means cancelled by

$$\exp(-\Delta H_d/kT);$$

in fact, $\exp(\Delta S_d/k)$ is by far the more significant term in the expression for the diffusion coefficient. Therefore one chooses to establish a criterion for diffusion by the ring mechanism in terms of D_0 rather than ΔH. From the discussion presented in the Introduction, it seems reasonable to presume that the contributions of ΔS^0_{vac} and ΔS^0_{con} to the entropy of activation may be neglected in an approximate comparison of the D_0's for diffusion by the respective mechanisms of vacancy and n-atom ring. Accordingly, the expected ratio of D_0's for self-diffusion in cubic lattices of high θ_D is obtained from eqns. (2), (22) and (28) as

$$D_{0\,\text{ring}}/D_{0\,\text{vac}} \cong (\alpha_{\text{ring}}/\alpha_{\text{vac}})(\theta_D/eT)^{2n-2}, \quad . \quad . \quad . \quad . \quad (29)$$

which has a value of about 10^{-5} for $n=4$ in b.c.c. lattices. Since the observed values of D_0 for self-diffusion in most cubic metals, which is presumed to occur by the vacancy mechanism, are generally of the order of unity, the present authors suggest that an appreciably lower value of measured D_0, perhaps of the order of 10^{-3} to $10^{-5}\,\text{cm}^2\,\text{sec}^{-1}$, is an experimental criterion for diffusion by the 4-atom ring mechanism. Further, the ring mechanism should be operative in cases where it has a sufficiently low ΔH to compensate for its low D_0, and, in view of the Arrhenius plot of $\ln D$ versus $1/T$, low temperatures should favour the ring mechanism.

§ 3. Comparison of the Present Theory with Observations

Paxton and Gondolf (1959) and Paxton *et al.* (1959) recently studied the self-diffusion of chromium (b.c.c.) from 1225 to 1550°K by three different radioactive-tracer techniques and concluded that the D_0 is of the order of $10^{-4}\,\text{cm}^2/\text{sec}$. $T/\theta_D \cong 3$ for this case†, and from eqn. (28), the contribution of probability of correct vibrational direction to the experimental entropy of activation for four atoms in ring diffusion is

$$\Delta S_d \cong -32\,\text{e.u.}$$

† $\theta_D = 485$°K.

According to eqn. (29) and the argument of the preceding section, the expected D_0 for diffusion by the 4-atom ring mechanism in chromium is $\cong 10^{-5}\,\mathrm{cm^2/sec}$. Therefore it is suggested that the self-diffusion in pure chromium may occur principally by this mechanism†.

Adda and Kirianenko (1958), Bochvar *et al.* (1958) and Rothman (1959, private communication) *et al.* measured the self-diffusion coefficient in b.c.c. uranium between 1070 and 1310°K and found D_0 to be about $1{\cdot}5 \times 10^{-3}\,\mathrm{cm^2/sec}$. The predicted D_0 according to the present theory is $\sim 10^{-7}\,\mathrm{cm^2/sec}$. Although the quantitative agreement is poor, it should be remembered that the present treatment assumes a high Debye θ, while θ_D for b.c.c. uranium is only 170°K (Rothman 1959, private communication). Actually, the departure from the theoretical prediction is in the direction to be expected for soft lattices. Thus it is suggested that the 4-atom ring mechanism of self-diffusion may be operative in b.c.c. uranium also.

Mayburg (1955) has given arguments to show that self-diffusion in germanium occurs by a ring mechanism. However, the observed D_0 is $7{\cdot}8\,\mathrm{cm^2\,sec^{-1}}$ (Letaw *et al.* 1955). Inasmuch as T/θ_D for germanium is about 4 at 1100°K, the present theory suggests that, if the ring mechanism is indeed operative, the number of atoms in the ring is less than 4. In fact, considering the diamond-cubic structure of germanium, direct interchange ($n=2$) might be expected, for which the predicted $D_0 \cong 10^{-2}$.

§ 4. Conclusions

(i) There are negative contributions to the experimental enthalpy and entropy of activation for diffusion in solids which may be evaluated through an alternative description of the activated state. In this treatment, the concentration of species in a state incrementally removed from the saddle-point state is calculated and assumed to equal the actual concentration of activated species. The requirement that jumping atoms have the correct direction of vibrational motion leads to a probability $p_d = 1/f_v^{2n}$, in the case of hard cubic lattices. This term gives rise to negative contributions to the enthalpy and entropy of activation given by $\Delta H_d = 2nk[d\ln f_v/d(1/T)]$ and $\Delta S_d = -2nk[\ln f_v + (d\ln f_v/d\ln T)]$. Invoking the assumption that the vibrational partition function in one degree of freedom $f_v \cong T/\theta_D$, these formulae simplify to $\Delta H_d = -2nkT$ and $\Delta S_d = -2nk[1+\ln(T/\theta_D)]$.

(ii) These expressions do not arise in standard treatments of diffusion by absolute rate theory, which assume the normal vibrational energy levels for the activated atom in the degrees of freedom orthogonal to the jump direction. Their presence here suggests that the orthogonal vibrational energy levels of the activated atom are high and hence only the lower ones are occupied.

† The interstitialcy mechanism is ruled out by energetic considerations (LeClaire 1953 a, b).

(iii) These negative contributions to ΔH and ΔS are unimportant for a process of single atomic jump ($n=1$), such as occurs in diffusion by the vacancy mechanism. However, they are important in diffusion by the 4-atom ring mechanism ($n=4$) where $\Delta H_d \cong -16\,000$ cal/mole and $\Delta S_d \cong -32$ e.u. in cubic metals of high Debye θ. In general, the contribution of ΔS_d to the diffusion coefficient is more significant than that of ΔH_d.

(iv) It is suggested that a low D_0, perhaps of the order of 10^{-4} cm^2/sec (versus unity for self-diffusion by the vacancy mechanism), is an experimental criterion for the 4-atom ring mechanism.

(v) The present theory suggests that the self-diffusion in pure chromium (b.c.c.) and pure uranium (b.c.c.) may occur principally by the 4-atom ring mechanism.

(vi) There are appreciable negative contributions to the experimental enthalpy and entropy of all thermally activated processes in solids which require simultaneous jump of n atoms, e.g. in certain movements of dislocation loops (Seeger 1956). However, in this latter case, the appropriate quantities for ΔH_d and ΔS_d in hard cubic lattices would be just half of those quoted in item (i) above, because vibrational motion is restricted in only one of the two degrees of freedom perpendicular to the jump direction. Nevertheless a low Arrhenius frequency factor is predicted for such processes.

Acknowledgments

The authors wish to express their thanks to Dr. Edward Hart of the General Electric Company Research Laboratory, Professor F. C. Frank of the University of Bristol, Professor Hill Huntington of the Rennslaer Polytechnical Institute, Professor R. F. Mehl of the Carnegie Institute of Technology, and Dr. Clarence Zener of the Westinghouse Research Laboratory for stimulating discussions and helpful criticisms.

This work was sponsored by the U.S. Office of Naval Research.

One of the authors (G. M. P.) gratefully acknowledges the assistance of a Fulbright Research Grant and a John Simon Guggenheim Fellowship.

References

Adda, Y., and Kirianenko, A., 1958, *C.R. Acad. Sci., Paris*, **247**, 744.
Adda, Y., and Philibert, J., 1958, *C.R. Acad. Sci., Paris*, **246**, 113.
Bochvar, *et al.*, 1958, Geneva Conference Report A, Conference 15, p. 2306.
Fumi, F. G., 1955, *Phil. Mag.*, **46**, 1007.
Glasstone, S., Laidler, K. J., and Eyring, H., 1941, *Theory of Rate Processes* (New York : McGraw-Hill).
Hirschfelder, J. O., and Wigner, E., 1939, *J. chem. Phys.*, **7**, 616.
Hollomon, J. H., Fisher, J. C., and Turnbull, D., 1948, *Trans. Amer. Inst. min. (metall.) Engrs*, **175**, 202.
Huntington, H. B., 1953, *Phys. Rev.*, **91**, 1092.

HUNTINGTON, H. B., and SEITZ, F., 1949, *Phys. Rev.*, **76,** 1728.
HUNTINGTON, H. B., SHIRN, G. A., and WAJDA, E. S., 1955, *Phys. Rev.*, **99,** 1085.
LANDERGREN, U. S., BIRCHENALL, C. E., and MEHL, R. F., 1956, *Trans. Amer. Inst. min. (metall.) Engrs*, **206, 73.**
LECLAIRE, A. D., 1953 a, *Progress in Metal Physics*, Vol. 4 (New York : Interscience), p. 265 ; 1953 b, *Acta Met.*, **1,** 438.
LETAW, H., Jr., PORTNOY, W. M., and SLIFKIN, L. M., 1955, *Bull. Amer. phys. Soc.*, **30,** 13.
MAYBURG, S., 1955, *Phys. Rev.*, **98,** 1134.
PAXTON, H. W., and GONDOLF, E. G., 1959, *Arch. Eisenhüttenw.*, **30,** 55.
PAXTON, H. W., PASIERB, E. J., and KUNITAKE, T., 1959 (to be published).
RICE, S. A., 1958, *Phys. Rev.*, **112,** 804.
SEEGER, A., 1958, *Dislocations and Mechanical Properties of Crystals* (New York : John Wiley), p. 502.
SHEWMON, P. G., and BECHTOLD, J. H., 1955, *Acta Met.*, **3,** 452.
SLATER, J. C., 1952, *Phys. Rev.*, **87,** 807.
VINEYARD, G. H., 1957, *J. Phys. Chem. Solids*, **3,** 121.
WERT, C., 1950, *Phys. Rev.*, **79,** 601.
WERT, C., and ZENER, C., 1949, *Phys. Rev.*, **76,** 1169.
YANG, L., SIMNAD, M. T., and MEHL, R. F., 1958, *Trans. Amer. Inst. min. (metall.) Engrs*, **212,** 412.
ZENER, C., 1950, *Acta Crystallogr.*, **3,** 346 ; 1951, *J. appl. Phys.*, **22,** 372 ; 1952, *Imperfections in Nearly Perfect Crystals* (New York : John Wiley and Sons), p. 289.

Total Cross Section of Lead for Slow Neutrons†

By M. F. Collins and G. Dolling
Cavendish Laboratory, Cambridge

[Received June 9, 1960]

Abstract

A beam of filtered neutrons with a mean wavelength of 8·4 Å has been used to measure the total cross section of lead as a function of temperature from 290°K to 840°K. The cross section is found to vary linearly with temperature in both solid and liquid phases to within 1°K of the melting point. There is a jump in cross section at the melting point of (9·4±0·6)%. The results in the solid are not in agreement with predictions based on the Debye theory.

§ 1. Introduction

In recent years, much attention has been given to the use of slow neutrons to investigate thermal motions in solids (for references see Kothari and Singwi (1959)). The present experiment was performed to study the behaviour of these motions in lead near the melting point, as reflected in the variation of its total inelastic cross section. A similar experiment of a preliminary nature has been performed by Squires (1954).

The total cross section was measured for lead over the temperature range 290°K to 840°K, by means of a beam of cold neutrons from the BEPO reactor, Harwell. Observations in the solid phase are compared with the predictions of the Debye theory and those in the liquid phase similarly analysed in terms of 'effective' Debye temperatures.

§ 2. Experimental

A collimated neutron beam was passed through a filter of bismuth metal in the form of shot (Egelstaff and Pease 1954) in order to remove all neutrons of wavelengths less than 6·5 Å. The resultant spectrum is roughly that of a Maxwellian of temperature 350°K with a sharp cut-off imposed at this wavelength. The filtered neutrons thus cannot suffer elastic Bragg scattering by the lead sample. A correction of about 0·7% was necessary to allow for imperfect filtering action.

The filtered-beam method has the great advantage (over neutron choppers or spectrometers) of high neutron flux resulting in good statistical accuracy and short counting times. It has the disadvantage of large incident wavelength spread. The total cross section of lead, however, is only a slowly varying function of neutron wavelength (Hughes and Schwartz 1958) over the range used (6·5 Å to 13 Å, longer wavelengths being present in negligible intensities).

† Communicated by the Authors.

The 99·99% pure lead sample is contained in a steel holder, an identical 'dummy' holder being used for 'out' counts. Both holders are heated in an oven specially designed for precise temperature control (to $\pm \frac{1}{4}$°K for many hours) of the specimen. The effective number of lead atoms in the beam was continually measured by observing the attenuation by the sample of a beam of epithermal neutrons (obtained by transmission through a cadmium sheet). The cross section for these neutrons is independent of the structure and thermal motions of the sample: it depends only on the number of lead atoms in the beam and on purely nuclear properties which may be measured in a subsidiary experiment.

The total cross section of lead is plotted (curve A) against temperature in fig. 1. The relation is linear in both the liquid and solid states over the temperature range with a discontinuity of $0{\cdot}239 \pm 0{\cdot}016$ barns (9·4%) on melting. We have investigated the linear relation in some detail near the melting point, as shown in fig. 2. It is found to hold to within 1°K of that point in both the solid and liquid states.

§ 3. Discussion

The total scattering cross section is the sum of a coherent and an incoherent part. The coherent scattering may be further divided into two parts, one representing the scattering by a single nucleus and the other the interference effect. To a first approximation, the interference term may be neglected. This is known as the 'incoherent approximation' and implies that the total coherent cross section has the same dependence on the atomic motions of the scattering system as does the total incoherent cross section.

For cubic crystals with Bravais lattices (e.g. lead) the total incoherent cross section depends only on the frequency distribution function and not on the detailed phonon dispersion relations. It can be shown that the use of the Debye approximation is quite adequate in this case. Moreover, Placzek (1954, 1957) has shown that the total incoherent cross section can be conveniently expanded in powers of the ratio of neutron to nuclear mass (mass expansion). Using this expression, which is very rapidly convergent, we have calculated the total inelastic incoherent cross section. In the present experiment the elastic coherent cross-section is zero for the solid. The results combined with the incoherent approximation give the total cross-section (σ_B) shown as curve B (Fig. 1).

We now consider the effect of interference on the scattering from the solid. Placzek and Van Hove (1955) have shown from theoretical considerations that the total coherent inelastic cross section depends on the precise form of the phonon dispersion relations and that the use of the Debye approximation will not, in general, give accurate values. The present experiment enables us to consider the adequacy of the Debye approximation in the case of lead.

The cross section was evaluated using a mass expansion. This conveniently divides into two parts: the first (and numerically the dominant) of which is identical with the mass expansion of the incoherent scattering

Fig. 1

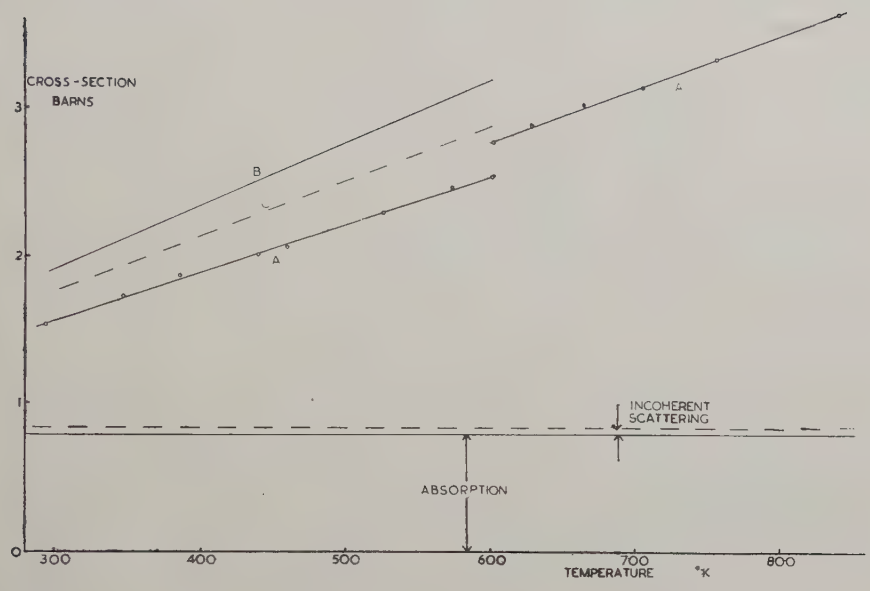

Total cross section of lead against temperature. A, experimental values ; B, theoretical cross section based on the incoherent approximation ; C, theoretical cross section with interference term.

Fig. 2

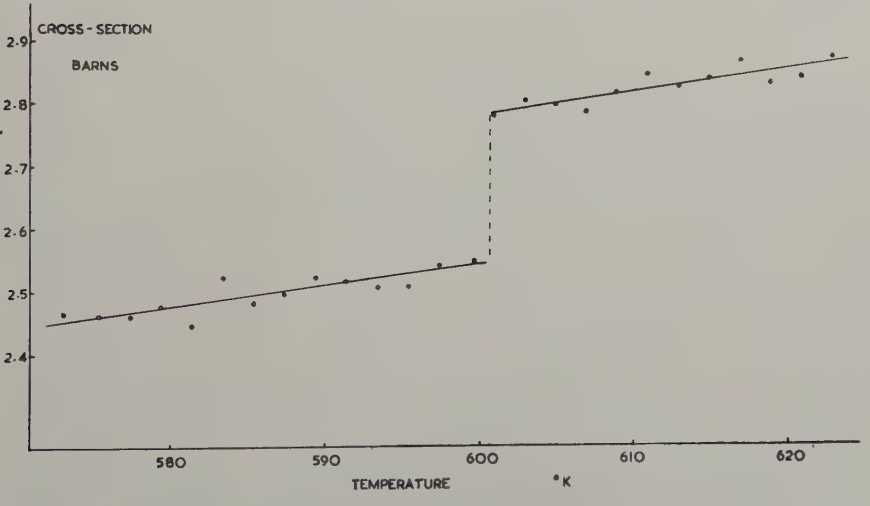

Total cross section of lead against temperature near the melting point.

cross section, and the second represents a ' correction ' term for interference effects. Marshall and Stuart (1959) have evaluated this correction term on the basis of the Debye approximation for an appropriate range of experimental conditions. When the correction term is added to the incoherent approximation curve B, we obtain curve C, which thus represents the total coherent cross section (σ_C) in the Debye approximation. Both σ_B and σ_C are average values over the expected beam spectrum assuming the file flux is Maxwellian.

To calculate the cross section at any temperature and incident wavelength we require a value of the Debye temperature, θ_D. Chipman (1959) has measured the variation of the Debye–Waller factor of lead with temperature using x-ray techniques. We have taken his values of θ_D for lead between 300°K and 600°K, given by

$$\theta_D = (98{\cdot}5 - 0{\cdot}045\,T)^\circ\text{K} \quad . \quad . \quad . \quad . \quad . \quad . \quad . \quad (1)$$

where T is the absolute temperature. The errors in these values are about 4°K.

The Debye–Waller factor involves a different average value over the frequency distribution than does the incoherent cross section, but, using more realistic frequency spectra due to Leighton (1958), we have estimated that the two 'effective' Debye temperatures are consistent to about $\frac{1}{2}\%$.

The mean wavelength of the beam, measured by means of a thin 1/v gold absorber, was 8·45 Å. The lead absorption cross section was taken as $0{\cdot}170 \pm 0{\cdot}002$ barns at 220 m/s (Hughes and Schwartz 1958), with a 1/v variation. We have taken the value of $0{\cdot}05 \pm 0{\cdot}03$ barns for the incoherent cross section of lead as given by Egelstaff and McCallum (1958). This figure gives rise to the greatest source of error in interpreting the results.

Figure 1 shows that curve C is a closer fit to the observations than the incoherent approximation. It is possible to obtain a fairly satisfactory fit using the Debye approximation if we take θ_D as given by the equation

$$\theta_D = (117 - 0{\cdot}040\,T)^\circ\text{K}. \quad . \quad . \quad . \quad . \quad . \quad . \quad . \quad (2)$$

The errors on these values are about 4°K. Values of θ_D given by (2) are much higher [$(21 \pm 6)^\circ$K] than those given by Chipman and other sources (Blackman 1955). We therefore conclude that the Debye theory is not adequate for predicting total coherent cross sections.

We assume that the part of the scattering from a single nucleus has been correctly calculated, so that the difference (B–A) on fig. 1 represents the effects of interference in the solid. If there is no change in the effects of interference on melting, the observed rise in cross section would imply a fall in θ_D of $(7 \pm 2)^\circ$K. It seems reasonable to expect these effects to be of less importance in the more disordered liquid state, in which case the change in θ_D would be an indeterminate amount smaller (and may even be of opposite sign). In view of the expansion on melting however, it is unlikely that θ_D in the liquid will be greater than in the solid. This discussion is, of course, based on a simple-minded solid-like representation of a liquid in which an 'effective' θ_D describes the atomic motions.

It should be noted that we have assumed that there will be no quasi-elastic scattering of neutrons of $\lambda > 6{\cdot}5$ Å by the liquid lead. Whether the 'cut-off' is sufficiently sharp to ensure this cannot be decided from existing neutron diffraction data for liquid lead (Chamberlain 1950, Sharrah and Smith 1953). If there is some quasi-elastic scattering, this would mean that the increase in the *inelastic* cross section at the melting point is *less* than the observed increase, again implying that the fall in θ_D is less than the value of 7 °K mentioned above.

In spite of all these uncertainties in interpretation, the outstanding feature of the results in the liquid still remains: viz. the surprisingly small change in cross section, at the melting point.

Acknowledgments

This work was carried out during the tenure of maintenance grants from the Department of Scientific and Industrial Research. We wish to thank Dr. Bretscher and the Director of A.E.R.E., Harwell, for kindly providing experimental facilities. We are grateful to Dr. W. Marshall for valuable discussions and for showing us the results of unpublished calculations. We are especially indebted to Dr. G. L. Squires for suggesting the problem and for much helpful discussion and advice.

References

Blackman, M., 1955, *Handbuch der Physik*, Vol. 7 (Berlin : Springer-Verlag), p. 325.
Chamberlain, O., 1950, *Phys. Rev.*, **77**, 305.
Chipman, D. R., 1959, MRL Rep. No. 67, Ordnance Materials Research Office, Watertown Arsenal.
Egelstaff, P. A., and McCallum, G. J., 1958, *Nature, Lond.*, **181**, 643.
Egelstaff, P. A., and Pease, R. S., 1954, *J. sci. Instrum.*, **31**, 207.
Hughes, D. J., and Schwartz, R., 1958, *Neutron Cross-Sections*, BNL 325, second edition.
Kothari, L. S., and Singwi, K. S., 1959, *Solid State Physics*, Vol. 8.
Leighton, R. B., 1948, *Rev. mod. Phys.*, **20**, 165.
Marshall, W., and Stuart, R. N., 1959, University of California, Lawrence Laboratory, Report UCRL–5568 ; and private communication.
Placzek, G., 1954, *Phys. Rev.*, **93**, 895 ; 1957, *Ibid.*, **105**, 1240.
Placzek, G., and Van Hove, L., 1955, *Nuovo Cim.*, **1**, 233.
Sharrah, P. C., and Smith, C. P. J., 1953, *J. chem. Phys.*, **21**, 228.
Squires, G. L., 1954, *Acta cryst., Camb.*, **7**, 674.

An X-ray Study of Deformation Stacking Faults at Low Temperatures in Lead, some Lead Alloys, and Aluminium†

By G. F. Bolling‡, T. B. Massalski§ and C. J. McHargue‖

[Received October 24, 1960]

Abstract

The deformation stacking-fault probability α, has been determined by the deformation of bulk specimens of zone-refined lead at 4·2° and 77°K. Aluminium (99·996%), α-brass (70 : 30), lead-0·1 at. % silver and lead-20·0 at. % indium were also examined at 4·2°K. It is shown that a major difference exists between aluminium and lead, the latter being copper-like in its value of α. The influence of increased deformation in increasing the value of α is demonstrated. Addition of indium to lead suppresses a measurable value of α which correlated with observations made on twinning in this alloy.

§ 1. Introduction

1.1. *Brief Review*

The stacking-fault energy, γ, is an important parameter in the theory of deformation of f.c.c. metals ; (see for example, Seeger (1957)). However, it has not been possible to predict γ adequately from theoretical considerations or to determine γ directly for any pure metal. In general, it is inferred that γ can be related to other measurable properties such as the twin boundary energy, creep rate, onset of cross slip or the stacking-fault probability, α, etc. ; it is thus possible to compare the values of γ for different metals by comparing the values of the properties to which it is related.

Data for copper have been used most frequently as a basis for comparison. Fullman (1951) determined the twin boundary energy in copper and from this, Seeger and Schöck (1953) estimated a value $\gamma_{Cu} \cong 40\,\text{ergs/cm}^2$; other data by Fullman (1950) was used to set a lower limit for aluminium, $\gamma_{Al} \gtrsim 200\,\text{ergs/cm}^2$. In the assessment by Seeger and Schöck (1953) of the role of γ in various deformation processes its value was considered high if $\gamma > 10^{-2}\mathbf{b}^2/s_{44}c$, and low if $\gamma \leqslant 2\times10^{-3}\ \mathbf{b}^2/s_{44}c$ where c is the spacing of glide planes for which the elastic coefficient of

† Communicated by the Authors.

‡ Westinghouse Research Laboratories, Pittsburgh 35, Pa.
§ Mellon Institute, Pittsburgh 13, Pa.
‖ Oak Ridge National Laboratory, Oak Ridge, Tennessee.

shear is s_{44}, and **b** is the Burgers vector of a whole dislocation. On this basis, copper has a low value of stacking-fault energy and aluminium a high value.

A comparison of γ for different metals may be obtained from their behaviour during deformation. Thornton and Hirsch (1958) interpreted creep data for several f.c.c. metals in order to determine values of γ; Haasen (1958) obtained a value for γ_{Ni} from an analysis of tensile tests on single crystals of Ni. However, the conclusions of both these investigations are based on the value of γ_{Cu} and the behaviour of copper as being typical of a metal having a low stacking-fault energy. Recently doubt has been cast on the relative measurements which employ γ_{Cu} as a standard by the tensile deformation analysis of copper single crystals made by Seeger *et al.* (1959). Using a theory relating the onset of cross slip to the value of γ, they determined an absolute value of $\gamma_{Cu} = 169\,\text{ergs/cm}^2$ by measurements of the strain-rate and temperature dependence of τ_{111}, the stress for initiation of cross slip. This value is much greater than the value determined from Fullman's data. Hence, a discrepancy exists.

The measurement by x-ray techniques of the stacking-fault probability, α, which is related to γ, seems to favour Fullman's value of γ_{Cu} when stacking-fault probabilities for copper and other metals and alloys are compared. Following a theoretical analysis of the x-ray pattern of deformed f.c.c. metals, Paterson (1952) predicted that a shift of certain reflections should occur in the presence of stacking faults. x-ray data may be conveniently described by a parameter α representing the fraction of close-packed planes which is in a faulted sequence. (Values of α for various metals and alloys are listed in table 6.) However, the true configuration of the faults produced during deformation which give rise to the shift in x-ray reflections is not known.

1.2. *Materials Chosen for Investigation*

All common f.c.c. metals except lead and aluminium are monovalent. Since the electronic structure of the polyvalent elements is complicated by Brillouin zone overlaps, it may be expected that a closer similarity should exist between the monovalent elements when compared with polyvalent elements. This might be reflected in different values of γ between the two types. However, although γ-values for the noble metals have been estimated, a good set of values for aluminium and lead is not available. In the investigation of aluminium nearly all the techniques give only lower limits for γ_{Al}. Viz.: Twins are found infrequently; and, as will be shown, α is almost too small to be measured; no stacking faults are seen in thin films by transmission electron microscopy.

High values of γ_{Pb} have been predicted (Seeger (1957), pp. 267 and 302) although an uncertainty has been expressed (Seeger (1955a)).

The deformation of single crystals by Feltham and Meakin (1957) indirectly supports a high value for γ_{Pb}. Only the determination of relative twin boundary energies (Bolling and Winegard (1958 a)) supports a low value for $\gamma_{Pb} \cong 20$ ergs/cm^2 which is intermediate in the range between 10^{-2} and $2 \times 10^{-3} \mathbf{b}^2/s_{44}c$; however, doubt can be expressed about the correlation between twinning frequency and γ. The creep data of Thornton and Hirsch (1958) was used to predict a value of γ_{Pb} within large enough limits so that it might be considered either high or low.

It became of interest, therefore, to examine the value of γ_{Pb} by other available techniques. An investigation by means of x-ray diffraction is described in the present paper†. Pure lead, two alloys of lead, aluminium and α brass were examined. The alloys contained 0·10 at. % Ag and 20·0 at. % In respectively. The 0·10 at. % Ag alloy was the same as that used earlier in the twin boundary energy experiments (Bolling and Winegard (1958 a)).

The Pb-20·0 at. % In alloy was selected as representative of a binary system based on lead in which the nominal electron-to-atom ratio decreases within the large range of primary solid solubility of indium in lead. This alloy has thus a lower nominal electron-to-atom ratio than pure lead, and it affords a comparison of any resulting change in the stacking fault probability with systems where e/a increases on alloying, as, for example, in Cu–Zn (Warren and Warekois (1955)). A brief investigation of twinning frequency in this alloy was also undertaken for comparison between the occurrence of annealing twins, stacking-fault probability and stacking-fault energy.

§ 2. Experiments

2.1. *Sample Preparation*

Lead was zone-refined from a starting material of 99·9999% purity. The two alloys were prepared from the zone-refined lead and 99·999% pure silver and 99·999% pure indium. The alloy with 0·10 at % Ag was of a composition which extends beyond the limits of primary solid-solubility at room temperature; however, no evidence of a second phase was observed either metallographically or in the x-ray study. As expected the alloy with 20·0 at. % In exhibited no second phase since the primary solid-solubility is more than 60 at. % In. The aluminium used was of 99·996% purity.

2.2. *The Cryostat*

The cryostat used was similar to that designed by Barrett and co-workers (Barrett (1956)). The specimen was held in a copper holder which was attached to the bottom of a liquid helium reservoir and was

† The deformation of lead single crystals at low temperatures was studied for the same purpose (Bolling *et al.* (to be published)).

surrounded by radiation shields at liquid nitrogen temperature. A nickel foil x-ray filter was used as a part of the radiation shield. The x-ray windows were of 0·030 in. thick beryllium. A pointed stainless steel rod entered the cryostat through a ball-and-socket joint and sylphon bellows. The cryostat was mounted on a General Electric XRD–5 spectro-goniometer.

A copper–constantan thermocouple and a carbon resistance thermometer were attached to the specimen. Temperatures other than liquid helium and nitrogen were attained by allowing the helium to evaporate and admitting air to the helium chambers. The thermal inertia of the system was such that this provided sufficient temperature control for this series of experiments.

2.3. *Cold Work*

The usual method of determining α is to cold-work the material by filing and to follow this by an x-ray examination. In the present method cold work was introduced into bulk specimens by scratching the surface with a pointed tool (as shown in the plate). This was not as satisfactory as could be desired; however, with proper care, the main part of the exposed surface could be severely worked at any temperature.

In order to compare the deformation which could be obtained by this method, an annealed bulk specimen of 70:30 α-brass was deformed at 4·2°K and the faulting frequency compared to that reported by Wagner (1957 a) who deformed his specimen by filing at 77°K.

2.4. *X-ray Method*

In the examination of bulk specimens, peak positions for the (111) and (200) reflections, prior to and after cold-working, were determined as the mid-point at half-peak height. However, for the (220) reflection in the unworked specimen a separation between $K\alpha_1$ and $K\alpha_2$ peaks was apparent. Therefore, as a rough measure, the mid-point at quarter-peak height was used to determine the peak position for all (220) lines.

The foregoing approach allowed a precision in the determination of peak separation of about 0·01° for the (200)–(111) pair and somewhat less for the (220)–(200) pair. The determination of peak separation for higher-order reflections was not attempted.

In a few cases the counting rate constant was changed between two peaks in order to give equal apparent line intensities. No measurable change in peak separation with change in counting rate was observed.

Copper Kα radiation ($\lambda = 1{\cdot}5418$ Å) was used and the scanning rate was 0·20°/min (2θ).

§ 3. Results

3.1. *Pure Lead Deformed at* 4·2°K

The bulk sample of pure lead was first deformed at 77°K in the cryostat then warmed up to between 160° and 170°K for one hour.

Recrystallization occurred and was indicated by the full recovery of the line broadening and peak intensities. (Barrett, private communication) has observed recrystallization at ~155°K in lead of comparable purity.) In this way, a fine grain bulk sample ('recrystallized') was obtained for subsequent deformation at 4·2°K. It can be seen from the data given in table 1 that the peak separation changed with cold-work. As expected, the (200)–(111) separation decreased and the (220)–(200) increased with deformation. Moreover, it is demonstrated that the change in separation increased with increasing cold-work. For comparison, a bulk sample of 70 : 30 α-brass was given the same treatment as the lead, producing a change $\Delta 2\theta_{(200)-(111)} = 0{\cdot}17°$.

3.2. *Lead Alloys Deformed at* 4·2°K

In table 2 the data for the alloy with 0·10 at. % Ag show that there was little difference in $\Delta 2\theta$, produced by cold-work, from that of the pure metal in table 1. Since the alloy had a fine initial grain size, no recrystallization treatment was given prior to measurement. On warming the $2\theta_{200}$–$2\theta_{111}$ peak separation recovered almost to the initial room-temperature value; whereas, the line intensities were only 20% recovered at this temperature. Recrystallization does not occur until higher temperatures are reached in this alloy (Bolling and Winegard (1958 b)).

The alloy with indium did not exhibit measurable faulting after cold work (table 2). The change in separation is on the border-line between a true change and a random measurement error. Therefore, the effect of indium has been to reduce or to eliminate the separation change.

3.3. *Pure Lead Deformed at* 77°K

In table 3 a sequence of measurements is presented for one sample that was deformed and examined both at 77°K and 4·2°K. The recrystallized state noted in the table was obtained after deformation as before, when the sample was warmed from 77°K to 172°K at a rate between 1 and 2°K/min. During this heating the lead recrystallized and the peak-separation change was recovered. It was noted from traces obtained at intermediate temperatures that the line broadening recovered at lower temperatures (viz.: ~135°K) than the peak-separation change (~170°K). An estimate of recovery may be made from changes in line broadening; however, only a crude estimate could be obtained. This is shown in the table by the half-width at half-intensity of the (111) trace.

The peak-separation change at 77°K is comparable to that at 4·2°K for heavy deformation as in table 1.

3.4. *Aluminium Deformed at* 4·2°K

The aluminium specimen was deformed and annealed to produce a uniform fine grain size. Peak separation changes were only obtained at

Table 1. Zone-refined Pb

Temp. °K	Treatment	$(2\theta_{200}-2\theta_{111})=\Delta 2\theta_1$	Change of $\Delta 2\theta_1$ with cold-work	$(2\theta_{220}-2\theta_{200})=\Delta 2\theta_2$	Change of $\Delta 2\theta_2$ with cold-work
4·2	Recrystallized	$5{\cdot}05_9$	—	$16{\cdot}12_7$	—
4·2	1st cold-work	$5{\cdot}02_9$	$-0{\cdot}03_0$	$16{\cdot}15_0$	$+0{\cdot}02_3$
4·2	2nd cold-work	$5{\cdot}01_1$	$-0{\cdot}04_8$	$16{\cdot}16_5$	$+0{\cdot}03_8$
68	On warming	$5{\cdot}01_1$	—	—	—
77	On warming	$5{\cdot}01_5$	—	—	—

Table 2. Pb Alloys

Temp. °K	Treatment	Pb—0·10 at. % Ag		Pb—20·0 at. % In	
		$(2\theta_{200}-2\theta_{111})=\Delta 2\theta_1$	Change of $\Delta 2\theta_1$ with cold-work	$(2\theta_{200}-2\theta_{111})=\Delta 2\theta_1$	Change of $\Delta 2\theta_1$ with cold-work
300	Recrystallized	$5{\cdot}01_5$	—	$5{\cdot}02_6$	—
77	Recrystallized	$5{\cdot}04_6$	—	$5{\cdot}05_8$	—
4·2	Recrystallized	$5{\cdot}04_5$	—	$5{\cdot}06_1$	—
4·2	1st cold-work	$5{\cdot}02_4$	$-0{\cdot}02_1$	$5{\cdot}06_0$	$-0{\cdot}00_1$
4·2	2nd cold-work	$5{\cdot}00_4$	$-0{\cdot}04_1$	$5{\cdot}05_4$	$-0{\cdot}00_7$
300	On warming	$5{\cdot}00_6$	—	$5{\cdot}02_5$	—

4·2°K and are shown in table 4. As can be seen, the change in peak separation is just measurable after heavy cold-work. Wagner (1957 b) has already shown that measurements on aluminium filings prepared and measured at 77°K reveal no change in peak separation with cold-work.

Table 3. Zone-refined Pb

X-ray exam. temperature °K	Treatment	Half-width (111) at $\frac{1}{2}I$, 2θ	$(2\theta_{200}-2\theta_{111})=\Delta 2\theta_1$	Change in $\Delta 2\theta_1$ with cold-work
77	From room temperature	0·12	$5{\cdot}05_0$	—
77	Recrystallized	0·09	$5{\cdot}04_5$	—
77	1st cold-work	0·21	$5{\cdot}02_0$	$-0{\cdot}02_5$
77	2nd cold-work	0·23	$5{\cdot}02_0$	$-0{\cdot}02_5$
77	3rd cold-work	0·24	$5{\cdot}00_5$	$-0{\cdot}04_0$
77	Recrystallized	0·11	$5{\cdot}04_0$	—
4·2	Recrystallized	0·11	$5{\cdot}04_0$	—
4·2	1st cold-work	0·14	$5{\cdot}02_0$	$-0{\cdot}02_0$
77	Recrystallized	0·11	$5{\cdot}04_0$	—
4·2	Recrystallized	0·11	$5{\cdot}04_5$	—

Table 4. Aluminium at 4·2°K

Treatment	$(2\theta_{200}-2\theta_{111})=\Delta 2\theta_1$	Change in $\Delta 2\theta_1$ with cold-work
Annealed	$6{\cdot}27_5$	—
1st cold-work	$6{\cdot}27_3$	$-0{\cdot}00_2$
2nd cold-work	$6{\cdot}26_0$	$-0{\cdot}01_5$
3rd cold-work	$6{\cdot}26_0$	$-0{\cdot}01_5$

3.5. *Stacking-fault Parameter*

Following the method described by Wagner (1957 a), α may be calculated as $\alpha . H=\Delta 2\theta_{hkl-h'k'l'}$, where H is a constant depending upon the particular reflections and radiation used. For CuKα radiation the following values were determined for H:

Pb 200–111 $H=-3{\cdot}7$
Pb 220–200 $H=+7{\cdot}8$
70:30 Brass 200–111 $H=-5{\cdot}0$
Al 200–111 $H=-4{\cdot}7$

In table 5 the value of α for the heaviest deformation used in this investigation is tabulated together with some other values taken from the literature. The values of α for pure lead calculated from $\Delta 2\theta_{220-200}$ are not included in table 5 because the determination of peak positions

Table 5. Stacking-fault probability for several f.c.c. metals

Metal	Deformation	C.W. Temp.	α	α^{-1}	Source
Pb	Cold-work II	4·2	0·013	77	Present investigation
Pb	Cold-work II	77	0·011	93	Present investigation
Pb–Ag (0·10)	Cold-work II	4·2	0·011	91	Present investigation
Pb–In (20)	Cold-work II	4·2	(0·002)	(500)	Present investigation
Al	Cold-work III	4·2	$0{\cdot}003_2$	312	Present investigation
Cu–Zn (30)	Cold-work II	4·2	0·034	29	Present investigation
Cu–Zn (27)	Filing	300	0·020	50	Smallman and Westmacott (1957)
Cu–Zn (30)	Filing	77	0·04	25	Wagner (1957 a)
Cu–Zn (30)	Filing	300	0·025	40	Warren and Warekois (1955)
Cu–Zn (42)	Filing	300	0·046	22	Massalski and Barrett (1957)
Cu	Filing	300	$0{\cdot}003_3$	300	Smallman and Westmacott (1957)
Cu	Filing	74	0·012	83	Smallman and Westmacott (1957)
Cu	Filing	77	$0{\cdot}012_5$	80	Wagner (1957 a)
Cu	Filing	300	$0{\cdot}006_3$	160	Greenough and Smith (1955)
Ni	Filing	300	$0{\cdot}001_7$	590	Smallman and Westmacott (1957)
Ni	Filing	300	$0{\cdot}003_4$	290	Christian and Spreadborough (1956)
Ag	Filing	77	0·017	60	Wagner (1957 a)
Al	Filing	77	$\sim$0·001	$>$1000	Wagner (1957 a)

of the (220) are less accurate. However, it can be seen from table 1 that the sign of the change in separation is consistent in giving a positive α. (For first and second cold working, α is respectively 0·003 and 0·005 as compared to the $\Delta 2\theta_{200-111}$ values 0·008 and 0·013.)

In table 6 the highest values of stacking-fault parameter determined at any temperature are compared with twin boundary energies. These are determined from relative energies (see, for example, Bolling and Winegard (1958a)) and the best values of grain-boundary energy. When the latter was not available, it was chosen as one-third of the surface-free energy.

Table 6. α_{max} compared to twin-boundary free energy

Metal	Highest α	$\gamma_{T.B.}$ ergs/cm^2	Method
Cu–Zn (30)	0·040	~ 20	Twinning more frequent than Cu, grain-boundary energy probably lower.
Ag	0·017	~ 15	Estimated relative energy as ~0·04
Pb	0·013	10	Measured relative energy
Cu	0·013	20	Measured relative energy
Ni	0·003	~ 32	Measured relative energy
A	$0{\cdot}003_2$	~120	Measured relative energy

§ 4. Discussion

4.1. *Correlation between α, γ and Twin-boundary Energies*

In table 6 a correspondence between twin-boundary energies and the stacking-fault parameter is apparent. It was also established that the temperature of deformation and the amount of cold-work introduced to the metal are important in determining the value of α. The temperature of measurement can also effect the value of α if any recovery occurs. If all these factors could be taken into account, a comparison of different techniques used to assess γ would have to include some type of comparative temperature scale for the metals of different melting points. It is possible that results obtained at two extremes of temperature might be suitably compared. For example, the relative twin-boundary energies for copper and lead were determined after long annealing near their respective melting points where the structures should be in a similar condition. On the other hand, it would probably be desirable to compare the values of α at the lowest possible temperature and for equally strained specimens. Nevertheless, the general trend in results confirms that lead should have a low numerical value of stacking-fault energy, which is comparable to copper in the temperature range 0–160°K where extensive cold-work can be obtained.

The data for lead alloys again show a general correlation between α and twin-boundary energies, but emphasize the difficulty of any direct correspondence. As shown in table 5, α decreases from 0·013 to 0·011 with addition of 0·10 at. % Ag to lead. This may not be a true change because the degree of cold-work may be smaller in the alloy which is harder than the pure metal. Bolling and Winegard (1958a) showed that the relative twin-boundary energy changed from $0{\cdot}050 \pm 0{\cdot}014$ to $0{\cdot}077 \pm 0{\cdot}016$ with the addition of 0·10 at. % Ag to lead. However, they attributed this change to a decrease in grain-boundary free energy in the alloy caused by the segregation of silver. If this conclusion were true, the lead–silver alloy is probably very much like pure lead with respect to the stacking-fault energy.

The addition of 20·0 at. % In to lead suppresses a measurable α as shown in table 5. Subsequent to the x-ray studies, samples of the same alloy were treated and examined for relative twin-boundary energy and twinning frequency in the manner used by Bolling and Winegard (1958a). Even after long annealing close to the melting point scatter in the data prevented an accurate determination of relative twin-boundary energies. However, on the average, the values obtained were higher than could be attributed solely to grain-boundary segregation of indium and a subsequent reduction in the free energy of grain boundaries. Moreover, the ratio of the number of twin boundaries to grain boundaries was reduced by a factor of six in the indium–lead alloy from that in pure lead. These results can be interpreted as indicative of an increase in twin-boundary energy, and hence they correlate with the decrease of α in this alloy.

4.2. *Electronic Interactions and Stacking-fault Energy*

The stacking-fault energy of a metal arises from particular electronic interactions within the structure. However, the way in which the influence of the electronic structure upon γ may be assessed is not clear. Aluminium is three-valent, and its first, and second, Brillouin zones are overlapped by a complex Fermi surface (Heine 1957), unlike the monovalent metals, copper, silver and gold. Hence, if the Fermi electrons and the nature of the Fermi surface are important in determining γ, one might expect aluminium to differ from the noble metals which do not exhibit overlap. For similar reasons all polyvalent f.c.c. metals might be expected to resemble aluminium (Seeger 1955b).

There is evidence that the first Brillouin zone, and higher zones of lead, are also overlapped by a multiply-connected Fermi surface (Gold 1958). Nevertheless, it is significant that the stacking-fault probability of lead falls with the noble metals rather than with Al. If the long-range electronic forces are responsible for the stacking-fault energy, the difference between Pb and Al may originate in the detailed difference between their respective Fermi distributions. This is suggested by reference to the Pb–In alloy.

For the purpose of assessing an alloy of lead, a group IV metal, with indium, a group III metal, it may be justifiable to assume that the electron concentration decreases on adding indium to lead. The electronic nature of lead–indium alloys has not been studied; however, interpretations exist for the lead–thallium system which shows a very close resemblance to lead–indium. In the lead–thallium alloys the changes of various electronic properties indicate that the density of states, $N(E)$, at the Fermi surface drops rapidly from the value of pure lead, reaching some fairly constant value at about 15% thallium (Gold 1960). This decrease of $N(E)$ has been interpreted in terms of changes in the Fermi distribution as the nominal electron concentration decreases. Similarity between the systems lead–thallium and lead–indium suggests that an analogous change in $N(E)$ may also occur in lead–indium alloys, and hence it is tempting to speculate about the connections between $N(E)$ and α. Since addition of 20 at. % In to lead produces a change in α from a copper-like metal to an aluminium-like metal, the above possibility deserves further detailed study.

4.3. *Summary*

1. At low temperatures the value of α for lead is similar to the value of α for the monovalent f.c.c. metals and about one-third of the value for 70 : 30 CuZn brass at 4·2°K.

2. The value of α for aluminium at 4·2°K is barely measurable, indicating that even at this temperature aluminium does not exhibit appreciable deformation faulting.

3. A finite stacking-fault probability in lead at low temperatures can be suppressed by the addition of 20 at.% In.

4. A correlation between the presence of annealing twins and the value of α is exhibited in the lead and lead alloys, even though it is clear that too many extraneous factors are present during the production of annealing twins for more than a qualitative comparison.

5. It has been demonstrated that the stacking-falt probability increases with the amount of deformation in the systems studied. Hence, it is difficult to compare α for different metals if the amount of strain is not assessed.

Acknowledgments

The authors thank Dr. P. A. Flinn for suggesting the investigation of the lead–indium alloy and for helpful discussions. Mr. J. C. Ogle contributed greatly to the experimental part of the investigation.

References

Barrett, C. S., 1956, *Acta cryst., Camb.*, **9**, 671.
Bolling, G. F., Hays, L. E., and Wiedersich, H. W. (to be published).
Bolling, G. F., and Winegard, W. C., 1958 a, *J. Inst. Met.*, **86**, 492 ; 1958 b, *Acta Met.*, **6**, 288.

Christian, J. W., and Spreadborough, J., 1956, *Phil. Mag.*, **1,** 1069.
Feltham, P., and Meakin, J. D., 1957, *Acta Met.*, **5,** 555.
Fullman, R. L., 1950, *Gen. Elect. Rep.* (RL-422); 1951, *J. appl. Phys.*, **22,** 488.
Gold, A. V., 1958, *Phil. Trans.* A, **251,** 85 ; 1960, *Phil. Mag.*, **5,** 70.
Greenough, G. B., and Smith, E. M., 1955, *Proc. phys. Soc. Lond.* B, **68,** 51.
Haasen, P., 1958, *Phil. Mag.*, **3,** 384.
Heine, V., 1957, *Proc. roy. Soc.* A, **240**, 340, 354, 361.
Massalski, T. B., and Barrett, C. S., 1957, *Trans. Amer. Inst. min. (metall.) Engrs*, **209,** 455.
Paterson, M. S., 1952, *J. appl. Phys.*, **23,** 805.
Seeger, A., 1955 a, *Phil. Mag.*, **46,** 1194 ; 1955 b, *Conf. on Defects in Crys. Solids* (Physical Society), p. 328 ; 1957, *Disl. & Mech. Prop. of Crystals* (Wiley), p. 243.
Seeger, A., Berner, R., and Wolf, H., 1959, *Z. Phys.*, **155,** 247.
Seeger, A., and Schöck, G., 1953, *Acta Met.*, **1,** 519.
Smallman, R. E., and Westmacott, K. H., 1957, *Phil. Mag.*, **2,** 669.
Thornton, P. R., and Hirsch, P. B., 1958, *Phil. Mag.*, **3,** 738.
Wagner, C. N. J., 1957 a, *Acta Met.*, **5,** 427 ; 1957 b, *Ibid.*, **5,** 477.
Warren, B. E., and Warekois, E. P., 1955, *Acta Met.*, **3,** 473.

Effect of Irradiation Growth on the Creep of Uranium Under a Uniaxial Load†

By W. S. Blackburn
Nuclear Research Centre of C. A. Parsons Ltd.,
Fossway, Newcastle upon Tyne, 6

[Received October 21, 1960]

Abstract

Theories are developed from two different assumptions to calculate the effect of irradiation growth on the creep of uranium under a uniaxial applied stress when the temperature is sufficiently high for the internal stresses set up by the differential expansions of the individual crystals to be insufficient of themselves to cause plastic flow. It is shown that the greater the irradiation growth the greater is the creep rate for a given stress ; the effect on creep rate is also greater at lower applied stresses for a given irradiation growth.

§ 1. Introduction

Anderson and Bishop (1957) have developed a theory for the effect of irradiation growth on the creep of uranium when the internal stress generated is sufficient for the material to become plastic. The theory presented here is similar to that derived (Blackburn *et al.* 1960) for thermal cycling effects and treats the case when the stresses are still in the elastic range. For simplicity, primary creep, variations with stress of Young's modulus and variations of the mechanical properties with time of irradiation are neglected, though these effects may be incorporated in the equations.

We obtain simultaneous differential equations, from which the creep rate may be determined by integration, from each of the following assumptions: (*a*) a uniform deformation; (*b*) a uniform internal stress which is the same as that generated if each crystal were prevented from deforming in the absence of the applied stress.

§ 2. Theory

To calculate the deformation of an aggregate of non-isotropic crystals from their individual properties, assumptions must be made, since the orientation and location of each crystal is not known. For simplicity we assume each crystal to undergo a homogeneous deformation. In general this prohibits the continuity of both stresses and displacements between the crystals. We require however on quasi-statical grounds

† Communicated by the Author.

that the mean of any component of the stress over the crystal orientations should equal the corresponding component of applied stress. Another assumption is also necessary. The simplest is that the stress is uniform (i.e. the same in all crystals). This however leads to the conclusions that the creep rate is the same under temperature variations as it would be if the temperature were maintained as its instantaneous value, in contradiction to the experimental evidence (Anderson and Bishop 1957, Blackburn *et al.* 1960).

Two other possibilities are to assume either that the deformation is uniform or that the stress components are the sum of those of the applied stress w and an internal stress which is uniform with respect to the crystal axes and independent of w. The first is probably more realistic but the second leads to simpler computation and can be pursued further. We will develop both.

In each case we assume that the strain rate of a crystal under homogeneous deformation is related to the stress, stress rate and rate of irradiation growth by

$$\frac{d\epsilon_{ij}}{dt} = \gamma_{ij} + \frac{1+\nu}{E}\frac{d}{dt}\left(\tau_{ij} - \frac{\nu}{1+\nu}g_{ij}\sum_k \tau_{kk}\right) + \left(\frac{3}{2}\right)^{(n+1)/2} C \exp\left(-\dot{B}/T\right)\sigma_{ij}J^{n-1}. \quad . \; . \; . \quad (1)$$

The first term on the right-hand side represents irradiation growth, the second is the derivative of the linear elastic strain stress relationship and the third is a generalization of the form of the one-dimensional secondary creep law for isothermal polycrystalline uranium as found experimentally. T is the temperature, t the time, E Young's modulus, ν Poisson's ratio, B, C and n creep constants ϵ_{ij}, g_{ij}, τ_{ij}, σ_{ij} the components of the strain, metric, stress and stress deviation

$$\left(\text{or reduced stress } \tau_{ij} - 1/3 g_{ij}\sum_k \tau_{kk}\right) \text{ tensors and } J^2 = \sum_{ij}\sigma_{ij}\sigma_{ij}.$$

We consider a uniaxial stress w acting along the z axis of a set of coordinate axes in the specimen. Without loss of generality we may choose the b axis of the crystal to lie in the (x, z) plane. We denote the angles between the b and z axes and between the (b, z) and (b, c) planes by $\frac{1}{2}\pi - \theta$ and $\frac{1}{2}\pi - \psi$. Then

$$\left.\begin{aligned} \gamma_{11} &= \gamma(\cos^2\theta - \cos^2\psi\sin^2\theta), & \gamma_{23} &= \gamma\cos\psi\sin\psi\cos\theta, \\ \gamma_{13} &= \gamma\cos\theta\sin\theta(1+\cos^2\psi), & \gamma_{22} &= -\gamma\sin^2\psi, \\ \gamma_{33} &= \gamma(\sin^2\theta - \cos^2\psi\cos^2\theta), & \gamma_{12} &= -\gamma\cos\psi\sin\psi\sin\theta. \end{aligned}\right\} \quad (2)$$

By adding the equations for the normal strain rates we find that,

$$\frac{d}{dt}\sum_k \epsilon_{kk} = \frac{1-2\nu}{E}\frac{d}{dt}\sum_k \tau_{kk}.$$

For a random orientation the mean of this is zero (since the mean of

$$\sum_k \tau_{kk}$$

is the applied stress w). Hence the creep rate $d\epsilon/dt$ is the mean rate of

normal strain deviation along the z axis. We note that the mean rates of strain deviation in the perpendicular directions are $-\frac{1}{2}$ of this and the mean tangential strains are zero.

We consider first the assumption that the deformation is uniform. Then eqns. (1) and (2) become:

$$\frac{d\sigma_{33}}{dt} = \frac{E}{1+\nu}\left\{\frac{d\epsilon}{dt} - (\tfrac{3}{2})^{(n+1)/2} C \exp(-B/T)\sigma_{33} J^{n-1} + \gamma(\cos^2\psi\cos^2\theta - \sin^2\theta)\right\},$$

$$\frac{d\sigma_{11}}{dt} = \frac{E}{1+\nu}\left\{-\tfrac{1}{2}\frac{d\epsilon}{dt} - (\tfrac{3}{2})^{(n+1)/2} C \exp(-B/T)\sigma_{11} J^{n-1} + \gamma(\cos^2\psi\sin^2\theta - \cos^2\theta)\right\},$$

$$\frac{d\sigma_{13}}{dt} = \frac{E}{1+\nu}\{-(\tfrac{3}{2})^{(n+1)/2} C \exp(-B/T)\sigma_{13} J^{n-1} - \gamma(1+\cos^2\psi)\cos\theta\sin\theta\},$$

$$\frac{d\sigma_{23}}{dt} = \frac{E}{1+\nu}\{-(\tfrac{3}{2})^{(n+1)/2} C \exp(-B/T)\sigma_{23} J^{n-1} - \gamma\cos\psi\sin\psi\cos\theta\},$$

$$\frac{d\sigma_{12}}{dt} = \frac{E}{1+\nu}\{-(\tfrac{3}{2})^{(n+1)/2} C \exp(-B/T)\sigma_{12} J^{n-1} + \gamma\cos\psi\sin\psi\sin\theta\}. \quad \ldots \quad (3)$$

We remember that σ_{22} may be obtained as $-(\sigma_{11}+\sigma_{33})$.

If we denote the properties of a crystal whose orientations, θ and ψ are $\theta_{(k)}$ and $\psi_{(h)}$ by bracketed subscripts and the frequency of its distribution by $S_{(k,\,h)}$, we have the additional equation:

$$\sum_{k,h} S_{(k,\,h)}\sigma_{33(k,\,h)} = \tfrac{2}{3} w \sum_{k,h} S_{(k,\,h)}.$$

Hence for random orientation it may be deduced from the first of eqns. (3) that

$$\frac{d\epsilon}{dt}\sum_{k,h} S_{(k,\,h)} = (\tfrac{3}{2})^{(n+1)/2} C \exp(-B/T)\sum_{k,h} S_{(k,\,h)} J^{n-1}(k,h)\sigma_{33(k,\,h)}. \quad \ldots \quad (4)$$

Integration of the simultaneous differential eqns. (3) and (4) for a small number of orientations yields the stresses and the creep rate.

We now investigate the consequences of the alternative assumption that the stress in a randomly orientated aggregate is the sum of the applied stress and a uniform internal stress. The value of the latter may be determined by putting $\theta = \pi/2$ and ψ and $d\epsilon/dt$ zero in eqn. (3). We denote the value of σ_{ij} when w is zero by s_{ij}.

s_{cc}, s_{ab}, s_{ac}, and s_{bc} are initially zero. We see that eqn. (3) is satisfied if they remain so. Also $s_{bb} = -s_{aa}$ where:

$$\frac{ds_{aa}}{dt} = \frac{E}{1+\nu}\{\gamma - (\tfrac{3}{2})^{(n+1)/2} C \exp(-B/T) s_{aa} I^{n-1}\} \quad \ldots \quad (5)$$

and

$$I^2 = \sum_{i,j} s_{ij} s_{ij}.$$

Hence we may write $s_{aa} = -s_{bb} = I/\sqrt{2}$ where

$$\frac{dI}{dt} = \frac{E}{1+\nu}\{\sqrt{2}\gamma - (\tfrac{3}{2})^{(n+1)/2} C \exp(-B/T) I |I|^{n-1}\}. \quad . \quad . \quad (6)$$

By integrating this equation, I may be determined, but it is often possible to approximate it by its asymptotic value:

$$\sqrt{\frac{2}{3}}\left[\frac{2\gamma}{\sqrt{3}C}\exp(B/T)\right]^{1/n}.$$

Table 1. Time for internal stress to approach asymptotic value at 403 °C in a flux of 3×10^{12} neutrons cm^{-2} sec^{-1}

t, hr	I, p.s.i.
43·65	4000
74·54	6000
101·44	7000
127·37	7500
154·41	7750
186·25	7875
∞	7950

Table 2. Asymptotic values of internal stress

T, °C	γ, yr^{-1}	I, p.s.i.
270	0·18	549000
305	0·14	162000
380	0·068	16600
400	0·046	8980
403	0·04	7950
450	0·01	1750

The times taken to approach this value at 403°C in a flux of 3×10^{12} neutrons cm^{-2} sec^{-1} are shown in table 1, using the values $n = 2{\cdot}52$, $\nu = 0{\cdot}23$, $\gamma = 0{\cdot}04$/yr, $B = 25\,300$°K, $E = 1{\cdot}86 \times 10^7$ p.s.i., $C = 8{\cdot}413$ hr^{-1} p.s.i.$^{-2{\cdot}52}$. With these constants, the asymptotic values of I at the temperatures for which γ is given by Finniston (1958) are presented in table 2. At the lower temperatures these stresses will not be attained since the material will previously have yielded plastically.

We now use the assumption that the stress is the sum of the applied and internal stresses. The mean creep rate over the various orientation simplifies from eqn. (1) to

$$\frac{d\epsilon}{dt} = \frac{1}{4\pi}(\tfrac{3}{2})^{(n+1)/2} C \exp(-B/T) \int_0^{2\pi} \int_{-\pi/2}^{\pi/2} \sigma_{33} J^{n-1} \cos\theta \, d\theta \, d\psi. \quad (7)$$

Then, as shown by Blackburn *et al.* (1960)

$$\sigma_{33} = s_{33} + 2w/3, \quad J^2 = I^2 + 2ws_{33} + 2w^2/3,$$

and the creep rate reduces to:

$$\frac{d\epsilon}{dt} = (\tfrac{3}{2})^{(n+1)/2} \frac{2(n+4)}{15} C \exp(-B/T) w I^{n-1}, \quad . \quad . \quad . \quad (8)$$

when w/I is small, and in general to:

$$\frac{d\epsilon}{dt} = \frac{1}{\pi} (\tfrac{3}{2})^{(n+1)/2} \exp(-B/T) C I^n \int_0^{\pi} \int_0^1 \left(\frac{2w}{3I} + \frac{\cos^2\psi(1-x^2) - x^2}{\sqrt{2}} \right)$$
$$\times \left\{ 1 + \frac{\sqrt{2}w[\cos^2\psi(1-x^2) - x^2]}{I} + \frac{2w^2}{3I^2} \right\}^{(n-1)/2} dx\, d\psi. \quad . \quad . \quad (9)$$

Thus the ratio of the creep rates in the presence and absence of irradiation growth is:

$$\frac{1}{\pi} (\tfrac{3}{2})^{(n+1)/2} \left(\frac{I}{w} \right)^n \int_0^{\pi} \int_0^1 \left(\frac{2w}{3I} + \frac{\cos^2\psi(1-x^2) - x^2}{\sqrt{2}} \right)$$
$$\times \left\{ 1 + \frac{\sqrt{2}w[\cos^2\psi(1-x^2) - x^2]}{I} + \frac{2w^2}{3I^2} \right\}^{(n-1)/2} dx\, d\psi. \quad (10)$$

With $n = 2{\cdot}52$ the constant appropriate to uranium this expression and the linearized approximation,

$$(\tfrac{3}{2})^{(n+1)/2} \frac{2(n+4)}{15} \left(\frac{I}{w} \right)^{(n-1)}$$

are presented in table 3 as function of w/I. The ratios of creep rates presented differ little from those which would obtain if the internal stress were caused by thermal cycling (Blackburn *et al.* 1960).

Table 3. Effect of irradiation on creep rate

w/I	Creep rate with irradiation / Creep rate without irradiation	Linearized approximation
0·25	14·9	14·6
0·5	5·5	5·08
0·75	3·25	2·74
1·0	2·34	1·77
1·5	1·63	0·955
2·5	1·23	0·44
5·0	1·06	0·153

It has been found experimentally (Rose 1957) that the secondary creep rate of uranium at 450°C under a stress of 2·7 t.s.i. does not differ markedly, with and without irradiation. This would be anticipated on this theory for the conditions reported but would not be true for small stress at this temperature.

§ 3. Conclusions

Theories have been derived to deduce the effect of irradiation growth on the creep of uranium under a uniaxial load when the stress is insufficient to cause plastic flow. The theory based on the assumption of uniform deformation is probably slightly more reliable, but the alternative assumption, of the stress being the sum of the applied stress and the internal stress that would exist if each crystal were prevented from deforming in the absence of applied stress, leads to a simpler formula for the creep rate. For w/I less than 1/3, the proportionate increase in creep rate is seen to vary approximately as $(I/w)^{n-1}$, while I tends to a value which varies in proportion to the nth root of the rate of irradiation growth.

Acknowledgments

The writer is grateful to Mr. D. Clarkson who performed the calculations on the digital computer and to C. A. Parsons & Co., Ltd., for permission to publish this work.

References

Anderson, R. G., and Bishop, J. F. W., 1957, UKAEA Reports IGR TN C, 681, 854 (to be published).

Blackburn, W. S., Stobo, J. J., and Harnby, G., 1960, *J. nucl. Energy*, **12**, 162.

Finniston, H. M., 1958, Australian Atomic Energy Symposium.

Rose, H. C., 1957, *J. Inst. Met.*, **86**, 122.

The Optical Properties of Liquid Germanium, Tin and Lead†

By J. N. Hodgson
University College, Keele, Staffs

[Received August 31, 1960]

Abstract

The optical constants of liquid germanium, tin and lead have been measured by a reflection method for wave numbers between 4000 and 27 000 cm^{-1} (wavelengths 2·5 to 0·37 microns). The temperature variation of the optical constants was measured for tin and lead. The experimental results follow approximately the Drude free electron formulae if the number of free electrons per atom, N_0, and their relaxation time, τ, are treated as adjustable parameters. The values of N_0 lie between 4·3 and 4·7, with a slight temperature variation. The values of the static conductivity calculated from N_0 and τ are compared with electrically measured values. Previous optical measurements on evaporated films of tin and lead have indicated values of N_0 between 1·2 and 1·4 for the solid metals.

§ 1. Introduction

The electronic band structure of a solid metal is determined by its crystal lattice structure. When the metal melts, the long-range order of the crystal lattice disappears but some short-range order remains. Knight *et al.* (1959) have suggested that this short-range order determines an electronic band structure for a liquid metal. For those metals in which the coordination does not increase markedly on melting, e.g. Al, Sn, Pb, the electronic structure of the liquid is similar to that of the solid. They quote experimental values of the changes of electrical conductivity and Knight shift in support of their suggestion. For example, the electrical conductivity of tin decreases by a factor 2·1 on melting and the Knight shift decreases by a factor 1·03. The change in the conductivity is in approximate agreement with the theory of Mott (1934), assuming no change in the number of free electrons when a metal melts. The small change in the Knight shift indicates a correspondingly small change in the electronic wave function. The behaviour of germanium and other metals for which the coordination increases on melting, is quite different and drastic changes in the electronic wave function must be assumed. The changes in the properties of germanium on melting are exceptionally large, with a ratio of electrical conductivity liquid/solid of about 15 at the melting point. Liquid germanium has a resistivity of $6{\cdot}0 \times 10^{-5}$ ohm-cm at the melting point, which is close to the value for liquid tin at the same temperature.

† Communicated by the Author.

Knight *et al.* also suggest that there is no simple connection between the optical properties of a liquid metal and its transport properties and Knight shift. The only values for the optical constants of liquid metals previously available, those of Kent (1919), are at variance with this suggestion. The electron densities and relaxation times deduced from Kent's values for the optical constants, lead to values for the electrical conductivity nearly equal to the electrically measured values. Since Kent made measurements over a small spectrum range and at only one temperature, this agreement might be considered a coincidence. To find out if this is so, the optical measurements on liquid metals are being repeated over a wider spectrum range, wave numbers 4000 to 27 000 cm^{-1}, and temperature variations are being measured where possible. This paper presents the results for three quadrivalent elements, germanium, tin and lead.

§ 2. Experimental Method

The optical constants were measured by the reflection method described in previous papers (Hodgson 1959, 1960). The metals were melted in silica or carbon crucibles enclosed in a tank filled with hydrogen. The temperature just below the centre of the crucible was measured with a chromel–alumel thermocouple. The experimental results are expressed in values of the dielectric constant, ϵ, and the conductivity, σ, in e.s.u. for various wave numbers, k, in cm^{-1}.

§ 3. Theory

A metal contains a certain density of conduction electrons, say N per cm^3. The motion of these electrons is damped by the thermal vibrations and lattice imperfections. The simplest representation of this damping is by a single parameter, the relaxation time, τ. Interaction with the atoms of the metal may also change the effective mass of the conduction electrons from the free electron value, $\boldsymbol{m}$, to $\boldsymbol{m}^*$. The theoretical formula for the static electrical conductivity, σ_0, due to these electrons is:

$$\sigma_0 = Ne^2\tau/\boldsymbol{m}^*. \quad . \quad . \quad . \quad . \quad . \quad . \quad . \quad . \quad . \quad (1)$$

At a non-zero frequency corresponding to a vacuum wave number k, the formulae for ϵ and σ due to the conduction electrons are:

$$\epsilon = 1 - k_0^2/(k^2 + k_R^2), \quad . \quad . \quad . \quad . \quad . \quad . \quad . \quad (2)$$

$$\sigma/\boldsymbol{c} = \tfrac{1}{2}k_0^2 k_R/(k^2 + k_R^2) \quad . \quad . \quad . \quad . \quad . \quad . \quad . \quad (3)$$

where

$$k_0^2 = e^2N/\boldsymbol{m}^*\pi\boldsymbol{c}^2 \quad \text{and} \quad k_R = 1/2\pi\boldsymbol{c}\tau. \quad . \quad . \quad . \quad . \quad (4)$$

The effective number of electrons per atom N_0, is defined by:

$$N_0 = (N/N_a) \times (\boldsymbol{m}/\boldsymbol{m}^*) \quad . \quad . \quad . \quad . \quad . \quad . \quad . \quad (5)$$

where N_a is the number of atoms per cm^3. At frequencies below the threshold for inter-band transitions, the effect of electrons in the filled bands can be represented by a small additional term in the expression for ϵ. This term has been neglected in the discussion of results.

§ 4. Discussion of Results

4.1. *Germanium*

The germanium used for these measurements had a room-temperature resistivity of about 1 ohm-cm corresponding to an impurity content of between 10^{15} and 10^{16} atoms per cm^3. About 40 g of germanium were melted in a silica crucible under a pressure of about 3 cm Hg of hydrogen. The hydrogen was constantly flowing through the tank containing the furnace. On first melting, the liquid germanium was covered with a cloudy, light scattering layer. This layer gradually cleared from the middle of the liquid germanium surface. The specularly reflecting area in the middle was sufficient for reflection measurements. The optical constants were measured and the germanium allowed to re-solidify. It was subsequently re-melted and the optical constants were measured again. The values were appreciably different from those of the first experiment, ϵ and σ having changed by $\sim 20\%$. This process was repeated about six times until the change of optical properties on solidification and re-melting was not more than the experimental error. These changes may be explained by the gradual reduction of an oxide film on the surface of the germanium. It was not possible to make reliable measurements of the temperature variation of optical properties because of the small temperature range available, 980 to 1050°C.

The final experimental values of ϵ and $\sigma/\mathbf{c}$ are given by the points in fig. 1. The estimated probable errors are shown by vertical bars where they exceed the diameter of the plotted circles. The theoretical curves have been drawn using formulae (2) and (3), choosing k_0 and k_R to give the best fit with the experimental points for $\log k < 4{\cdot}2$, i.e. in the infra-red. The general trend of the experimental points agrees with the theoretical curves but there are significant differences in detail.

4.2. *Tin*

Optical measurements were made on two samples of tin of different purities, 99·999 and 99·99%. The tin was melted in a silica crucible under a pressure of about 5 cm Hg of hydrogen. As with germanium, the optical constants changed on successive melting and solidification until stable values were found. The final values for both samples of tin were not appreciably different. Tin is a convenient metal for the measurement of temperature variation because of the low melting point, 232°C, and the high boiling point, ~2000°C.

The final experimental values are given by the points in fig. 2. The theoretical curves have again been fitted to the experimental points for $\log k < 4{\cdot}2$. Only a few points show significant deviations from the curves.

Some experimental values of ϵ and σ for evaporated films of tin are available for comparison (Motulevich and Schubin 1957 and Hodgson

Fig. 1

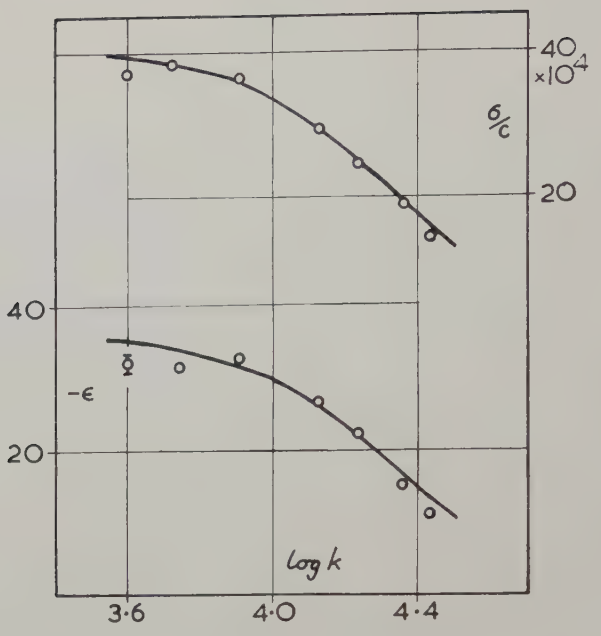

Liquid germanium.

ϵ = dielectric constant, σ = conductivity in e.s.u., k = wave number in cm^{-1}. Experimental points for 998°C. Theoretical curves for $N_0 = 4{\cdot}30$, $\sigma_0/c = 40{\cdot}7 \times 10^4$.

Fig. 2

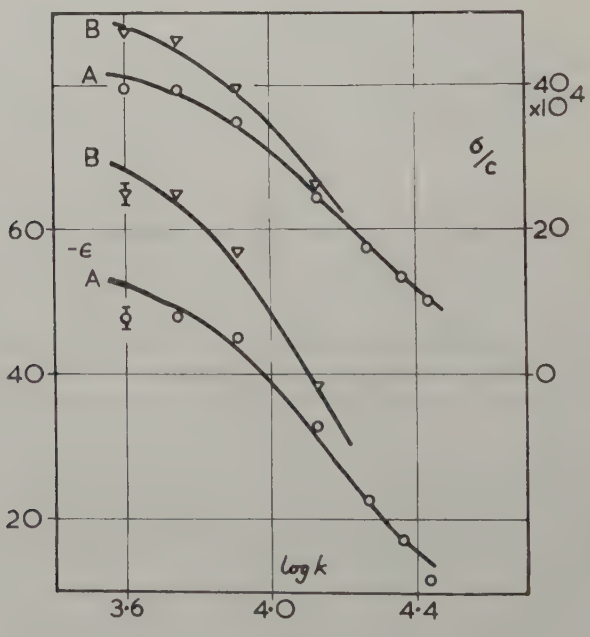

Liquid tin.

ϵ = dielectric constant, σ = conductivity in e.s.u., k = wave number in cm^{-1}. Experimental points : ○ for 858°C, ▽ for 446°C. Theoretical curves : A for $N_0 = 4{\cdot}59$, $\sigma_0/c = 43{\cdot}8 \times 10^4$; B for $N_0 = 4{\cdot}68$, $\sigma_0/c = 52{\cdot}4 \times 10^4$.

1955). These measurements on evaporated films are not exactly reproducible and further experimental work is needed before such values can be accepted as standard values for solid tin. They should be accurate enough, however, to show some general features of the optical properties of the solid metal. The experimental values are shown by the points in fig. 3 and the theoretical curves have been fitted to the points for $\log k < 3{\cdot}6$. The experimental points for σ lie consistently above the curve for $\log k > 3{\cdot}6$. The general agreement of the experimental points with the curves for $\log k < 3{\cdot}6$ indicates that the corresponding values of N_0 and τ

Fig. 3

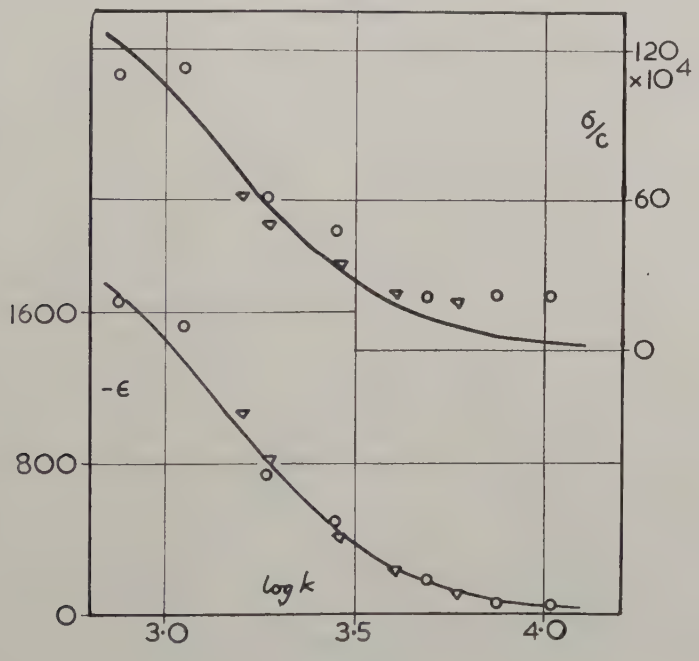

Solid tin.

ϵ = dielectric constant, σ = conductivity in e.s.u., k = wave number in cm^{-1}. Experimental points : ▽ Motulevich and Schubin (1957), ○ Hodgson (1955). Theoretical curves for $N_0 = 1{\cdot}33$, $\sigma_0/c = 1{\cdot}53 \times 10^6$.

are significant. The optical value of $\sigma_0/\boldsymbol{c}$ is smaller than the electrical value, but a similar discrepancy has been noticed in measurements on evaporated films of other metals. For example, infra-red measurements on a silver film (Hodgson 1955), gave $N_0 = 1{\cdot}08$ and $\sigma_0/\boldsymbol{c}$ (optical) $= 0{\cdot}38\ \sigma_0/\boldsymbol{c}$ (electrical). The value of N_0 for the silver film agrees with the value suggested by other experiments and by theory. The value of N_0 deduced from the infra-red measurements on a tin film should therefore be significant for the solid metal.

4.3. *Lead*

Lead of 99·99% purity was melted in a carbon crucible under a pressure of about 3 cm Hg of hydrogen. The optical properties of liquid lead did not change appreciably on repeated solidification and melting. The lead could be heated to 800°C without appreciable evaporation on to the tank windows. The optical constants were measured at two temperatures about 200°C apart. The experimental values for the higher temperature are given by the points in fig. 4. The theoretical curves were fitted to the points for $\log k < 4{\cdot}2$, but all the points lie close to the curves. The agreement between experimental points and theoretical curves is similar at the lower temperature but these have been omitted from fig. 4 for the sake of clarity.

Fig. 4

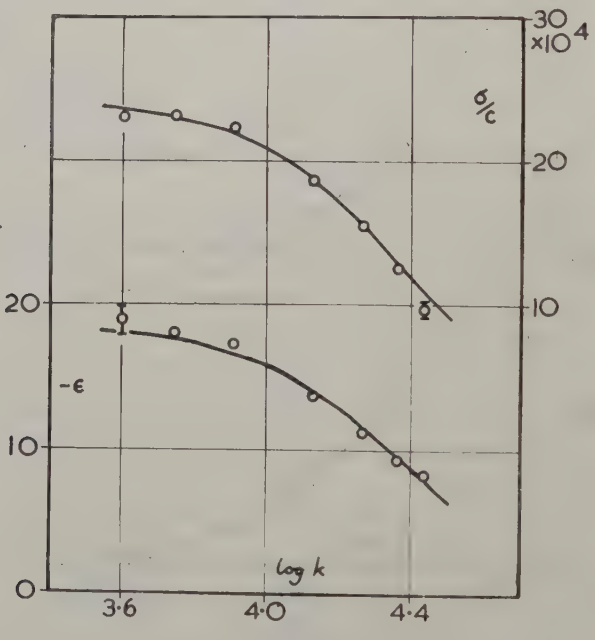

Liquid lead.

ϵ = dielectric constant, σ = conductivity in e.s.u., k = wave number in cm^{-1}. Experimental points for 786°C. Theoretical curves for $N_0 = 4{\cdot}57$, $\sigma_0/c = 24{\cdot}2 \times 10^4$.

The optical constants of an evaporated film of lead have been measured by Motulevich and Schubin. Their results have been analysed to give approximate values of N_0 for solid lead.

§ 5. Conclusions

The values of N_0, τ and σ_0/c (optical) corresponding to the curves in figs. 1 to 4, are set out in the table. The latitude in fitting the curves to the experimental values leads to an uncertainty of about $\pm 1\%$ in the tabulated

values. For all the liquid metals, the effective number of electrons per atom, N_0, is greater than 4·0, the number of valence electrons. In other words, the effective mass is apparently less than the electronic mass. The decrease of N_0 for liquid tin and lead when the temperature increases is just large enough to be significant. N_0 for liquid tin and lead is larger by a factor of between three and four than N_0 for the solid metals. This is in contrast to the small difference between the Knight shifts for solid and liquid tin.

Metal	t	N_0	τ	σ_0/c (optical)	σ_0/c (electrical)
Ge (l)	998	4·30	2·47	40·7	49·5
Sn (l)	446	4·68	3·90	52·4	56·1
Sn (l)	858	4·59	3·52	43·8	47·2
Sn (s)	20	1·33	37·4	153	276
Pb (l)	567	4·68	2·30	26·8	28·4
Pb (l)	786	4·57	2·18	24·2	25·9
Pb (s)	20	1·26	29·9	103	145
	°C		$\times 10^{-16}$ sec	$\times 10^4$	$\times 10^4$

(l) liquid, (s) solid, t temperature, N_0 effective number of electrons per atom, τ relaxation time, σ_0 static conductivity in e.s.u.

The optical values of $\sigma_0/\boldsymbol{c}$ for the liquid metals are all less than the electrically measured values. The difference decreases in the sequence germanium, tin, lead. A similar but larger discrepancy is noted for the evaporated films of tin and lead. These discrepancies may be due to the fact that the surface layer of a metal does not have the same properties as the bulk metal. The surface may cause extra damping of the electronic motions above that found in the bulk metal. The temperature variations of $\sigma_0/\boldsymbol{c}$ (optical) for liquid tin and lead are closely correlated with the changes in $\sigma_0/\boldsymbol{c}$ (electrical). This lends support to the original view of Kent (1919) that in these liquid metals the same valence electrons are responsible for both the optical properties and electrical conduction.

Acknowledgments

I would like to thank Professor D. J. E. Ingram for valuable discussion of this paper and the Mullard Company for the loan of the germanium used in these experiments.

References

Hodgson, J. N., 1955, *Proc. phys. Soc., Lond.* B, **68**, 593 ; 1959, *Phil. Mag.*, **4**, 183 ; 1960, *Ibid.*, **5**, 272.

Kent, C. V., 1919, *Phys. Rev.*, **14**, 459.

Knight, W. D., Berger, A. G., and Heine, V., 1959, *Ann. Phys., New York*, **8**, 173.

Mott, N. F., 1934, *Proc. roy. Soc.* A, **146**, 465.

Motulevich, G. P., and Schubin, A. A., 1957, *Optika i Spektrosk.*, **2**, 633.

The Alpha-particle Component of the Primary Cosmic Radiation over Northern England†

By G. R. Stevenson and C. J. Waddington
H. H. Wills Physical Laboratory, University of Bristol

[Received October 18, 1960]

Abstract

Alpha-particles of the primary cosmic radiation have been studied in a stack of nuclear emulsions exposed over northern England on July 29, 1959. A flux of 167 ± 12 α-particles/m² ster sec was found. The energy spectrum was examined between the cut-off energy of about 250 Mev per nucleon and an energy of 1·5 Bev per nucleon. It was not found to be significantly different from that observed during solar maximum. The energy spectrum was also examined as a function of zenith angle. An apparently significant linear relationship was established between neutron monitor counts recorded at sea level and primary α-particle flux values. A value of $24{\cdot}0 \pm 2{\cdot}4$ cm has been determined for the mean free path of α-particles in nuclear emulsions, which is somewhat higher than previously reported values.

§ 1. Introduction

In the last few years there have been a number of experiments to investigate the behaviour of the α-particle component of the primary cosmic radiation. In particular, much effort has been directed towards studying the variations in the flux and energy spectrum that have occurred during the solar cycle. These measurements have been summarized in a recent review article (Waddington 1960 a). Of special interest is the distribution of the lower energy particles, because of the particular sensitivity of these particles to any alterations in the conditions of the inter-planetary medium they traverse. In order to investigate these slow particles it is necessary to make exposures at latitudes where the geomagnetic cut-off energy is as low as possible. Due to the position of the magnetic pole, this means that, over Europe, exposures should ideally be made at geographic latitudes higher than about 60° N, compared with the 45° N that is adequate over northern America. For this reason a series of flights was made in the summer of 1959 over northern England, with the intention of recovery in Northern Ireland; the results obtained from the emulsions carried on one of these flights are considered in this paper.

These flights were planned to take place at a time when the sun's activity was appreciably diminished from that at solar maximum, 1957–58, since it was hoped that it would be possible to study the process of recovery from the low flux values recorded during those years. An observation of the energy spectrum during such a period of recovery

† Communicated by the Authors.

would be of particular interest. It has been pointed out by McDonald and Webber (1959) that the change in the spectrum from solar minimum to solar maximum was in good agreement with that predicted by the electric de-acceleration theory of Nagashima (1953), in which each particle passes through a constant retarding field; and does not accord with any of the qualitative results of those theories that invoke magnetic modulation in one form or another. While not entirely conclusive, an observation that the higher energy particles recover before those of lower energy would be strong evidence in favour of a magnetic modulation theory, while equal recovery of particles of all energies would favour the electric modulation theory.

Unfortunately, these flights chanced to occur during a temporary, but very active, period of renewed solar activity which produced intense geophysical activity, and the consequent failure to observe any significant difference from the 1957–58 data may have been a temporary consequence, or may mean that no recovery had yet occurred. If the apparent relationship established later in this paper between sea level neutron monitor counts and α-particle fluxes is valid at all times in the solar cycle, then no significant difference could have been expected.

§ 2. Exposure Details

A stack of 100 Ilford G5, 600 μ stripped emulsions, measuring 20×15 cm, was exposed on July 29, 1959. The balloon carrying the stack was launched from Duns, Berwickshire (55° 47′ N, 2° 20′ W) and the equipment fell at Omagh, Co. Tyrone, Northern Ireland (54° 36′ N, 7° 18′ W). The flight curve is shown in fig. 1. While the balloon was at ceiling it drifted almost due west, so that the flight was assumed to be at a constant geomagnetic latitude of 57·7° N. The cut-off rigidity predicted by Quenby and Webber (1959) for this location is 1·65 BV, corresponding to a cut-off energy of 310 Mev per nucleon for α-particles. This is not as low as might be desired, but is as far north in the British Isles as is consistent, under normal meteorological conditions, with making a balloon flight of useful duration and still recovering the equipment.

§ 3. Experimental Procedure

Twelve emulsions near the centre of the stack were each scanned for 10 cm along a line 2 cm below the top edge. The scan-line had to be placed so far below the top edge because of the serious curvature of the emulsions in the top centimetre. Tracks crossing the scan line were recorded if:

(i) They had a projected length of greater than 1 cm.

(ii) They had an ionization greater than about three times the minimum value.

(iii) They had a zenith angle, ϑ, less than or equal to 60°

In recent years, it has been customary to use smaller values of ϑ in similar experiments, in order to reduce the uncertainties of the corrections to the top of the atmosphere and to minimize the geomagnetic effects that occur at large zenith angles. How serious these geomagnetic effects are has not been considered in detail. For this reason, the data obtained in this experiment have been separated into two groups of particles, those with $\vartheta < 30°$, and those with $30° \leqslant \vartheta \leqslant 60°$. These two groups have been examined for any significant differences.

Fig. 1

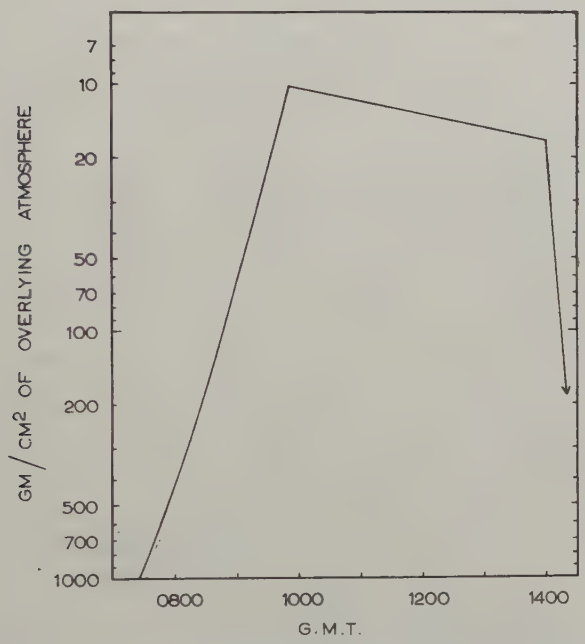

The time-altitude curve of the balloon used to expose the emulsions.

The efficiency of detection of α-particles achieved by the scanners in this experiment was checked by applying the usual tests.

(i) Re-scanning. The scanning of the emulsions was done at two different times, and so the data have been divided into two sets (*a*) and (*b*). There were three scanners, and their efficiencies, as determined from re-scanning, were 98%, 90% and 88%. In set (*a*), each plate was rescanned, and the overall scanning efficiency was 99%. Only one plate was re-scanned in set (*b*), and so the average scanning efficiency was only 94%.

These results indicate that there was a small random scanning loss, but the determination of efficiencies by cross-scanning does not exclude the possible existence of serious systematic losses. Some workers appear

to have assumed recently that the demonstration of a high efficiency in re-scanning is sufficient to prove a high overall detection efficiency. It must be pointed out that such an assumption implicitly assumes that all particles have an equal intrinsic probability of being detected. Experimentally, this assumption is probably not true. It appears reasonable to expect that particles lying near the glass interface, and those with a projected length near the minimum accepted, may be more difficult to detect than those more favourably situated. For this reason additional tests have been applied to the data.

(ii) Depth Distribution. The depth of each track in the emulsion at the scan line was measured, and a depth distribution plotted for sets (*a*) and (*b*) separately. There was evidence for the missing of tracks in the region of the emulsion nearest the glass in set (*a*), and so tracks found in the lower 10% of the emulsion were omitted and the scanning area appropriately reduced for the flux calculations. There was no indication of the missing of tracks at any depth in set (*b*).

(iii) Length Distribution. The projected length of each α-particle track was measured and the distribution plotted for sets (*a*) and (*b*). In set (*b*), it appeared that some tracks whose length was only slightly greater than 1 cm had been lost, and so the minimum accepted length for the flux calculations was set at 1·1 cm. There was no evidence for such a loss in set (*a*).

The tracks found by this scanning were aligned along the axis of a microscope and inspected in order to distinguish between singly and doubly charged particles. In those cases where this inspection did not result in an unambiguous identification, a measurement was made of the multiple scattering and grain density.

Each track identified as having been produced by an α-particle was traced back to the top of the stack to verify that it had not been produced by the break-up of a heavier nucleus. Those which were not incident on the stack were discarded. The remainder were then followed down into the stack until they either interacted or left. All α-particles on which there was more than 2 cm of track length situated more than 1 cm from an outside edge were then examined further. A measurement of multiple scattering was made on each of these tracks employing techniques similar to those used previously, Fowler and Waddington (1956). A basic cell size of 500 μ was used, and two and three times overlap calculated. Noise was eliminated by assuming that it varied as the square root of the cell size. The momentum, and thus the energy of each particle was then calculated using a scattering constant of 30·7 (Freier *et al.* 1959).

§ 4. The Mean Free Path

The α-particles found in this experiment were followed through the stack until they interacted or left. While this tracing was primarily to ensure that each particle was incident on the stack, and that there was sufficient track length available for scattering measurements, it

was also possible to obtain a value for the interaction mean free path, λ. In all, in the 2493 cm of track length which was available for the observation of interactions, 103·5† events were found, of which three were α_{in}–α_{out} interactions. The resulting interaction mean free path was $24{\cdot}0 \pm 2{\cdot}4$ cm. This may be compared with the rather smaller value of $\lambda = 18{\cdot}7 \pm 0{\cdot}6$ cm, which is the weighted mean of those values found previously by Waddington (1956a), Hanni (1956), Appa Rao *et al.* (1956), Shapiro *et al.* (1956) and Lohrmann and Teucher (1959). The reason for this apparent discrepancy is not clear.

This mean value is calculated from the assumption that λ is independent of energy between a few hundred Mev and at least 10 Bev per nucleon, since the median energies of the samples used by these investigators range between $\sim 1{\cdot}5$ and 12 Bev per nucleon.

In order to investigate further this assumed independence with energy, the data obtained in this experiment have been separated, by the scattering measurements, into those particles with $E < 1$ Bev per nucleon, and those with $E \geqslant 1$ Bev per nucleon. For those with $E < 1$ Bev per nucleon, median energy 0·6 Bev per nucleon, 38·5 stars were observed in a length of 659 cm, where this figure includes a correction for the length necessary for the measurement of the energy of each particle.

The resulting value of λ was $17{\cdot}1 \pm 2{\cdot}8$ cm. For those particles with $E \geqslant 1$ Bev per nucleon, median energy 2·65 Bev per nucleon, 50 stars were observed in a corrected length of 1310 cm, giving $\lambda = 26{\cdot}2 \pm 3{\cdot}7$ cm. These values may be compared with those of $22{\cdot}0 \pm 4{\cdot}2$ cm and $19{\cdot}95 \pm 3{\cdot}8$ cm found for samples also separated at 1 Bev per nucleon, with median energies of 0·70 and about 2·0 Bev per nucleon, respectively, by Waddington (1955). Combining these values gives $\lambda = 18{\cdot}6 \pm 2{\cdot}3$ cm for $E < 1$ Bev per nucleon and $\lambda = 23{\cdot}2 \pm 2{\cdot}6$ cm for $E \geqslant 1$ Bev per nucleon, which are not significantly different.

§ 5. Flux

The flux of α-particles crossing the scan line, $J(x, \vartheta)$, for $\vartheta \leqslant 60°$ was found, after correction for the ascent and descent of the balloon, to be $105{\cdot}0 \pm 6{\cdot}6$ α-particles/m^2 ster sec. For $\vartheta < 30°$ it was $109{\cdot}0 \pm 9{\cdot}0$ and for $30° \leqslant \vartheta \leqslant 60°$, $106{\cdot}0 \pm 10{\cdot}6$ α-particles/m^2 ster sec. These values were corrected for absorption in the overlying emulsion, using a mean free path of 20 cm, and for absorption and production in the overlying atmosphere, using an absorption mean free path of 50 g/cm^2. The fluxes at the top of the atmosphere, $J(0, \vartheta)$, were then:

167 ± 10 α-particles/m^2 ster sec for $\vartheta \leqslant 60°$;

160 ± 14 α-particles/m^2 ster sec for $\vartheta < 30°$;

and

183 ± 18 α-particles/m^2 ster sec for $30° \leqslant \vartheta \leqslant 60°$.

† One track could not be traced from one emulsion to the next, and it was assumed that this was probably due to a small, undetected interaction. This was given a weight of one-half.

It is apparent that there is no significant difference between the fluxes for $\vartheta < 30°$ and for $30° \leqslant \vartheta \leqslant 60°$. Hence the value at the top of the atmosphere has been taken as:

$$J_{\alpha^0} = 167 \pm 12 \ \alpha\text{-particles/m}^2\,\text{ster}\,\text{sec}$$

where a possible error of 10% in the absorption mean free path in the atmosphere has also been taken into account. No allowance has been made for any error in the assumed thickness of the emulsions since measurements made on at least four stacks in the last two years have shown that the manufacturers have recently kept the average thickness very close to the nominal value.

Fig. 2

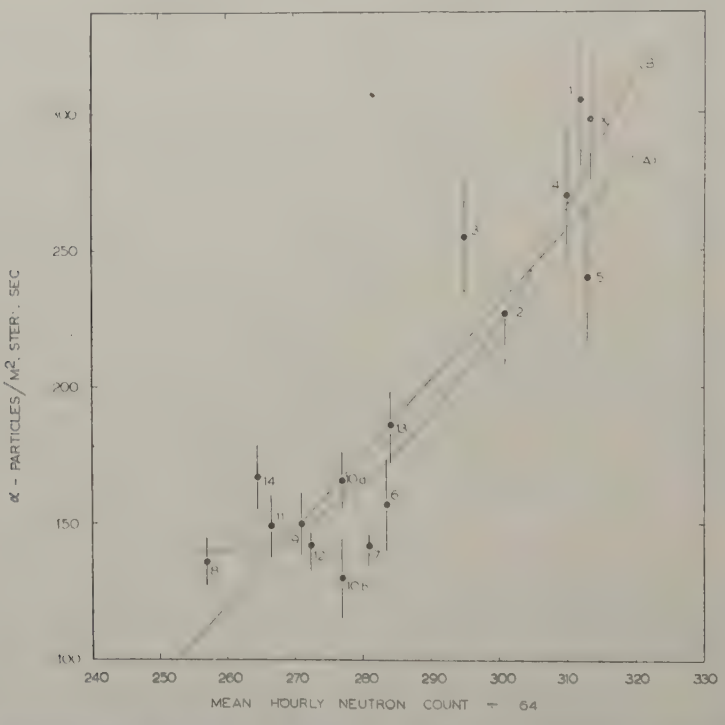

The α-particle flux values as a function of Ottawa neutron monitor counts. Curves (A) and (B) show relations (1) and (2).

It will be seen later, § 6.3, that this flux value is for α-particles having an energy above between 200 and 300 Mev per nucleon. In table 1 this value is compared with other α-particle flux values measured at similar cut-off energies since 1955. Also given in this table are the hourly mean neutron counts recorded by the Ottawa neutron monitor on the day of each experiment. Figure 2 shows these flux values as a function of the neutron counts. A linear relation has been fitted to these data by

Table 1. Alpha-particle flux values measured since 1955 at low cut-off energies.

	J α-particles/m² ster sec	Neutron counts hourly means ÷6·4 Ottawa	Cut-off energy Bev/n	Date	Technique	Reference
1	305 ± 25	3124	280	7.7.55	Cerenkov	McDonald (1957)
2	227 ± 23	3012	280	13.3.56	Cerenkov	McDonald (1957)
3	255 ± 20	2959	150	17.5.56	Emulsions	Fowler *et al.* (1958)
4	270 ± 25	3104	280	17.8.56	Cerenkov	McDonald (1957)
X	298 ± 25†	3134	200	21.8.56	Cerenkov	McDonald (1958)
5	240 ± 26	3133	130	18.9.56	Emulsions	Duke (1960)
6	157 ± 17	2837	225	17.5.57	Emulsions	Freier *et al.* (1958)
7	151 ± 9	2829	200	30.7.57	Emulsions	Engler *et al.* (1959)
8	136 ± 9	2573	200	1.9.57	Emulsions	Freier *et al.* (1959)
9	150 ± 12	2713	225	16.2.58	Cerenkov	McDonald (1959)
10 *a*	171 ± 11	2771	200	14.6.58	Emulsions	Freier (priv. com.)
10 *b*	130 ± 15					Duke (1960)
11	149 ± 12	2665	160	2.7.58	Cerenkov	McDonald (1959)
12	142 ± 10	2728	256	16.5.59	Cerenkov	McDonald and
13	186 ± 14	2838	240	2.6.59	Cerenkov	Webber (1960)
14	167 ± 12	2645	200–300	29.7.59	Emulsions	Present experiment

† This value was not discovered until after relations (1) and (2) had been calculated. It was not thought worth while to repeat these calculations.

assuming that the errors in the hourly neutron counts, N, are negligible compared with those in J_{α^0}. This relation has the form

$$(J_{\alpha^0}-189)\pm 7{\cdot}2=(2{\cdot}73\pm 0{\cdot}41)(N-285). \quad . \ . \ . \quad (1)$$

However, due to the preferential removal of lower energy particles during flux decreases and the greater effectiveness of high energy particles in producing counts in neutron monitors, the sensitivity of N to changes in J_{α^0} should increase as J_{α^0} decreases. Hence it might be expected that the relationship between these two quantities is not linear but at least quadratic. The following quadratic was derived from the data:

$$J_{\alpha^0}-189=-(13{\cdot}4\pm 9{\cdot}9)+(N-285)(2{\cdot}48\pm 0{\cdot}41)$$
$$+(N-285)^2(0{\cdot}043\pm 0{\cdot}0024). \quad . \ . \ . \ . \ . \quad (2)$$

These two relations are shown in fig. 2.

Relation (2) is obviously not vaid for $N\lesssim 255$, since then dJ_{α^0}/dN becomes negative. However, for larger values of N relation (2) appears to be at least as consistent with the data as relation (1), and has an added physical significance.

The neutron counts are predominantly caused by the primary protons of the cosmic radiation, and thus the existence of a simple relation between the α-particle fluxes and neutron counts can be interpreted as meaning that the ratio of the α-particle flux to the proton flux has remained constant over the wide range of observed values. An observation of an α-particle flux associated with a neutron count which significantly diverged from these relations would suggest that, at the time of that particular experiment, this ratio had altered. Due to the rather wide experimental spread of the data the possibility that small variations may have occurred during these experiments cannot be excluded.

The fact that the flux obtained here is somewhat higher, although barely significantly, than those obtained in 1957 and 1958 is supported by the observations made on the ending particles in these emulsions, Waddington (1959, 1960 b). In this stack, exposed according to Quenby and Webber (1959) at a cut-off rigidity of $\sim 1{\cdot}65$ BV, the rate of production of ending particles, ρ, was 486 ± 35 enders/cm^3 h. This value may be compared with the very similar value of

$$\rho=485\pm 21 \text{ enders/cm}^3\text{ h}$$

obtained in 1957–58 from stacks exposed at the lower cut-off rigidity of $\sim 1{\cdot}0$ BV.

The flux of primary protons has also been measured in this stack by examining the interactions produced by singly charged particles, Waddington (1960 c)†. In the emulsions the flux of singly charged particles was determined as 1270 ± 180 particles/m^2 ster sec. When corrected to the top of the atmosphere using the curves given previously the flux was 810 ± 117 protons/m^2 ster sec, correction (d), or

$$860\pm 125 \text{ protons/m}^2\text{ ster sec},$$

† *Footnote added in proof.*—Here a factor of $1{\cdot}74\pm 0{\cdot}04$ has been used to correct for the loss of small stars, instead of the value of $1{\cdot}56\pm 0{\cdot}13$ used previously.

correction (*d*). Accepting this latter value the proton–alpha ratio is $5{\cdot}15 \pm 0{\cdot}77$, which is comparable with the value of $6{\cdot}23 \pm 0{\cdot}63$ found by McDonald (1959) on a flight flown on February 16, 1958.

§ 6. Energy Spectrum

The energy values found by scattering, and corrected for the energy loss in the material between the top of the atmosphere and the point of measurement, are shown in fig. 3, separated into those with $\vartheta < 30°$ and those with $30° \leqslant \vartheta \leqslant 60°$. These energy values have been used to construct integral and differential energy spectra.

Fig. 3

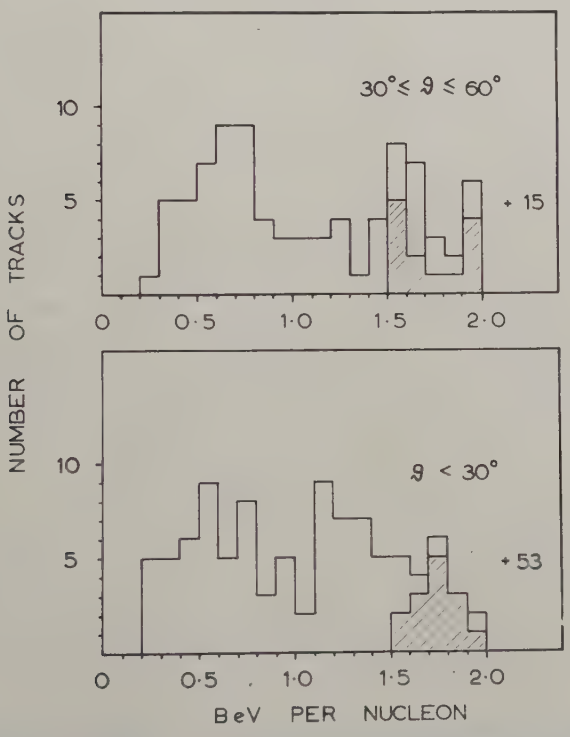

The distribution in energy at the top of the atmosphere, divided into those particles with $\vartheta < 30°$ (*a*) and those with $30° \leqslant \vartheta \leqslant 60°$ (*b*). Values which are lower limits are shown shaded.

6.1. *Integral Energy Spectrum*

Figure 4 shows the integral energy spectrum for all ϑ. The flux of α-particles, having an energy greater than some value T, $J(\geqslant T)$, is plotted as a function of the total energy, $T = m_0c^2 + E$, expressed in Bev per nucleon. Also shown are the integral energy spectra obtained by similar experimental techniques in 1957 (Freier *et al.* 1959) and

in 1950–54 (Fowler and Waddington 1956). The spectrum obtained in this experiment can be seen to lie between these two, which are respectively regarded as being characteristic of solar maximum and solar minimum. It should be noted that the errors shown on each point are not independent, since each point includes all those particles of higher energy. The apparent difference between this spectrum and that obtained in 1957 is only as significant as that between the two fluxes.

Fig. 4

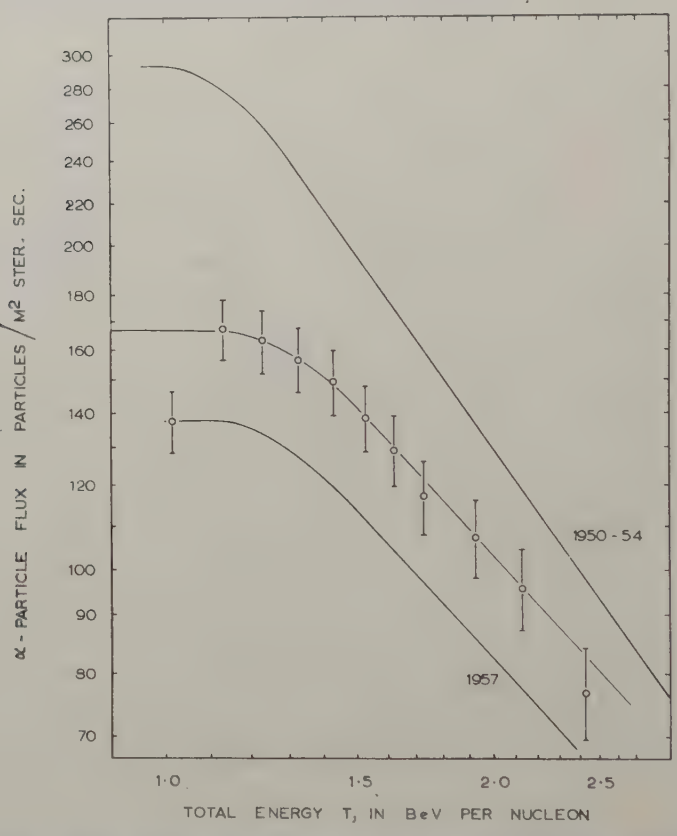

The integral energy spectrum at the top of the atmosphere obtained in this experiment. Also shown are the spectra obtained in 1957 and 1950–54.

Assuming that these spectra may, over a restricted range of energies, be represented by a simple power spectrum of the form $J(\geqslant T)=C\,.\,T^{-\gamma}$, where C and γ are constants, the values of these constants were determined by putting this expression into differential form $dJ=K\,.\,T^{-\beta}dT$, where $\beta=\gamma+1$ and $K=-C\,.\,\gamma$, and considering the values of $J(\geqslant T)$ at $T=1{\cdot}43$ and $2{\cdot}13$ BeV per nucleon. The result, for all ϑ, was $\beta=2{\cdot}12\pm0{\cdot}12$, $\gamma=1{\cdot}12\pm0{\cdot}12$ and $C=222\pm31$. These values may be

compared with those found in 1957 of $\gamma = 1{\cdot}17 \pm 0{\cdot}14$ and $C = 185 \pm 30$; and in 1950–54 of $\gamma = 1{\cdot}48 \pm 0{\cdot}12$ and $C = 360 \pm 40$.

Separating the particles into those with $\vartheta < 30°$ and with $30° \leqslant \vartheta \leqslant 60°$, β, over the same range of energies, is $1{\cdot}94 \pm 0{\cdot}14$ and $2{\cdot}42 \pm 0{\cdot}24$ respectively. The ratio of these is $0{\cdot}80 \pm 0{\cdot}10$. An examination of the detailed energy spectrum shows that this apparent difference is due to additional low energy particles at large zenith angles, or a lack of such particles at small angles. For $\vartheta < 30°$ the fluxes above and below 1 BeV per nucleon are 111 ± 11 and 49 ± 8 α-particles/m^2 ster sec respectively, whereas for $30° \leqslant \vartheta \leqslant 60°$ they are 103 ± 13 and 80 ± 12 α-particles/m^2 ster sec.

Thus, while the total fluxes at the top of the atmosphere of the two zenith angle groups agree to within one standard deviation, the exponents of the energy spectra differ by two standard deviations. The probability of observing such a difference by chance is about 1 in 20, which is not negligible. If this difference is real it could only be due to the change in cut-off energy with azimuth angle, which should result in a higher cut-off energy for particles coming from the east and a lower one for those coming from the west. Assuming that the stack rotated during the flight the net effect would be a function of the difference between these two directions. A consideration of the theory of these geomagnetic effects (Schwartz 1959), suggests that the net effect would be a *decrease* in the number of low energy particles at large zenith angles, which is the opposite to what is actually observed. Therefore it was concluded that not only was there no real difference between particles at different zenith angles but there was no physical justification for expecting a difference observable under the conditions of this experiment.

6.2. *Differential Energy Spectrum*

The differential energy spectrum is shown in fig. 5, where dJ, expressed in α-particles/m^2 ster sec 100 MeV, is plotted as a function of E, the kinetic energy in BeV per nucleon. The individual values are listed in table 2. These values have been compared with values calculated from previously published data obtained in 1957 and 1958 by Freier *et al.* (1958)†, Aizu *et al.* (1959) and the joint Rochester–Oxford–St. Louis group (Engler, private communication).

While the limited statistical weight of these results makes it difficult to draw any firm conclusions from this comparison, it appears that the spectrum obtained in this experiment is not too dissimilar from that observed previously. There is some indication of an increase in the number of particles above 1 BeV per nucleon, which could be evidence in favour of a magnetic modulation mechanism, but it is hardly significant. The divergence at low energies must be due to the operation of a cut-off mechanism.

† But not including that data obtained during the Forbush decrease of August 31, 1957.

Fig. 5

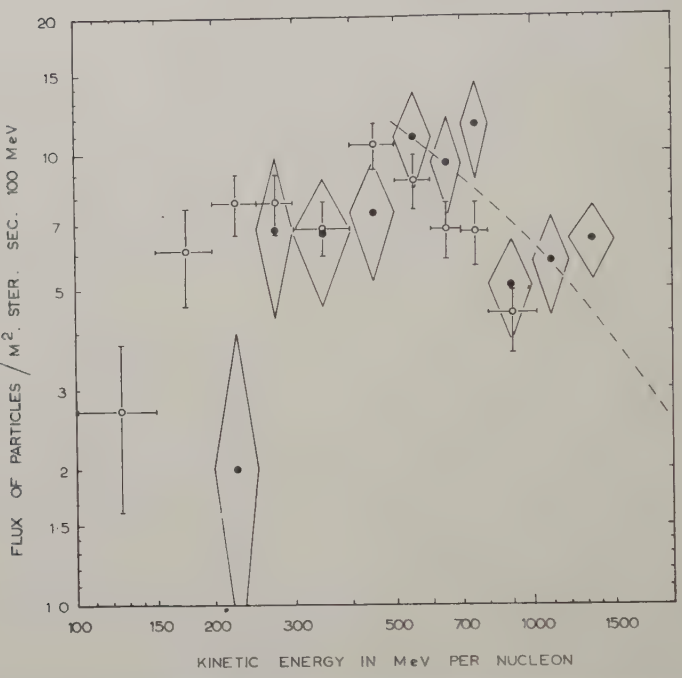

The differential energy spectrum at the top of the atmosphere in this experiment, shown by lozenge-shaped points, compared with the mean values found previously. The differential energy spectrum above 500 MeV per nucleon derived from the integral spectrum is shown as a dotted line.

Table 2. Differential energy flux values

dE 100 MeV per nucleon	dJ_{α° α-particles/m² ster sec 100 MeV			
	All	Present experiment		1957–58 Previous exp
		$\vartheta < 30°$	$30° \leqslant \vartheta° \leqslant 60°$	
1·0–1·5	—	—	—	$2·7 \pm 1·1$
1·5–2·0	—	—	—	$6·1 \pm 1·5$
2·0–2·5	$2·0 \pm 2·0$	$2·0 \pm 2·0$	—	$7·8 \pm 1·2$
2·5–3·0	$6·8 \pm 3·0$	$8·6 \pm 4·4$	$3·6 \pm 3·6$	$7·8 \pm 1·2$
3·0–4·0	$6·7 \pm 2·1$	$5·4 \pm 2·4$	$8·8 \pm 3·9$	$6·8 \pm 0·9$
4·0–5·0	$7·4 \pm 2·2$	$6·5 \pm 2·7$	$8·8 \pm 3·9$	$10·4 \pm 1·2$
5·0–6·0	$10·8 \pm 2·7$	$9·7 \pm 3·2$	$12·3 \pm 4·7$	$8·7 \pm 1·2$
6·0–7·0	$9·5 \pm 2·5$	$5·4 \pm 2·4$	$15·8 \pm 5·3$	$6·8 \pm 1·0$
7·0–8·0	$11·5 \pm 2·8$	$8·6 \pm 3·1$	$15·8 \pm 5·3$	$6·7 \pm 1·1$
8·0–10·0	$5·1 \pm 1·3$	$4·3 \pm 1·5$	$6·1 \pm 2·3$	$4·4 \pm 0·8$
10·0–12·0	$5·7 \pm 1·4$	$5·9 \pm 1·8$	$5·3 \pm 2·2$	—
12·0–15·0	$6·4 \pm 1·2$	$6·8 \pm 1·5$	$5·3 \pm 1·8$	—

6.3. *The Cut-off Energy*

In previous experiments to measure geomagnetic cut-off energies in emulsions (Waddington (1956 b), Fowler and Waddington (1956), Freier *et al.* (1959)), the cut-off energy has been sufficiently great to justify the assumption that the integral energy spectrum rises steadily to the cut-off value. In this experiment γ clearly varies appreciably before the cut-off energy is reached and information on the cut-off can only be obtained from a comparison of the differential spectrum with that obtained previously. Such a procedure is obviously much more sensitive to statistical fluctuations.

Fig. 6

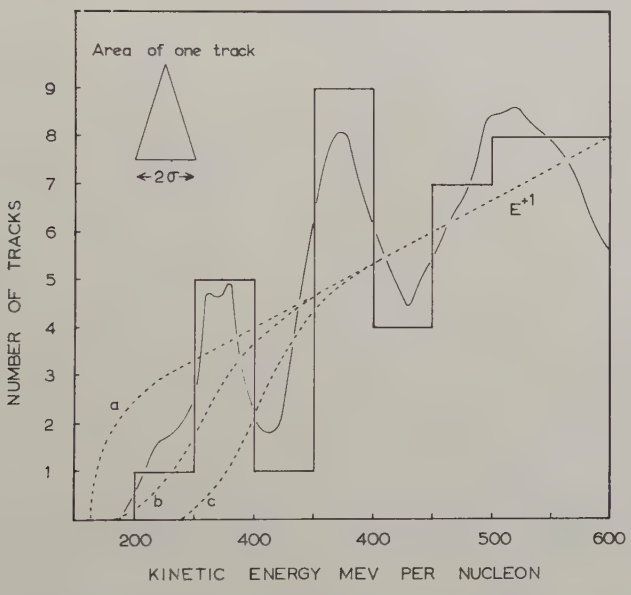

Histogram of energies at the top of the atmosphere lower than 600 MeV per nucleon. See text for explanation of curves.

Figure 6 shows a histogram of those energy values below 600 MeV per nucleon, normalized to a curve obtained by plotting each value as a triangle of constant area and base width of two standard deviations. Also shown is a curve which, while not precisely normalized, represents a differential spectrum in this energy range of the form $E^{+1\cdot0}$. The effects of cut-off energies at 300 and 250 MeV per nucleon are shown by curves *c* and *b* respectively, while that of the cut-off imposed by the overlying atmosphere is shown by curve *a*. It can be seen that while a sharp cut-off at 250 MeV per nucleon is in best agreement with the experimental distribution, it is impossible to unambiguously distinguish between this cut-off and one at 300 MeV or one lower than the air cut-off value. This result is not inconsistent with the value of ~ 310 MeV per nucleon predicted by Quenby and Webber (1959).

Acknowledgments

We are grateful to Professor C. F. Powell for the facilities of his laboratory. Professor D. C. Rose kindly provided the Ottawa neutron monitor data. This experiment was only made possible by the balloon flying team of this laboratory, and the scanning of Mrs. M. W. Dyer, Miss J. Maggs and Miss P. Smedley. One of us, G. R. Stevenson, wishes to acknowledge a maintenance grant from the Department of Scientific and Industrial Research.

References

Aizu, H., Fujimoto, Y., Hasegawa, S., Koshiba, M., Mito, I., Nishimura, J., Yokoi, K., and Schein, M., 1959, *IUPAP Moscow Conf.*, **3,** 100; 1961, *Phys. Rev.*, **121,** 1206.

Appa Rao, M. V. K., Daniel, R., R., Neelakanton, K. A., 1956, *Proc. Indian Acad.*, **43,** 181.

Duke, P. J., 1960, *Phil. Mag.*, **5,** 1151.

Engler, A., Kaplon, M. F., Klarmann, J., Kernan, A., Fichtel, C., and Friedlander, M. W., 1959, *IUPAP Moscow Conf.*, **3,** 153.

Fowler, P. H., Freier, P. S., and Ney, E. P., 1958, *Nuovo Cim.*, Suppl., **8,** 492.

Fowler, P. H., and Waddington, C. J., 1956, *Phil. Mag.*, **1,** 637.

Freier, P. S., Ney, E. P., and Fowler, P. H., 1958, *Nature, Lond.*, **181,** 1319.

Freier, P. S., Ney, E. P., and Waddington, C. J., 1959, *Phys. Rev.*, **114,** 365.

Hanni, F., 1956, *Helv. phys. acta*, **29,** 281.

Lohrmann, E., and Teucher, M. W., 1959, *Phys. Rev.*, **115,** 636.

McDonald, F. B., 1957, *Phys. Rev.*, **107,** 1376; 1958, *Ibid.*, **109,** 1367; 1959, *Ibid.*, **116,** 462.

McDonald, F. B., and Webber, W. R., 1959, *Phys. Rev.*, **115,** 194; 1960, *J. geophys, Res.*, **65,** 767.

Nagashima, R., 1953, *J. Geomag. Geoelec.*, **5,** 141.

Quenby, J. J., and Webber, W. R., 1959, *Phil. Mag.*, **4,** 90.

Schwartz, M., 1959, *Nuovo Cim.*, Suppl., **11,** 27.

Shapiro, M. M., Stiller, B., and O'Dell, R. W., 1956, *Bull. Amer. phys. Soc.*, **1,** 319.

Waddington, C. J., 1955, Ph.D., Thesis, University of Bristol; 1956 a, *Phil. Mag.*, **1,** 105; 1956 b, *Nuovo Cim.*, **3,** 930; 1959, *Ibid.*, **14,** 1205; 1960 a, *Progr. Nucl. Phys.*, **8,** 1; 1960 b, *Nuovo Cim.*, **18,** 820; 1960 c, *Phil. Mag.*, **5,** 1105.

Dislocation Decoration by Precipitation in Gold-Cobalt Alloys†

By R. B. Campbell‡
Franklin Institute Laboratories, Philadelphia, Pennsylvania
and L. Muldawer§
Institut Fourier, University of Grenoble

[Received October 11, 1960]

Abstract

Precipitation from an alloy of gold +5 atomic % cobalt has been observed by electron microscopy using replication and transmission techniques. The precipitate particles form a rectangular grid of lines when observed on {100} faces and mainly parallel lines when observed on {110} faces. The simplest explanation is that dislocations on {110} planes are decorated by cobalt precipitation. These dislocation walls are presumed to have arisen from polygonization during ageing. Geometrical arguments are presented.

In a study of the magnetic nature of cobalt precipitation in a gold matrix, we studied the course of the precipitation process by means of electron microscopy using replication and transmission techniques. Single crystals of the gold + 5% cobalt alloy were solution treated at 950°C, quenched, and then aged at temperatures up to 450°C. Before replication, the specimens were etched, with gold being preferentially removed leaving surface bumps of cobalt rich precipitate. For {100} faced samples, the cobalt particles appear to precipitate along lines which intersect at 90°. These lines, within 20°, were along ⟨110⟩ directions. Figure 1‖ shows this effect in a micrograph obtained by replication using silicon monoxide. In {110} faced specimens, the precipitate particles appear to come out along parallel lines; occasionally there are deviations with lines shifting by 20 to 35 degrees. Figure 2 is a good example of a replica electron micrograph obtained from {110} faced samples.

Using transmission electron microscopy and diffraction on thin foil samples (rolled to a few thousands of an inch, homogenized, quenched, aged, electropolished) of the same composition, we determined the orientation of the rows of precipitate particles with respect to the gold matrix (fig. 3). The foil plane was usually {110}, sometimes {100}. This is in

† This research was supported in part by the United States Air Force through the Air Force Office of Scientific Research (ARDC). Communicated by the Authors.

‡ Now at Crucible Steel Company of America, Pittsburgh, Pennsylvania.

§ On Sabbatical Leave from Temple University, Philadelphia, Pennsylvania.

‖ All figures are shown as plates.

agreement with the rolling texture from face-centred cubic metals. For the {110} foils, the precipitate particles were always along a ⟨111⟩ direction. As well as could be determined for the {100} foils, the rows of precipitate particles were in ⟨110⟩ directions. In some {110} cases the particles formed an almost perpendicular grid of lines, one of which was ⟨111⟩. It should be noted that the situation for foils differs in that they were severely cold-worked before the solution anneal.

The regularities shown in figs. 1, 2 and 3 must be related to some substructure of the alloy and a plausible mechanism would be that precipitation occurs along dislocations. Such dislocation decoration has been noted by Castaing (1949) and by Wilsdorf and Kuhlmann-Wilsdorf (1954) working with aluminium–copper alloys, by Dash (1956) working with silicon + copper, by Mitchell (1957) with working silver halides, and by Amelinckx (1956) working with NaCl.

Inasmuch as there is a real question as to whether the precipitates are decorating dislocations or whether the precipitates are producing dislocations (Elbaum 1959, p. 237) we shall show the reasonableness of the former hypothesis. The production of dislocations may be due to vacancy precipitation, thermal or external mechanical shear strains, or to shear strains resulting from abrupt changes in composition. The density of dislocations in pure, slowly cooled gold foil was found to be $5 \times 10^8/\text{cm}^2$ (Silcox and Hirsch 1959). It is to be expected that the quenched specimens would show higher dislocation concentrations, especially since alloys should show higher vacancy concentrations (Sosin and Rachal 1959). Even if the only dislocations produced are those from vacancy migration to form discs and their subsequent collapse, it is expected that this would occur before cobalt precipitation. In gold–nickel alloys, gold diffuses faster than nickel (Reynolds *et al.*, 1957) and, in a 5 atomic % nickel alloy, this means that vacancy diffusion is faster than that of nickel. Since the Goldschmidt radius of cobalt is about 5% larger than that of nickel, we expect a similar situation in Au + 5% Co. Also, it is rather difficult to conceive of a mechanism whereby precipitation would occur with some geometrical regularity without some guidance.

A lower limit to the number of nucleation centres present, as measured by counting the number of precipitate particles after brief anneals, was about $5 \times 10^8/\text{cm}^2$. Silcox and Hirsch (1959) obtained a value of $10^{10}/\text{cm}^2$ for the dislocation density of quenched gold foil. However, since their pure gold was annealed at temperatures up to only 250°c and our gold alloys were annealed at 450°c before investigation, this difference is not unreasonable. Furthermore, the methods of observation were different, the compositions were different, and our number was obtained for solid single crystals and theirs for polycrystalline foils.

There are several ways in which plane arrays of dislocations can be produced. One would be to have dislocations (produced by deformation) migrate to form simple sub-boundaries; these would tend to be planes perpendicular to the active slip planes (Burgers, 1940). For gold the

slip plane is {111} and planes perpendicular to {111} include {110}, {211}, {321}. Quenching strains have generated dislocations in silicon and germanium and it is expected that an even greater production would be obtained in metals (Elbaum 1959, p. 238). For a second mechanism we look to the collapse of vacancy discs to form dislocation loops on close packed planes. These have been observed in gold by Silcox and Hirsch (1959). Arrays of such loops would be expected to form on the {111} planes (Cottrell 1949) and again sub-boundaries could be formed (Amelinckx and DeKeyser, 1959). However, relatively high temperatures would be required for the needed dislocation mobility and it is unlikely that sufficient time is available during quenching.

Our micrographs of replicas show precipitate lines which, according to the first mechanism given above, are probably traces of planes of dislocations on the plane of observation. The square array of precipitate lines can be produced by having two planes of dislocations of type {100}, {110}, {111}, {211}. We shall assume that dislocations lie only on two planes of a given $\{hkl\}$. The requirement then, when we look at the micrographs for the {110} faced sample, is to obtain parallel traces from a pair of planes producing perpendicular traces on {100} faces. This cannot be done with {211} planes. Our calculations also show that arrays on {110} faces might include lines at 54·1° and 70·5° for {110} and {111} traces and 90° for {100} traces. Small line segments at angles near 55° and 70° were actually observed. Square arrays of precipitate lines on {100} faces have been seen in deformed silver halide (Mitchell 1957) and alkali halides (Amelinckx and Dekeyser 1959) with the traces in ⟨110⟩ directions. Mitchell states that, in his silver halides, slip has occurred on (101) and (011) planes and that dislocations concentrate on these planes. In the case of fig. 1, a possible explanation is that slip has occurred along (111) planes, almost horizontal traces, and that there are polygonized walls along orthogonal $(1\bar{1}0)$ planes (Friedel, 1960). In this case, the traces will also be orthogonal. However, it is not clear why the precipitate decoration in the slip planes and in the polygonized walls should then be so similar.

In the transmission electron micrographs rows of particles in ⟨111⟩ directions were observed for {110} foils; this requires that the plane producing the trace satisfy $h+k+l=0$. This condition is met by planes of the type $(1\bar{1}0)$, $(2\bar{1}\bar{1})$, $(3\bar{2}\bar{1})$ but not by {100} or {111}. The ⟨110⟩ directions for {100} foils give us the condition $h+k=0$; this is met by (001), (110), $(1\bar{1}1)$, $(1\bar{1}2)$ planes. Thus it seems most probable that the dislocation lines are found in {110} or {211} planes. This would mean that the dislocation walls are probably produced as a result of distortion during quenching and subsequent polygonization.

We believe the same geometry is effective in the case of quenched single crystals of the alloys. There is good agreement between figs. 2 and 3; this indicates that the reliability of the replicas is good. However, since the directions obtained in these replicas were good only to 20°, we

cannot be sure that the same mechanism is effective. The angular separation between traces of (110) and (111) planes on {110} planes is only 18°. It may well be that both mechanisms (polygonization and collapse of vacancy discs) are operative and are responsible for the complexities of some precipitate patterns. We have used {110} above rather than {211}; only when selected {211} planes are used do we obtain the results as given above.

It may be of interest here to state some results obtained through magnetic measurements. Torque and rotational hysteresis data indicate that the particles were crystallographically aligned, that the initial precipitate was face-centred cubic cobalt coherent with the gold matrix, and that with increasing time of ageing the f.c.c. cobalt transformed to the hexagonal variety and the particles become elongated along the *c* axis.

Our conclusions are that precipitates are present where we would expect to find dislocation walls, that the precipitate particles probably nucleated on dislocations, and that the dislocation walls are probably the result of polygonization. Furthermore, we believe that most of the dislocations originated as a result of quenching strains and that the polygonization occurred early during the ageing process.

Acknowledgments

One of us, R. B. Campbell, wishes to thank the Office of Scientific Research for partial support; the other, L. Muldawer, wishes to thank Temple University for Sabbatical Leave. Thanks are also due to Drs. J. Friedel and H. Wilsdorf for helpful suggestions. A portion of this paper was used by R. B. Campbell in his Ph.D. Dissertation, Temple University, 1959.

References

Amelinckx, S., 1956, *Phil. Mag.*, **1**, 269.
Amelinckx, S., and Dekeyser, W., 1959, *Solid State Physics*, Vol. 8, p. 327 (New York : Academic Press).
Burgers, J. M., 1940, *Proc. phys. Soc. Lond.*, **52**, 23.
Castaing, R., 1949, *C.R. Acad. Sci., Paris*, **228**, 1341.
Cottrell, A. H., 1949, *Progr. Met. Phys.*, Vol. 1, p. 77 (New York : Pergamon Press).
Dash, W. C., 1956, *J. appl. Phys.*, **27**, 1193.
Elbaum, C. 1959 *Progr. Met. Phys.*, Vol. 8, p. 203 (NewYork : Pergamon Press).
Mitchell, J. W., 1957, *Dislocations and Mechanical Properties of Crystals* (New York : Wiley), p. 69.
Reynolds, J. E., Averbach, B. L., and Cohen, M., 1957, *Acta Met.*, **5**, 29.
Silcox, J., and Hirsch, P. B., 1959, *Phil. Mag.*, **4**, 72.
Sosin, A., and Rachal, L., 1959, *Bull. Amer. phys. Soc.*, **4**, 458.
Wilsdorf, H., and Kuhlmann-Wilsdorf, D., 1954, *Phil. Mag.*, **45**, 1096.

Precipitation and Irradiation Hardening in Iron†

By D. Hull‡ and I. L. Mogford
Atomic Energy Research Establishment, Harwell, Berks

[Received September 21, 1960]

Abstract

Precipitation of carbon from α-iron during irradiation and thermal ageing has been studied using thin film electron transmission microscopy. During irradiation at 100°c precipitates formed with a density of 2×10^{14} cm^{-3} and saturated at 400 Å diameter after 72 hours in a flux of

$1{\cdot}5 \times 10^{11}$ neutron cm^{-2} sec^{-1} > 1 Mev.

The precipitates were in the form of plates parallel to {100} and occurred individually in the matrix and in rows on dislocation lines. Thermal ageing at 100°c produced clusters of plates with a density of 3×10^{13} cm^{-3} and rows of plates on dislocation lines. At higher ageing temperatures the plate-like precipitates were replaced by larger dendritic particles at 200°c and needle-shape particles at 250°c with a density of 3×10^{12} cm^{-3}. The defects produced during irradiation, which are responsible for irradiation hardening, were not detected. Tensile experiments showed that the hardening was most pronounced when precipitation did not occur.

§ 1. Introduction

A great deal of empirical information has been gathered concerning the hardening effects produced by neutron irradiation of various structural steels and this work has been reviewed recently by Harries (1960). However, relatively little is known about the actual mechanism of hardening, which results in an increase in yield stress and a rise in the temperature of the transition from brittle to ductile fracture. It has been shown from tensile hardening experiments (Churchman *et al.* 1957, Hull and Mogford 1958) that in a low carbon steel the hardening can be accounted for by an increase in the resistance to dislocation movement rather than by an increase in the stress to unpin a dislocation from its atmosphere, and it is suggested that this is due to the interaction of the moving dislocation with radiation induced defects, e.g. clusters of point defects. Irradiation hardening is also produced in pure iron (Kunz and Holden 1954, Konobeevsky *et al.* 1955). In the work of Kunz and Holden it was found that the hardening annealed out with an activation energy of 3·1 ev suggesting a process involving self-diffusion.

† Communicated by the Authors.
‡ Present address : Department of Metallurgy, University of Liverpool.

The development of thin film transmission electron microscopy has enabled direct observation of collapsed vacancy aggregates as dislocation rings such as those found in face-centred cubic metals quenched from just below their melting point (Hirsch *et al.* 1958). Closed dislocation loops ~300 Å diameter have been observed in irradiated copper (Silcox and Hirsch 1959, Makin *et al.* 1961, Barnes and Mazey 1960). However, it is difficult to correlate the observed irradiation hardening with the formation of dislocation loops.

The present paper describes work originally undertaken to examine the nature of the irradiation defects which resist the movement of dislocations in ferrous materials. After irradiating iron for only a few hours, observation of thin films in the electron microscope revealed a large number of defects 100 Å to 300 Å diameter many of which gave a contrast similar to that produced by dislocation rings. However, further experiments indicated that these defects were a product of irradiation and thermal ageing at the pile temperature, and it is believed that they are produced by precipitation of interstitial atoms, e.g. carbon, from solid solution. This has led to a comparison of precipitation of carbon in iron with and without the influence of neutron irradiation. The effect of precipitation and irradiation on the tensile properties of the iron has also been determined.

§ 2. Experimental Details

The iron used in this work was supplied by the National Physical Laboratory. The analysis is given in table 1.

Table 1. Analysis of material used (all values wt. %)

C	Si sol.	Si insol.	S	P	Mn	Al sol.	Al insol.
0·004	0·007	< 0·001	0·0056	< 0·001	< 0·005	0·003	0·001
Cr	**Ni**	**Cu**	**Mo**	**N**	**O**		
< 0·001	< 0·001	0·001	0·003	0·001	0·0005		

The $\frac{1}{2}$ in. diameter hot rolled bar was cold swaged to 0·040 in. diameter rod with intermediate anneals for 1 hour at 900°C *in vacuo* followed by slow cooling, after every 35% reduction in area. Foil for transmission electron microscopy was prepared from the rod by cold rolling to 0·001 in. This was then thinned electrolytically using a solution of chromic acid in glacial acetic acid and the final foils examined in the Siemens Elmiskop Ib electron microscope at 100 kv. It was not possible to determine the final thickness of the foil but in calculating the number of precipitates and concentration of defects a foil thickness of 3000 Å was assumed (McLean 1960). The electrolytic thinning was carried out after the thermal and irradiation treatments.

Tensile tests were made on the 0·040 in. diameter rod in a hard beam autographically recording tensile machine (Adams 1959) with a strain rate of $5{\cdot}7 \times 10^{-4}$ sec^{-1}.

The final heat treatment given to the foils and tensile specimens before ageing or irradiation was either (i) furnace cool from 900°C or (ii) air cool in the evacuated silica tube from 900°C. In the following sections these will be referred to as 'slow cool' and 'fast cool' respectively.

The specimens were irradiated with neutrons in BEPO graphite moderated reactor in a flux of 1 to 2×10^{11} neutron cm^{-2} sec^{-1} > 1 MeV to doses between $2{\cdot}7 \times 10^{15}$ and $7{\cdot}8 \times 10^{16}$ neutron cm^{-2} > 1 MeV. The temperature of irradiation was between 60°C and 100°C. Thermal ageing treatments to simulate the irradiation conditions were carried out *in vacuo*.

§ 3. Experimental Results

3.1. *Precipitation During Irradiation*

Foils examined in the electron microscope before irradiation contained a low density ($< 10^8$ cm $^{-2}$) of dislocations which appeared quite free from precipitation. In the fast-cooled material small black spots were observed in the matrix in addition to the dislocations. The density of the spots was $8{\cdot}5 \times 10^{12}$ cm^{-3} and they were about 100 Å diameter. Some of the defects had contrast similar to dislocation loops.

Table 2. Effect of irradiation on diameter and number of defects

Time of irradiation hours	Dose, neutron cm^{-2} > 1 MeV	Diameter of precipitates Å	Number of precipitates cm^{-3}
5	$2{\cdot}7 \times 10^{15}$	100	$1{\cdot}7 \times 10^{14}$
12	$6{\cdot}5 \times 10^{15}$	130	$2{\cdot}7 \times 10^{14}$
24	$1{\cdot}3 \times 10^{16}$	170	$2{\cdot}0 \times 10^{14}$
72	$3{\cdot}9 \times 10^{16}$	380	$1{\cdot}8 \times 10^{14}$
144	$7{\cdot}8 \times 10^{16}$	380	$2{\cdot}3 \times 10^{14}$

When foils were annealed at 900°C for ½ hour followed by a fast cool and then irradiated, precipitation could be induced after very low doses. The first definite signs of precipitation, in the form of small black spots ~ 100 Å diameter, were formed after 5 hours, with a density of nearly 2×10^{14} cm^{-3}. The damage produced after 12 hours is shown in fig. 1†. After 24 hours the spots could be resolved into irregular loops. The diameter of the loops increased with the irradiation time up to 72 hours but the density of loops was approximately independent of time (table 2).

† Figures 1–9 are shown as plates.

In fig. 2 dark streaks ~ 350 Å long can be seen in addition to loops and it is assumed that these are produced when the plane of the loop is normal to the plane of the foil, i.e. the loops appear edge-on. The appearance of the loops depends on the orientation of the foil and the results can be summarized as follows :

(*a*) In {100} foils two sets of streaks at right angles parallel to ⟨100⟩, no loops (fig. 3).

(*b*) In {110} foils one set of streaks parallel to ⟨110⟩ and loops : the ratio of streaks to loops is approximately unity (fig. 2).

(*c*) In {111} foils only loops are observed.

In addition to apparently homogeneous precipitation throughout the material precipitation occurred on dislocations. After 5 hours' irradiation some dislocations were surrounded by an indistinct envelope ~ 100 Å across and after 12 hours definite precipitation could be seen (fig. 1). The appearance of the precipitate varied with the orientation of the foil and in some foils after 72 hours irradiation there was definite formation of a row of loops along the dislocation which appeared similar to the loops formed independent of the dislocation, fig. 4 at A–B. Figure 4 shows a network of dislocations at C–D in which some segments have complicated precipitates whilst others are completely free suggesting that there is preferential precipitation on dislocations with certain Burgers vectors. There is a zone around the network, about 5×10^{-5} cm wide, free from loops and the precipitation on dislocation A–B is clearly more pronounced away from the network.

When foils were annealed at 900°C for $\frac{1}{2}$ hour followed by a slow cool and then irradiated no precipitation effects could be detected after six days. The dislocations were free from precipitation prior to irradiation.

3.2. *Precipitation During Thermal Ageing*

All the experiments were made on foils fast cooled from 900°C. The first ageing experiments were conducted at 60°C which was believed to be the most likely pile irradiation temperature. After three days the foil contained precipitates having an average diameter of about 400 Å with a density of 2×10^{13} cm^{-3}. A foil given such a treatment was cut in half and one half aged for a further three days at 60°C. The precipitates were less regular and had increased in diameter, however the density of precipitates was approximately the same (table 3).

The other half of the foil was irradiated for three days and fig. 5 shows that there were two forms of precipitates ; large precipitates, somewhat larger than those in the foil aged at 60°C for six days, but with the same morphology, and fine precipitates (table 3). The growth of the large precipitates to 625 Å diameter during irradiation compared with 500 Å for the six-day aged specimen suggests that the pile temperature is higher than 60°C and subsequent ageing treatments were carried out at 100°C.

In material aged at 100°C for successively longer times the formation of defects was somewhat similar to ageing at 60°C. After 1 hour small loops about 350 Å diameter were formed and after three days the precipitates had a complex morphology (fig. 6). Table 4 gives details of ageing at 100°C. Dislocations were decorated with precipitates and

Table 3. Ageing and irradiation at 60°C

Treatment	Diameter of precipitates Å	Number of precipitates cm^{-3}
Aged 72 hrs at 60°C	400	2×10^{13}
Aged 144 hrs at 60°C	500	3×10^{13}
Aged 72 hrs at 60°C followed by 72 hrs irradiation	625 150	$4{\cdot}5 \times 10^{13}$ 3×10^{14}

Table 4. Ageing at 100°C

Time, hours	Diameter of precipitates, Å	Number of precipitates, cm^{-3}
1	350	2×10^{13}
72	800	3×10^{13}
120	925	3×10^{13}

again their appearance depended on orientation. When the foil was close to {111} the precipitates in the matrix often appeared as a cluster of plates with six-fold symmetry (fig. 6). In {100} foils the precipitates, either as individual particles or on dislocations, appeared as streaks in two directions at right angles (fig. 7) along ⟨100⟩ in the foil.

3.3. *Annealing of Foils Containing Precipitates*

Foils which contained precipitates formed by ageing for three days at 100°C or by three days' irradiation were further heated for 1 hour periods at 140°C, 175°C, 200°C and 250°C respectively before thinning. In the irradiated foils no change occurred after 1 hour at 140°C, but after 1 hour at 175°C the precipitates had become larger and more complicated and the concentration reduced significantly. At 200°C dendritic particles were formed and at 250°C the precipitates assumed the form of Widmanstatten-like needles. These changes are illustrated in figs. 8 (*a–c*) and the changes in shape and concentration are listed in table 5. In the aged foils no change was observed below 200°C at which temperature the precipitates appeared more dense and became elongated, and at 250°C the structure was identical to the irradiated foil. In foils parallel to {110}

the precipitate needles formed at 250°c were at 60° to each other and were along ⟨111⟩.

Table 5. Effect of heating foils containing precipitates

Treatment	Diameter of precipitates Å	Number of precipitates cm^{-3}	Shape
Three-day irradiation	350	3×10^{14}	Discs
+1 hour 140°c	350	3×10^{14}	Discs
+1 hour 175°c	550	9×10^{13}	Complicated aggregates
+1 hour 200°c		5×10^{12}	Dense dendrites about 1500 Å long and 650 Å across
+1 hour 250°c		1×10^{12}	Needles or rods about 5000 Å long and 350 Å across
Three-day thermal ageing at 100°c	800	3×10^{13}	Complicated aggregates
+1 hour 175°c	850	2×10^{13}	Complicated aggregates
+1 hour 200°c		2×10^{13}	Dense dendrites about 1600 Å long and 600 Å across
+1 hour 250°c		3×10^{12}	Needles or rods about 5000 Å long and 200 Å across

A number of foils were irradiated and thinned and then heated on the hot stage in the electron microscope. Figure 9 (*a*) is a typical field prior to heating which contains loops with and without a black spot in the centre, clusters of loops and decorated dislocations. Heating for a few minutes between 150°c and 180°c produced no change in the structure but at 180°c the single loops were observed to shrink very rapidly (e.g. loops at A, fig. 9) and disappear within 1 or 2 minutes. The decoration on the dislocation lines also disappeared in a similar way. The more complicated loops at B in fig. 9 shrank slowly, leaving behind a black spot (often associated with a small piece of dislocation line) which was still visible after heating to 235°c. No massive precipitation was observed at this temperature similar to that formed in the specimen heated outside the microscope before thinning.

3.4. *Tensile Experiments*

A limited number of tensile tests were made to determine whether any relation exists between the irradiation hardening and the formation of irradiation induced precipitation. The increase of yield stress $\Delta\sigma_y$ for tests at -78°c are recorded as a function of irradiation or thermal ageing time in fig. 10. For specimens annealed at 900°c and slow cooled

$\Delta\sigma_y$ increased continuously with the irradiation time but for specimens annealed at 900°C and fast cooled, there was little change in $\Delta\sigma_y$ between 5 and 24 hours' irradiation. In specimens aged at 100°C after a fast cool from 900°C no appreciable increase in yield stress was detected after 72 hours.

Fig. 10

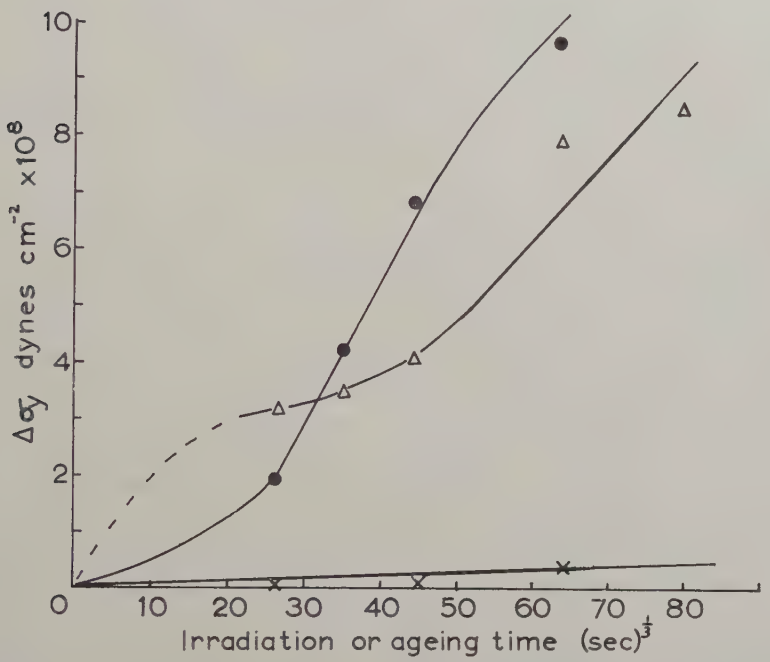

Increase in yield stress, $\Delta\sigma_y$, as a function of irradiation or ageing time.
△ Specimens fast cooled from 900°C and irradiated, curve (i);
● specimens slow cooled from 900°C and irradiated, curve (ii);
× specimens fast cooled from 900°C and aged at 100°C, curve (iii).

§ 4. Discussion

4.1. *Precipitation During Irradiation*

Irradiation of iron for 72 hours after a fast cool from 900°C, produced a high density of loops, 2×10^{14} cm^{-3}, about 400 Å diameter. The loops gave a contrast effect similar to loops of dislocation line produced in aluminium and copper after quenching from just below the melting point and in copper after neutron irradiation, i.e. they consisted of a dark ring with little or no contrast in the centre and the contrast could be altered by rotating the specimen in the stereo holder of the microscope. In copper and aluminium the dislocation loops are formed by the collapse of platelets of vacancies and the present observations were explained initially in a similar way; thus, if it is assumed that each primary

knock-on in iron produces 100 Frenkel pairs, an irradiation of 4×10^{16} fast neutrons cm^{-2} would produce a concentration of approximately 10^{-5} point defects. The concentration of defects that would be required to produce the observed number of loops after such an irradiation is approximately 5×10^{-5}. However, there are a number of observations that indicate that the loops in iron are not collapsed vacancy aggregates. Firstly, the number of loops saturates after only 5 hours' irradiation and the diameter of loops saturates after 72 hours, whereas, no saturation would be expected if the loops were formed by point defects created continuously during irradiation. Secondly, loops were not observed in slow cooled material after irradiation. Thirdly, somewhat similar loops were observed in foils aged at the pile temperature in the absence of irradiation.

We propose, therefore, that the loops are produced by precipitation of interstitial carbon atoms in a thin layer probably one atom thick. The appearance of the loops in foils of different orientation is consistent with them lying parallel to {100} planes† in the iron lattice; hence in {110} foils one set of loops is seen edge-on parallel to ⟨110⟩ and in {100} foils two sets of edge-on loops occur at right angles, parallel to ⟨100⟩, in {111} foils no loops appear edge-on. In fig. 2 three streaks appear parallel to ⟨100⟩, e.g. at A, and they are probably produced by loops lying on {100} planes inclined at 45° to the plane of the foil which have intersected the foil surface, so that only a small portion of the precipitate lies within the foil The most favourable interstitial site in the body-centred cubic cell is 0, 0, $\frac{1}{2}$ and if all such sites in a (100) plane are occupied by carbon atoms the iron atoms parallel to this plane will be displaced about 1 Å normal to the plane. The arrangement of atoms around such a layer will be somewhat similar to a closed loop of edge dislocation in the (100) plane.

Since the solubility of carbon in iron at 100°C is very small, $\sim 10^{-7}$ wt. %, practically all the carbon will precipitate from solid solution. After 72 hours' irradiation, precipitation appears to be complete and assuming that the precipitates are monatomic layers of carbon, the density and size of the loops are equivalent to approximately 0·001 wt. % carbon. This is close to the solubility of carbon expected in this material fast cooled from 900°C. Thus it is considered that precipitation under irradiation conditions consists of the growth of a monatomic plate of carbon atoms.

In the presence of grain boundaries and individual dislocations, the distribution of the loops was considerably modified. The free zone around dislocations, low angle boundaries and grain boundaries presumably results from the preferential diffusion of carbon to these sites. In many cases the precipitation on the dislocations can be resolved into definite

† This is a correction to a preliminary report of this work (Hull and Mogford 1960) which stated that the loops were parallel to {110} in the iron lattice.

particles which have the same contrast appearance as the individual precipitates, e.g. dislocation A–B in fig. 4, and it is possible that these precipitates also consist of monatomic layers of carbon. The decoration on dislocations is similar to the effects produced during thermal ageing which will be discussed below.

4.2. *Precipitation During Ageing at* 100°C

When specimens were aged at the same temperature at which they were irradiated, precipitation occurred on dislocations and throughout the lattice. At the dislocations the first sign of precipitation was a dark zone previously observed by Hale and McLean (1960, private communication) and after 24 hours this could be resolved into individual particles. In foils with {001} orientation the particles appeared as short streaks on two sets of planes at right angles to each other along ⟨100⟩ directions indicating that they consisted of small plates parallel to {100} planes. The precipitates formed away from dislocations were more complicated than in the irradiated specimens and had a much lower density, 3×10^{13} particles cm^{-3}. They appeared to consist of a cluster of plates and again in {100} foils aggregates with plates at right angles could be seen. It is possible that the clusters of plates formed by successive growth of individual plates and this explains the formation of clusters containing 2, 3, 4, 5 and 6 plates in fig. 6.

The similarity in the appearance of the particles formed on irradiation, the particles on dislocation lines in both aged and irradiated foils and the individual particles in the clusters formed in aged foils suggests that the plate form is common to all. In addition the size of the unit plate is practically constant, i.e. about 400–500 Å diameter in all cases. If it is assumed that the platelets are monatomic layers of carbon atoms, comparison of the aged and irradiated foils, when all the carbon is precipitated, i.e. 72 hours, requires that the average number of plates in the clusters in the aged foils should be the ratio of the number of precipitates in the irradiated and aged foils respectively,

$$\text{i.e. } \frac{2 \times 10^{14}}{3 \times 10^{13}} \simeq 7$$

which agrees with the observations.

4.3. *Nature of the Nuclei*

One of the most important differences between ageing and irradiation is the difference in the number of particles. This is most clearly illustrated by fig. 5 which shows that a concentration of 3×10^{13} particles cm^{-3} is formed on ageing at 60°C and that irradiation produces quite independently a concentration of 2×10^{14} particles cm^{-3}. The concentration of precipitates produced during irradiation was constant after about 5 hours. The most probable source of nuclei is displacement spikes. The arrangement of point defects in this spike can be represented as a small region with

a large number of vacancies ~ 10–100 surrounded by a much wider region containing interstitials. This central region may provide a ready sink for carbon atoms. The number of displacement spikes, calculated as the product of the total neutron flux, density of atoms in the metal, and the neutron cross-sectional area for elastic scattering, produced in 5 hours is about 2×10^{14} which agrees closely with the observed number of particles. Presumably further nuclei produced are unstable with respect to the previously formed nuclei and carbon precipitation continues on the existing precipitates. There is good evidence that small precipitates can redissolve during irradiation from the width of the free zone around dislocations and sub-boundaries. After 12 hours the zone is about 10^{-5} cm wide and after 72 hours it is about 5×10^{-5} cm.

The width of the free zone is close to that expected from the diffusion rate of carbon in iron. The diffusion distance $x = (Dt)^{1/2}$ can be calculated from t the diffusion time in seconds, and D which is given by :

$$D = D_0 \exp(-\Delta H/RT).$$

Using the values $\Delta H = 20\,400$ cal/g mol and $D_0 = 3{\cdot}16 \times 10^{-2}$ cm^2 sec^{-1} obtained by Thomas and Leak (1954) at 100°c, $D = 4 \times 10^{-14}$ cm^2 sec^{-1}. Thus after 12 hours $x = 4100$ Å and after 72 hours $x = 10\,000$ Å. However, diffusion may not be the rate controlling factor in the deposition of carbon atoms on platelets. When the concentration of precipitates is 2×10^{14} cm^{-3}, i.e. after irradiation, the average distance apart is about 1700 Å so that the growing plate will require a diffusion distance of 850 Å for complete precipitation. Precipitation is only complete after 72 hours, $x = 10\,000$ Å.

The nature of the nuclei in the aged foils is less certain. There appears to be a low density of defects after cooling and after 1 hour at 100°c there are 2×10^{13} cm^{-3} loops about 300 Å diameter. It is possible that the nuclei are quenched in from the higher temperatures either as aggregates of carbon atoms or clusters of vacancies. As in the irradiated specimens the distance between particles, i.e. 3200 Å, is much smaller than the diffusion distance estimated from the diffusion coefficient and activation energy, although the exact time when precipitation was complete in aged specimens was not determined.

4.4. *Effect of Heating Foils and Ageing at Higher Temperatures*

Although the experiments in which specimens were aged at higher temperatures are far from complete the results in table 5 clearly show that a marked change in the character of the precipitation occurs between 175°c and 250°c. In the irradiated specimens the loop defects, density 3×10^{14} cm^{-3}, were replaced at 175°c by complicated precipitates, and with dense dendritic precipitates after ageing for 1 hour at 200°c. After an hour at 250°c the precipitates had grown into rods 5000 Å long and 350 Å diameter lying along ⟨111⟩ directions. It is not possible to establish whether the rod-shaped precipitates, which are probably Fe_3C (Leslie

et al. 1959), form as a completely new precipitate or by a rearrangement of atoms of the existing precipitates, although the concentration is reduced by about 10^2. No appreciable change is observed in the aged foils held at 175°C for 1 hour but at 200°C and 250°C the morphology and density of the precipitates are identical to those in the irradiated foils. We can therefore recognize two or three stages in precipitation, (1) ageing at 100°C results in the formation of platelets, individually or in clusters, depending on the number of nuclei available, throughout the lattice and in rows along dislocation lines, (2) between 175°C–200°C these dissolve and complex dendritic precipitates are formed, and (3) at 250°C a Widmanstatten array of rods is formed.

4.5. *Irradiation Hardening*

The present experiments have provided little information on the nature of the defects producing an increase in σ_y on irradiation. It is immediately clear from fig. 10 that precipitation is not producing an appreciable increase in hardness during irradiation ; for specimens in curve (i) precipitation is expected, but there is no increase in σ_y between 5 and 24 hours' irradiation, whereas in curve (ii) for specimens in which no precipitation could be detected after 14 days, σ_y increases continuously with irradiation time. This implies for curve (i) that either the irradiation hardening is cancelled out by softening induced by ageing, or that the irradiation induced point defects, which produced hardening in curve (ii), are not effective in the presence of precipitate particles. Curve (iii) suggests that no softening occurs when specimens are aged, so it is possible that the point defects become associated with the carbon platelets and do not produce hardening.

Since nothing can be seen in slow cooled foils after an irradiation of 14 days, even though there is an appreciable increase in σ_y, it follows that the irradiation induced defects are extremely small. Further work is necessary to determine whether it is possible with higher doses to observe irradiation induced defects in material free from carbon or nitrogen. It is also important to make a detailed correlation, in the early stages of precipitation, between the tensile properties and the appearance of precipitation on dislocation.

§ 5. Conclusions

1. The defects produced during neutron irradiation of iron at 100°C, which increase the resistance to the movement of dislocations and hence increase to yield stress, have not been detected in the electron microscope for the irradiation doses used.

2. Irradiation creates nuclei for the precipitation of carbon from solid solution and they are probably produced at the disorder caused by displacement spikes. It is possible that irradiation will provide nuclei for precipitation in other supersaturated systems and hence affect the rate of transformation.

3. At 100°C carbon precipitates in the form of platelets which grow in size to about 400 Å. When a large number of nuclei are present, as in the irradiated material, the platelets form individually and when there are fewer nuclei the platelets form in clusters. Dislocations provide nucleation sites and the platelets form in rows along the dislocations.

4. In the electron microscope the platelets, which lie along {001} planes in the iron lattice, produce a contrast similar to closed dislocation loops, and it is suggested that their structure consists of a monatomic layer of carbon in the 0, 0, $\frac{1}{2}$ interstitial sites. The amount of carbon, estimated from the size and density of the plates when precipitation is complete, agrees with the amount expected in solid solution before precipitation.

5. Whilst it has been assumed in the discussion that only interstitial carbon atoms are precipitating, the experiments do not differentiate between carbon and nitrogen.

Acknowledgments

The authors are grateful to Professor W. S. Owen, Mr. R. S. Barnes and Dr. J. Burke for useful discussions, and Dr. M. J. Whelan for assistance with the heating stage experiments.

References

Adams, M. A., 1959, *J. sci. Instrum.*, **36**, 444.
Barnes, R. S., and Mazey, D. J., 1960, *Phil. Mag.*, **5**, 1247.
Churchman, A. T., Mogford, I. L., and Cottrell, A. H., 1957, *Phil. Mag.*, **2**, 1271.
Harries, D. R., 1960, *J. Iron St. Inst.*, **194**, 289.
Hirsch, P. B., Silcox, J., Smallman, R. E., and Westmacott, K. H., 1958, *Phil. Mag.*, **3**, 897.
Hull, D., and Mogford, I. L., 1958, *Phil. Mag.*, **3**, 1213 ; 1960, *Bull. Inst. Metals*, **5**, 49.
Konobeevsky, S. T., Pravdynk, N. F., and Kutaitsev, V. I., 1955, Geneva Conf. on Peaceful Uses of Atomic Energy, Paper 680.
Kunz, F. W., and Holden, A. N., 1954, *Acta Met.*, **2**, 817.
Leslie, W. C., Fisher, R. M., and Sen, N., 1959, *Acta Met.*, **7**, 632.
McLean, D., 1960, *Bull. Inst. Metals*, **5**, 49.
Makin, M. J., Whapham, A. D., and Minter, F. J., 1961, *Phil. Mag.*, **6**, 465.
Silcox, J., and Hirsch, P. B., 1959, *Phil. Mag.*, **4**, 1356.
Thomas, W. R., and Leak, G. M., 1954, *Phil. Mag.*, **45**, 986.

The Formation of Sub-grain Structure by Alternating Plastic Strain†

By J. Holden
National Engineering Laboratory, East Kilbride, Glasgow

[Received September 14, 1960]

Abstract

A micro-beam x-ray technique has been applied to the fracture surfaces produced by slow-growing fatigue cracks. The cracks were propagated in metal sheets subjected to pulsating tension such that the rate of growth of the crack was proportional to its instantaneous length. The fracture surfaces showed a highly developed sub-grain structure with large mis-orientations $>13°$. The sub-grain size was found to be independent of the range of cyclic stress used to propagate the crack and to be characteristic of the metal. The progressive development of the sub-grain structure was followed in torsion specimens subjected to large ranges of plastic-strain $\sim 10^{-2}$.

If the process of sub-grain formation is regarded as an essential feature of the mechanism of fatigue crack propagation then the order of susceptibility of metals to fatigue crack growth and the phenomenon of non-propagating surface cracks can be interpreted.

§ 1. Introduction

The emphasis in many recent physical investigations of the effects of cyclic stressing has been upon the origin of the fatigue crack. In a series of experiments Thompson *et al.* (1956) have shown, for example, how the life of a copper specimen is correlated with the development, at an early stage, of persistent slip bands which eventually behave as cracks. The metallographic changes accompanying the cyclic stressing of aluminium and its alloys have been classified by Forsyth (1952) and several structural conditions which are associated with the nucleation of surface cracks have been identified. In particular, the coarse slip striations, which are characteristic of cyclic deformation and which have been described by other workers (Hempel *et al.* 1955, Wood 1956), appear to cause a surface profile which can be identified with the initial crack as calculations by May (1960) suggest.

Although, therefore, the nucleation of fatigue cracks at an early stage of the life of the specimen has been related to the behaviour of cyclic slip bands at free surfaces the limitations of the resultant physical viewpoint are seriously felt when the growth of the initial cracks is considered. The transition from the formation of a surface crack to the commencement of

† Communicated by the Author.

steady crack growth is particularly important since analyses of crack growth have shown that the slow, reproducible growth which occurs at low cyclic stress ranges, ceases if either the stress range or crack length is too small.

This phenomenon of non-propagation of fatigue cracks has been shown by Frost and Dugdale (1958) to underlie the behaviour of notched mild steel fatigue specimens. Notches with high theoretical stress concentration factors, K_t, form non-propagating cracks at the notch root at alternating stress ranges given by the intrinsic fatigue limit divided by K_t. Fracture of the specimen is, however, only produced by raising the alternating stress to a propagation value which is characteristic of the material and the length of the surface crack formed at the notch root.

In the present paper, experimental observations resulting from the application of an x-ray micro-beam technique to the fracture surfaces formed by slow fatigue crack growth, are presented. The cracks were grown in centrally notched sheets under pulsating tension at ranges of applied nominal alternating stress σ, and mean stress, such that the crack growth obeyed the relations found by Frost and Dugdale (1958):

$$\left.\begin{aligned} \frac{dl}{dN} &= kl, \\ \ln\frac{l}{l_0} &= kN, \end{aligned}\right\} \quad \ldots\ldots\ldots \quad (1)$$

where l = current half-length of crack, N = number of cycles, l_0 = initial half-length. The coefficient of proportionality k is given by σ^3/N_s where N_s depends upon the metal and is independent of mean stress for the metals and mean stresses employed in the present observations.

The observations (on aluminium, mild steel and zinc) showed that the fracture surfaces produced under these conditions possessed a highly developed sub-grain structure characteristic of the metal and involving large misorientations. The structure was independent of the alternating stress range used to produce the fracture and of the initial state of working of the material. In order to follow the gradual development of the sub-grain structure prior to the state characteristic of fracture it was considered that torsion specimens subjected to conditions of large plastic strain range, ϵ_{pl} (giving lives up to 5×10^4 cycles) would be most suitable. Under these conditions Coffin and Tavernelli (1959) have shown that the relation $\epsilon_{pl} \cdot N^{1/2} = \text{const.}$ holds, a relation which is again relatively free from the scatter characteristic of plain fatigue testing.

§ 2. Experimental Method

The x-ray micro-beam technique introduced by Hirsch and Kellar (1952) depends for its application upon the dislocations in the deformed metal being so distributed that they form arrays or boundaries, thus defining sub-grains which are relatively free from dislocations. Information about the distribution of the dislocations can be obtained if the volume irradiated is not too large compared with the sub-grain dimensions and if

the difference in dislocation density between sub-grain and boundary is sufficiently large. The application of the method to metals deformed by rolling by Gay *et al.* (1954) required the use of very fine micro-beams but, as will be shown below, the structures formed by cyclic stressing involve larger and better resolved sub-grains, factors which enable the technique to be applied in a relaxed form using beams down to 70 μ diameter only.

When the deformed metal is irradiated with a sufficiently fine beam of x-rays the Debye–Scherrer ring is observed to be made up of individual spots. If the spots are well-enough defined to be counted, the mean sub-grain size can be deduced since the number of reflections on a Debye–Scherrer ring is given by (Hirsch 1952):

$$N = \tfrac{1}{2}\frac{At}{v}.p\cos\theta\,(d\theta + \Delta)$$

where A = area of cross section of beam, t = effective penetration of beam, v = volume of sub-grain, p = multiplicity factor, θ = Bragg angle, $d\theta$ = divergence of beam, Δ = angle over which the sub-grain reflects due to distortion, small size and wavelength spread.

Further information about the sub-grain in addition to its size can be obtained from the radial and tangential spread of individual spots on the Debye–Scherrer ring and from the contrast between a spot and the general level of background in the Debye–Scherrer ring. When the volume irradiated is such that only a few original grains are included, the Debye–Scherrer ring may be incomplete and consist of separate arcs. The total range of misorientation within the grain, due to deformation, can then be estimated since $\sin\beta/2 = \cos\theta\sin\psi/2$ (Hirsch 1952) where ψ is the angle subtended by the arc at the centre of the ring and β is the maximum angle between normals of the reflecting planes of sub-grains within the original grain.

§ 3. Experimental Observations

3.1. *Aluminium*

In their initial rolled condition the $\frac{1}{8}$ in. thick aluminium sheets of commercial purity (99·8%), used for crack growth, had a wide variation of grain size ranging from 20–40 μ at the outside surfaces to $\sim 300\,\mu$ in the centre. Using a 250 μ diameter beam of divergence 2×10^{-3} radians the Debye–Scherrer rings from the rolled metal were found to be continuous. In the central region of the sheet where the grain size was large the rings were incomplete and made up of arcs which again had a continuous intensity distribution. A fracture surface was formed in such material by growing a fatigue crack at $3 \pm \frac{1}{2}$ ton/sq. in., the crack growing so as to extend approximately 1 cm in 10^7 cycles at 2000 c/m. Using the same camera geometry the fracture surface was examined and showed prominent spottiness of the Debye–Scherrer rings. Figure 1† illustrates the change in detail of the Debye–Scherrer ring for the camera geometry employed. By

† All figures are shown as plates.

irradiating the mid-section of the sheet and obtaining arcs instead of complete rings it was also evident that the building-up of sub-grains by cycling involved an increased spread of the arcs. Thus the range of misorientation within a rolled grain increased as the sub-grains formed. The effect of the localized cyclic stressing at the crack tip had, therefore, been to drive the dislocations into boundaries defining sub-grains of greater size and misorientation than had been produced by the initial rolling deformation.

The fracture surface structure was found to be localized since removal of a 50 μ layer from the fracture surface revealed material producing continuous Debye–Scherrer rings. This fact precluded any micro-structural study of the sub-grains. It was argued that the fracture surface structure might be simulated in a plain direct-stress specimen if the range of stress was high enough, since, although the fatigue crack was grown slowly, it would have advanced for distances of the order of the sub-grain size in a matter of minutes. Plain direct-stress specimens of the commercial purity Al were tested for some 30 000 cycles at stress levels which were known to give endurances of the order of 100 000 cycles. Using both annealed and unidirectionally strained initial structures the effect of cycling was found to be the production of well-developed sub-grains, a structure which was found to be common to the interior as well as the exterior of the plain specimens. Figure 2 illustrates, for the case of a single grain, how the characteristic tensile deformation, as shown in a Transmission Laue diagram, is built up into a sub-grain structure by cyclic deformation.

Closer examination of the plain specimens showed that the fracture surface structure had not been completely simulated. Although numerically similar, the shapes of the individual diffraction spots on the Debye–Scherrer rings were quite different. For the same camera geometry the fracture surface spots were more sharply defined, smaller and free from radial and tangential distortion. These features suggest that the interior of the sub-grains in the fracture surface are more free from residual dislocations than the direct-stress specimens and that the sub-grain boundaries are more sharply defined. It was found impossible to simulate the fracture surface structure in respect of the spot shape by any high range of direct stress on a plain specimen. It was concluded that the initiation and rapid growth of a surface crack was occurring before the dislocations could be driven into boundaries to the extent which occurs at the crack tip in the propagation-type specimen. In order, therefore, to follow the development of the sub-grain structure as far as possible, torsion specimens were employed. Aluminium of purity 99·99% was also used for these specimens so that metallographic methods could be used to show up the sub-grain structure. For specimens containing a few large grains in the gauge length the same grain could be irradiated after increasing numbers of cycles. Figure 3 shows the development of structure within a grain at a plastic strain range of $\sim 10^{-2}$. After a few hundred cycles the deformation of the crystal has reached the stage where the spreading Laue spots have begun

to show a sub-structure and the misorientation range is such that parts of Debye–Scherrer rings emerge. By 2000 cycles the build-up of sub-grains is illustrated by the increase in extent of the spread of the spotty Debye–Scherrer arcs. At 4000 cycles the surface of the specimen shows many small cracks, particularly at grain junctions, but the misorientation range of the sub-grain structure can be observed to increase for a further 2000 cycles since, under torsion conditions, the test is not terminated by the propagation of a crack.

The misorientation at a sub-grain boundary is large enough to allow polarized-light techniques to be used to show the range of sub-grain sizes and their development. Figure 4 (*a*) shows the characteristic short-slip lines (Seeger 1956) on a torsion specimen after a few hundred cycles at a plastic-strain range $\sim 10^{-2}$, fig. 4 (*b*), shows the same field under polarized light. The sub-grains are observed to be forming in the regions between the slip-line traces. With increasing number of cycles many cracks appear in torsion specimens in the regions of well-developed sub-grain structure. In polycrystalline specimens the sub-grain structure is concentrated in the region of grain-boundary junctions due to stress-concentration effects and, therefore, the cracks tend to be associated with grain boundaries. In single-crystal specimens, however, the cracks have a surface trace with irregularities on the same scale as the sub-grain size.

It is noteworthy that the cyclic sub-grain structure is also readily formed at -196°c. Thin slices of single-crystal specimens showed prominent double-Bragg reflection effects (Atkinson 1959) when examined in transmission. The cyclic structure is also resistant to recrystallization, an anneal of four hours at 330°c, which readily caused complete recrystallization in an aluminium specimen deformed to 15% strain in tension, failed to cause any new grains to appear in the cyclic sub-grain structure. A partial recrystallization developed after a further four hours at 420°c.

The characteristics of the sub-grain structures found in the various specimens are tabulated in tables 1 and 2.

3.2. *Mild Steel and Iron*

Fracture surfaces in annealed 0·05%C mild steel of uniform grain size $\sim 20\,\mu$, resulting from the growth of cracks at 5 ± 3 tons/sq. in. and 12 ± 3 tons/sq. in. were examined with beam diameters of $75\,\mu$ and divergences between 1 and 5×10^{-3} radians. It was found possible to estimate the particle size and to measure the total angular misorientation within a grain. In contrast, specimens of the same mild steel pulled in tension to strains of up to 10% displayed quite continuous Debye–Scherrer rings for the same camera geometry.

As in the case of aluminium, plain direct-stress specimens of mild steel were subjected to high stress levels in short-time tests in an attempt to simulate the fracture surface structure. Although the Debye–Scherrer rings showed spottiness compared with the unidirectionally strained specimen measurements were not possible. Specimens of an iron were next

Table 1. Reflection

Specimen $v^{1/3}$	Average size of sub-grain $v^{1/3}$ (μ)	Total misorientation range β	Mean angle between sub-grains $\alpha=\beta/3$	Broadening $\overline{d\phi}$
Fracture surface Al 99·8% $3\pm\frac{1}{2}$ ton/sq. in.	4–6	$>40°$	$>13°$	$\sim 1\times10^{-4}$
Fracture surface Al 99·8% 3 ± 1 ton/sq. in.	4–6	$>40°$	$>13°$	$\sim 1\times10^{-4}$
Torsion specimen, Al 99·9% 6000 cycles at $\epsilon_{pl}=10^{-2}$	4–8	$>40°$	$>13°$	$\sim 5\times10^{-4}$
Torsion specimen, Al 99·9% 80 000 cycles at $\epsilon_{pl}=3\times10^{-3}$	4–8	$>40°$	$>13°$	$\sim 5\times10^{-4}$
Direct stress, Al 99·9% 30 000 cycles at $\epsilon_{pl}=8\times10^{-3}$	5–8	25°–36°	8°–12°	$\sim 1\times10^{-3}$

Table 2. Transmission

Direct stress, Al 99·9% 30 000 cycles at $\epsilon_{pl}=8\times10^{-3}$	5–8	30°–40°	12°	1×10^{-3}

Table 3. Reflection

Specimen	Average size of sub-grain $v^{1/3}$(μ)	Total misorientation range β	Mean angle between sub-grains $\alpha=\beta/3$
Fracture surface mild steel $5\pm2\frac{1}{2}$ tons/sq. in.	1–2	25°–38°	8°–13°
Fracture surface mild steel 12 ± 3 tons/sq. in.	1–2	25°–38°	8°–13°
Direct stress, iron 30 000 cycles at $\epsilon_{pl}\sim10^{-3}$	1–2	20°–28°	7°–9°

used in direct stress and these proved to have a sub-structure upon which measurement was possible. The measurements are summarized in table 3.

Sheets containing growing fatigue cracks were examined metallographically with the plane of section normal to the mean direction of crack growth. The crack front was always found to be slightly bowed forward so that sections could be made with the leading part of the crack in the middle of the sheet. From such sections, taken at intervals of a few microns right through the position of the front, it could be seen that the trace of the crack at completely broken sections owed its irregularity to the fact that it was formed from the joining up of many independent cracks formed ahead of the completely broken section at any stage of propagation. Figure 5 (*a*) shows detail of one end of a bowed front at a section where the outside faces of the sheet are unbroken down to a depth of 20% of the sheet thickness. Figure 5 (*b*) shows a final section of the leading cracks in the middle of a sheet; removal of a further 3 μ at this section eliminated all traces of cracks. The irregularities in the small independent cracks are on the scale of the observed sub-grain structure. In the case of the mild-steel specimens it was notable that these elementary cracks were not found to bear any relation to the known form of elementary brittle cracks in the mild steel or to the particular inclusions which were known to play a part in the ductile fracture of the material.

3.3. *Other Metals*

With the micro-beam geometry developed for mild steel attempts were made to detect sub-grain structures on fracture surfaces of other metals. These were unsuccessful in the cases of copper, stainless steel and two aluminium alloys, one of duralumin type, L. 71, and the other a Zn, Mg alloy DTD. 687A. In the case of a Zn sheet of 99% purity, well-developed sub-grains were detected and measurements would have been possible with the 75 μ beam. In the case of copper torsion specimens a local sub-structure associated with twin boundaries was observed metallographically after x-ray observations had indicated the existence of sub-grains.

§ 4. Discussion

The structure detected by the micro-beam method can be related to some long-standing observations on the effect of cyclic stressing. The sharpening of Debye–Scherrer rings from iron deformed by cycling was observed by Hempel and Möller (1954) and was considered to be a result of the reduction of strains between crystals. The formation of sub-grains in annealed super-pure aluminium and in iron was observed metallographically by Forsyth (1952) who considered the effect to be most pronounced at high ranges of alternating strain and interpreted the structure as due to polygonization consequent upon the production of vacancies in the fatigue test. The micro-beam observations show that the cyclic sub-structure develops in previously deformed crystals and is, therefore, not simply a breaking-down structure but a structure which is formed by the dislocations

reaching a preferred distribution under cycles of large alternating strain. This distribution develops at $-196°$C so that the dislocations are not dependent upon diffusion mechanisms to form the sub-grain arrays, but must reach their positions by cross-slip processes.

The cyclic structure is shown to reach an extreme condition, i.e. large misorientation between particles, α, and sharply defined diffraction spots, in material subject to the stress concentration that exists at the tip of a slow growing crack. The sub-grain formation is the same for the specimens from fracture faces irrespective of the range of alternating stress used to produce the fracture. The sub-grain structure appears, therefore, to be characteristic of the fracture condition at the crack tip and not of any intervening state of plastic deformation. We would expect, therefore, that a dislocation model which complies with the data determined by the micro-beam technique would contain features suggestive of the mode of fracture at the slowly growing crack.

Following Hirsch (1952) the sub-grain structure can be described in terms of the density of excess dislocations of one sign in the boundaries, D_b, and the residual density of dislocations left within the particles D_i. In this way the cyclic structure may be compared with the structure found in rolled super-pure aluminium. Table 4 gives the comparative data.

Table 4

Specimen	Average sub-grain size $v^{1\ 3}(\mu)$	Total misorientation range β	Mean angle between sub-grains α	Density of dislocations	
				In boundary D_b	In sub-grain D_i
Super-pure Al rolled to 57% original thickness Hirsch (1952)	2	15°	1·5°	$4{\cdot}5\times10^{9}$	6×10^{8}
Al 99·8% fracture surface $3\pm\frac{1}{2}$ ton/sq. in.	4–6	>40°	>13°	$2\text{–}3\times10^{10}$	$\sim1\times10^{7}$

In the case of rolled aluminium, Hirsch considered that the resultant sub-grain structure was best described by a polygonized arrangement of dislocations such that $\alpha=\beta\,.\,v^{1/3}/T$ and $D_b=\beta/\mathbf{b}T$ where T was the original grain size and **b** the Burgers vector. The cyclic sub-structure can, however, be observed with polarized-light techniques known to be insensitive to small misorientations, so that the data for this structure are interpreted in table 4 on the basis that the sub-grains are not polygonized but misoriented about a mean position such that $\alpha=\beta/3$ and $D_b=\beta/3\mathbf{b}\,.\,v^{1/3}$

(Hirsch 1952). The value D_i is estimated in the same way for the two deformation structures on the basis that there is a random distribution of dislocations within the sub-grains (Hirsch 1952).

The values of D_b and D_i in table 4 show that the main feature of the cyclic sub-structure is the accumulation of high dislocation densities in sub-grain boundaries brought about by the removal of dislocations from the sub-grain interior. The cyclic sub-grain structure would not be expected to be a strong source of hardening (Ball 1957) of the metal, but the misorientation of regions of crystal through such large angles, α, would cause stresses to develop in adjacent parts of a grain and the densely packed sub-boundary regions might be expected to be sites of micro-cracks. Such micro-cracks would not be expected to propagate immediately after formation since the material within the sub-grains would be still quite ductile. The first micro-cracks would serve to cause further local stress concentration and aid the formation of cyclic sub-structure at the region of the main crack tip. This is in accord with two features connected with slowly growing fatigue cracks, that no large micro-hardness changes can be detected around the cracks and that the crack front consists of many small elementary cracks unconnected with the metallurgical features known to be effective in brittle and ductile fracture.

Table 5

Metal	Thornton and Hirsch (1958) Seeger (1956) γ	Relative rate of crack propagation Frost (1959)
Stainless steel, 18/8	13 ergs/cm^2	0·7
Mild steel	—	1·0
Copper	40	4·0
Aluminium	200	12·0
Zinc	Large	150·0

If the dislocations are considered to perform a symmetric random walk before becoming trapped in sub-boundary arrays the density of dislocations in the arrays would increase as $N^{1/2}$ multiplied by the number of dislocations which were moving cyclically. Under cyclic conditions of constant plastic strain range, ϵ_{pl}, the number of moving dislocations would be proportional to ϵ_{pl} and cracks would appear when $\epsilon_{pl} . N^{1/2}$ reached a large enough value as is experimentally observed in some metals (Coffin and Tavernelli 1959). The ease with which the sub-grain structure could form would depend upon the ability of the dislocations to cross-slip and thus upon the stacking-fault energy, γ. It is, therefore, of interest to tabulate the stacking-fault energy and the relative rate of crack propagation (at unit alternating stress and same crack length) for various metals.

The hypothesis can therefore be made that, under the cyclic conditions prevailing at a slowly growing crack tip, the dislocations tend to form

regions of high and low density. The resultant misorientations within a grain are detected as well-defined sub-grain boundaries in metals of high stacking-fault energy; this ease of forming sub-grains favours the formation of the micro-cracks which are an essential stage in the progression of the fatigue crack. On this basis some further features of crack propagation in sheets can be understood. Thus, if the micro-cracks formed in the densely-packed boundaries are unable to propagate but serve only to advance the cyclic, sub-grain structure formation, the progress of the main crack front will depend on the formation of a sufficient number of independent micro-cracks until the applied maximum tensile stress pulls off the remaining necks of material between the micro-cracks. This pulling-off effect is minimized on the crack surfaces examined in the present work since the maximum tensile stress of the cycle was small and the crack length was only a small proportion of the sheet width in which the crack was growing. It has been observed, however (Frost 1959), that, as the crack increases in length beyond this condition, the fracture surface roughens and, in thin sheets, goes over from a position normal to the loading axis to an inclined position. The onset of the transition correlates with the maximum tensile stress of the cycle and would be interpreted as being due to the gradually increasing effectiveness of the pulling-off stage which contributes to the mechanism of advance of the main crack front.

The further main feature of the model of growth is that, since the first micro-cracks are dependent upon the formation of high dislocation density boundaries defining particles in the range of size of several microns, it is clear that an adequate volume of material at the crack tip must be subject to alternating cyclic strain. If this is not so a sufficient number of sub-grains with their associated stress effects due to their large misorientations will not be formed. The range of alternating stress, σ, and the crack length, l, determine the volume of the region subject to alternating strain and these quantities appear in the crack growth parameter $\sigma^3 l$ in eqns. (1). The process of crack growth as opposed to surface crack initiation can, therefore, be defined as occurring when:

(i) a large-enough volume of material is subject to cyclic plastic strain sufficient to cause the development of cyclic sub-grain structure to the extent that micro-cracks form at the sub-boundaries; and

(ii) a sufficient normal stress is present to pull off the necks of material which remain between sub-boundary micro-cracks.

The many processes whereby surface cracks can be formed are regarded, therefore, as controlling the fatigue process only until the surface crack is long enough to satisfy condition (i) for the stress system on the specimen. The length of the surface crack before crack growth as defined commences will be much larger, for example, for copper than for aluminium on account of the large difference in ease of development of cyclic sub-grain structure due to the difference in stacking-fault energy. The importance of chemical attack by the atmosphere will also be greater for materials

which have a longer period of their fatigue-life taken up in forming a crack long enough to grow by the sub-boundary crack mechanism. As regards diffusion effects, the cyclic sub-structure will resemble a grain-boundary system, with the condition that the small size of the sub-grains will extend the temperature range over which grain boundaries are usually regarded as being effective in contributing to bulk diffusion.

The failure of surface cracks to propagate is met with experimentally when either the cycle of deformation is wholly compressive or the value of the parameter $\sigma^3 l$ falls below a critical value. Condition (ii) is not fulfilled for the compressive cycle and it is suggested that the critical value of $\sigma^3 l$ for propagation is due to the need to fulfil condition (i). Measurements (Frost 1959) on mild steel of the critical value of $\sigma^3 l$ lead to a value of $l \sim 50\,\mu$ for values of σ equal to the plain fatigue limit. The processes which form surface cracks on plain specimens, e.g. the development of surface notches as calculated by May, would have, therefore, to cause a $50\,\mu$ surface crack before growth by the sub-grain mechanism would take over for a range of applied stress equal to the fatigue limit. The scatter associated with fatigue tests on plain specimens at long endurances is associated in the hypothesis with the formation of surface cracks rather than with their growth. In this connection it may be noted that, in experiments in which steps are taken to initiate the surface crack by an additional process, e.g. as in fretting, the scatter in the fatigue test tends to be diminished.

§ 5. Conclusions

1. Under large ranges of alternating plastic strain the dislocations in aluminium and α-iron form sub-grain boundaries irrespective of the initial state of distribution.

2. The cyclic sub-grain structure tends to a characteristic limiting condition of sub-grain size, misorientation and dislocation density within the sub-grains with increasing number of cycles. The limit is reached when micro-cracks form at the sub-grain boundaries. The most developed sub-grain structure, i.e. largest misorientation and lowest density of dislocations within the sub-grains, is observed on the fracture surfaces formed by slow fatigue cracks.

3. The commencement of fatigue crack growth is, therefore, associated with the fracture process based upon the formation of sub-grain cracks, a phenomenon not connected with the metal surface.

4. Two aspects of fatigue crack growth can be interpreted on this model. (*a*) The order of susceptibility to fatigue-crack growth in metals relates to the ease of formation of sub-grains and hence to the stacking-fault energy; (*b*) the phenomenon of non-propagation of surface cracks is expected when the volume of material ahead of the surface crack which is subject to the range of alternating strain is too small to allow the characteristic sub-grain structure to develop.

Acknowledgment

The work described has been carried out as part of the research programme of the National Engineering Laboratory of the Department of Scientific and Industrial Research and the paper is published by permission of the Director.

References

Atkinson, H. H., 1959, *J. appl. Phys.*, **30**, 637.
Ball, C. J., 1957, *Phil. Mag.*, **2**, 1011.
Coffin, L. F., and Tavernelli, J. F., 1959, *Trans. Met. Soc. AIME*, **215**, 794.
Forsyth, P. J. E., 1952, *J. Inst. Met.*, **80**, 1340.
Frost, N. E., 1959 a, *Proc. Inst. mech. Engrs* (in the press); 1959 b, *J. mech. eng. Sci.*, **1**, 151.
Frost, N. E., and Dugdale, D. S., 1958, *J. mech. phys. Solids*, **6**, 92.
Gay, P., Hirsch, P. B., and Kelly, A., 1954, *Acta cryst., Camb.*, **7**, 41.
Hempel, M., Wever, F., and Schrader, A., 1955, *Arch. Eisenhüttenw.*, **26**, 739.
Hempel, M., and Möller, H., 1954, *Arch. Eisenhüttenw.*, **25**, 425.
Hirsch, P. B., 1952, *Acta cryst., Camb.*, **5**, 168; 1959, *Internal Stresses and Fatigue in Metals* (London : Elsevier).
Hirsch, P. B., and Kellar, J. N., 1952, *Acta cryst., Camb.*, **5**, 162.
May, A. N., 1960, *Nature, Lond.*, **185**, 303.
Seeger, A., 1956, *Dislocations and Mechanical Properties of Crystals* (London : Chapman & Hall).
Thornton, P. R., and Hirsch, P. B., 1958, *Phil. Mag.*, **3**, 738.
Thompson, N., Wadsworth, N. J., and Louat, N., 1956, *Phil. Mag.*, **1**, 113.
Wood, W. A., 1956, *Fatigue in Aircraft Structures* (New York : Academic Press).

The Half-life of Vanadium–50†

By A. McNair
Atomic Weapons Research Establishment, Aldermaston, Berkshire

[Received October 26, 1960]

Abstract

The half-life of the naturally occurring odd–odd isotope ^{50}V for electron capture decay to the first excited state of ^{50}Ti is shown to exceed 8×10^{15} years and for negatron decay to the first excited state of ^{50}Cr to exceed $1{\cdot}2 \times 10^{16}$ years.

§ 1. Introduction

In 1952 Johnson showed by mass measurements that the odd–odd isotope ^{50}V was unstable with respect to beta decay to its even–even neighbours, to ^{50}Ti by $(2{\cdot}39 \pm 0{\cdot}13)$ Mev and to ^{50}Cr by $(1{\cdot}18 \pm 0{\cdot}12)$ Mev. Early attempts to measure the half-life merely agreed that it was long (Sheline 1954, Strome 1954, Selig 1954, Heintze 1955). ^{50}Ti, however, has a first excited state, presumably 2+, at 1·58 Mev (Pieper 1952). ^{50}V has a ground state spin of 6 units (Kikuchi *et al.* 1952, 1953, Baker *et al.* 1952) and presumably even parity, since the odd neutron and proton are likely both to be in $f_{7/2}$ configurations. Hence the fastest mode of decay in the electron capture branch is expected to be the fourth forbidden (4, no) transition to the 1·58 Mev state of ^{50}Ti since the ground to ground transition involves two more units of spin change. Recent attempts to measure the half-life for this mode of decay (by finding the rate of emission of 1·58 Mev gamma rays from vanadium) agreed that the half-life is around 4 to 5×10^{14} years (Glover and Watt 1957, Bauminger and Cohen 1958). However, unless the log *ft* value for a fourth forbidden beta transition is considerably smaller than would be expected from the trend of values shown by first, second and third forbidden transitions, this half-life seems to be one or two orders of magnitude too short. It seemed worth investigating the decay again to see if this discrepancy from the expected log *ft* value for a fourth forbidden transition were real.

The recent discovery (Porter *et al.* 1958) of an excited state in ^{50}Cr at 0·78 Mev which fits in well with the general systematics of the first excited 2+ states of even–even nuclei permits us to examine another fourth forbidden transition mode from ^{50}V, that by negatron decay to ^{50}Cr via this excited state, by searching for 780 kev gamma rays from ^{50}V. A search for both 1·58 Mev and 780 kev gamma rays from vanadium in order to arrive at a value for the half-life of ^{50}V is described below.

† Communicated by Dr. S. C. Curran.

§ 2. Apparatus

A $4\frac{1}{2}$ in. $\times$ $4\frac{1}{2}$ in. cylinder of NaI(Tl) was used as the detector and the pulses were amplified, and recorded on a 100-channel kicksorter. The source, 500 g of V_2O_5 was compacted in a thin copper holder which sat snugly over the crystal, so that the source covered the crystal top and side.

§ 3. Method

Since the counting rates from the two gamma rays were expected to be extremely low, the experiment was designed so that the results would be as significant as possible by particular attention to three points: Reduction of detector background by massive iron and lead shielding and by geiger anti-coincidence techniques, good source-detector geometry combined with large quantities of source, and precautions in the method of analysis against long term gain drifts. This last precaution consisted of taking short $\sim$2–3 hours runs of background and background plus source alternately, with frequent energy calibration of the system. In each set the two spectra were subtracted and the count rates within a gamma ray peak width about 1·58 Mev and 780 kev were determined and recorded. A large number of separate such runs gradually built up useful integrated count rates, and in this way gain drifts could be counteracted.

§ 4. Results and Discussion

Normally one would simulate the source in such an experiment by suitable inactive materials for use in the background measurements. Slightly variable ^{40}K contamination proved to be troublesome, however, so the background was taken with the crystal alone. The increased gamma ray interaction in the source material was estimated by measuring count rates in the difference spectra at energies above and below the expected positions of the two ^{50}V gamma-ray energies. The trend shown by these counts was taken to indicate the true background and the count rates at 1·58 Mev and 780 kev related to this value. Corrections were applied to allow for the slight ^{40}K contamination of the source. The small extra uncertainties introduced by the corrections have been allowed for mathematically in calculation of the statistical error in the results.

In fact, several separate experiments involving a total counting time of about 500 hours agreed in showing that the emission of gamma rays from the vanadium was undetectable and that the count rate in the 1·58 Mev and 780 kev regions of the spectrum did not rise above background. The efficiency of the system was calibrated using potassium (assuming a gamma emission rate of $3{\cdot}36 \pm 0{\cdot}10$ gammas $\sec^{-1}\,g^{-1}$ of natural potassium) and ^{22}Na. The final results, allowing for crystal efficiency, were

(-2 ± 29) 1·58 Mev gammas per 100 g natural vanadium per hour.

$(+6 \pm 14)$ 780 kev gammas per 100 g natural vanadium per hour.

The statistical limits show that the half-life of ^{50}V for electron capture decay to the first excited state of ^{50}Ti must exceed 8×10^{15} years, and for

negatron decay to the first excited state of ^{50}Cr must be greater than $1{\cdot}2 \times 10^{16}$ years. These results give $\log ft$ values $> 22{\cdot}1$ and $> 22{\cdot}5$ respectively which approach more nearly to what would be expected for a fourth forbidden (4, no) beta transition.

§ 5. Conclusion

As expected from consideration of the $\log ft$ value, the half-life of ^{50}V for electron capture decay to the first excited state of ^{50}Ti has been shown to be much larger than previous measurements of 4 to $4{\cdot}8 \times 10^{14}$ years and is not less than 8×10^{15} years. The half life for negatron decay to the first excited state of ^{50}Cr is similarly shown to exceed $1{\cdot}2 \times 10^{16}$ years.

Acknowledgments

The author wishes to thank the Director of the Establishment for permission to publish this paper, and Dr. H. W. Wilson for the interest which he has taken in the work.

References

Baker, J. M., and Bleaney, B., 1952, *Proc. phys. Soc. Lond.*, A, **65**, 952.
Bauminger, E. R., and Cohen, S. G., 1958, *Phys. Rev.*, **110**, 953.
Glover, R. N., and Watt, D. E., 1957, *Phil. Mag.*, **2**, 697.
Heintze, J., 1955, *Z. Naturf.* A, **10**, 77.
Johnson, W. H., 1952, *Phys. Rev.*, **87**, 166.
Kikuchi, C., Sirvetz, M. H., and Cohen, V. W., 1952, *Phys. Rev.*, **88**, 142 ; 1953, *Ibid.*, **92**, 109.
Pieper, G. F., 1952, *Phys. Rev.*, **88**, 1299.
Porter, W. C., Van Patter, D. M., Rothman, M. A., and Mandeville, C. E., 1958, *Phys. Rev.*, **112**, 468.
Selig, H., 1954, Thesis, Carnegie Inst. Tech.
Sheline, R. K., 1954 (unpublished).
Strome, F. C., 1954, Thesis, University of Michigan.

The Half-life of Rubidium-87†

By A. McNair and H. W. Wilson
Atomic Weapons Research Establishment, Aldermaston, Berkshire

[Received October 26, 1960]

Abstract

A 4π proportional counter system capable of examining thin sources of extended area has been used to determine the half-life of ^{87}Rb, which was found to be $(5{\cdot}25 \pm 0{\cdot}10) \times 10^{10}$ years. Corrections for absorption of electrons and for scattering in the source and in the source supporting foil are discussed.

§ 1. Introduction

Recent advances in rubidium–strontium geochronology have shown that the method can give self-consistent ages which are more or less in agreement with ages derived from uranium–lead and potassium–argon analyses when the half-life of ^{87}Rb is assumed to be near 5×10^{10} years (Aldrich and Wetherill 1958). Lately, differences in the ages derived by the Rb–Sr and K–A methods have been shown to indicate the more recent thermal history of an ancient rock system, since heating of the rock by late volcanic intrusions will be expected to reduce the amount of argon retained in the mineral whilst leaving the ^{87}Rb/^{87}Sr ratio relatively unchanged (Giletti 1959). The increasing use of the ^{87}Rb–^{87}Sr method in dating studies has made careful evaluation of the half-life of ^{87}Rb a matter of some importance, because the accuracy of a measured age depends on the accuracy to which the half-life of the transition is known. Independent physical measurements of the half-life are therefore necessary to check the value of 5×10^{10} years usually accepted by geochronologists on the basis of correspondence between ages determined by the different methods.

The $^{87}\text{Rb} \rightarrow {}^{87}\text{Sr}$ decay is known to be a third-forbidden (3, yes) beta transition with a highly forbidden spectrum shape which shows no maximum but appears to rise steadily as the energy decreases (Flynn and Glendenin 1959, MacGregor and Wiedenbeck 1954, Lewis 1952, Curran *et al.* 1951). Although the energy of the transition is about 275 kev the shape of the spectrum is such that the average energy of the beta particles is low, about 45 kev, and care must be taken to reduce and correct for losses caused by absorption

† Communicated by Dr. S. C. Curran.

of the softest electrons in the source or source mount. Values of the half-life ranging from $4{\cdot}3 \times 10^{10}$ to $6{\cdot}4 \times 10^{10}$ years have been reported, and are summarized by Aldrich and Wetherill (1958). The most recent experiments by Huster and Rausch (1956) using thin sources in a 4π counter gave $4{\cdot}95 \times 10^{10}$ years, but there seemed still to be some doubt about this value and later work by Huster (1957), using absorbers and extrapolating to zero thickness, gave a half-life of $4{\cdot}6 \times 10^{10}$ years. In experiments using scintillation counting Flynn and Glendenin (1959) derived a half-life of $(4{\cdot}7 \pm 0{\cdot}1) \times 10^{10}$ years. The only earlier experiment in which source and support absorption should not have raised any problem was that of Lewis (1952) who used a RbI scintillation spectrometer and measured a half-life of $5{\cdot}9 \times 10^{10}$ years. Insensitivity to low energy electrons would, however, tend to make this a high value.

In the present work we aimed at reducing absorption of the softest beta particles by using very thin uniform sources (produced by evaporation *in vacuo* from a tantalum strip) deposited on thin supporting films. The use of enriched rubidium ($> 99\%$ ^{87}Rb) and large source areas helped to improve the counting statistics for thin layers. Further improvements in statistics were made by shielding the counter in 8 in. of iron and operating it in anti-coincidence with the output from a surrounding ring of geiger counters to reduce background counts. Internal background was kept to a minimum by lining the counter with carefully cleaned copper sheet. The amount of ^{87}Rb present in the sources was determined to high accuracy by isotopic dilution and mass spectrometer analysis. Counting in 4π geometry was considered essential in order to keep back-scattering corrections within manageable limits, but in addition to the 4π count we simultaneously recorded separate counts from each side of the source and used these counts to estimate the effect of absorption and back-scattering within the supporting film.

§ 2. Basic Assumptions and Theory

The detector which was used in our study of ^{87}Rb was a large 4π proportional counter tube. A solid source gas counter was chosen in preference to a scintillation detector because counting could be extended to much lower energies. Of gas counters, the proportional was used in preference to the geiger counter, since proportional counters appear to be more tolerant of changes in the nature of the cathode surface than do geigers and also, in our experience, are much more stable over long counting periods.

The source was mounted on one side of a foil and three simultaneous counts taken, as in fig. 1 (*a*). N_1 is the count rate, extrapolated to zero energy, on the side of the counter facing the source. N_2 is the count rate observed at the back of the supporting foil and N_s is the count rate obtained when the outputs of the two sides of the counter are added together. It follows that electrons scattered from one side of the counter, through the foil and source, to the other side count only once in the N_s channel and once in each of N_1 and N_2. The block diagram of the system is shown in fig. 1 (*b*).

Suppose now that N electrons actually leave the source and that the source support transmits a fraction a of the electrons entering it. (N is not the absolute decay rate but is somewhat less due to source absorption.) Of the electrons entering the foil and not transmitted let a fraction b be back-scattered, and let a fraction s of the electrons counting in either side of the counter be scattered backwards in the direction of the other side (cross-scattered electrons). Then

$$N_1 = \frac{N}{2} + b(1-a)\frac{N}{2} + sa^2\frac{N}{2},$$

$$N_2 = a\frac{N}{2} + sa\left[\frac{N}{2} + b(1-a)\frac{N}{2}\right],$$

$$N_s = \frac{N}{2} + b(1-a)\frac{N}{2} + a\frac{N}{2}.$$

Fig. 1

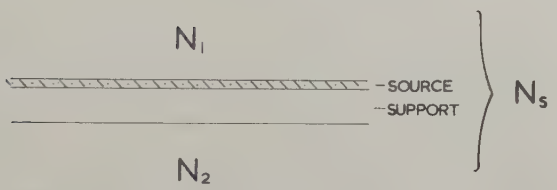

(*a*)

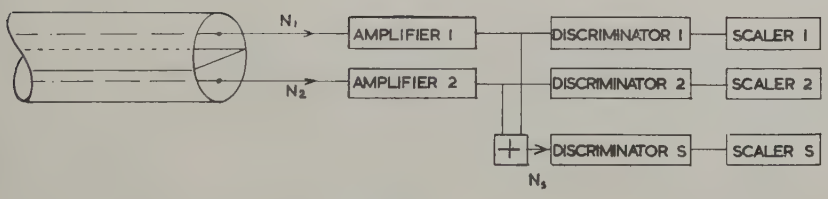

(*b*)

Counter system.

We allow for the effect of source absorption on cross-scattered electrons by taking measurements with different thicknesses of source as described later and extrapolating to zero source thickness. Double cross-scattering or scatter in the gas followed by back-scattering from the support does not affect the argument, since these events do not increase the count rate, because of the integrating action of the counter.

We are, of course, assuming that degradation of the energy spectrum of the electrons in traversing matter does not seriously interfere with the value of a, s or b. As we shall show later, we can arrive at essentially the same answer for the half-life of ^{87}Rb by a completely independent path without making any assumptions about absorption or scattering, so that

our postulates would appear valid. It may be that the shape of the low energy spectrum of ^{87}Rb does not alter much on further degradation by passage through matter.

From the above equations we can derive an expression for N, the number of beta particles escaping from the source,

$$N = \frac{2N_s}{2N_s-(N_1+N_2)}\left[N_s - \frac{N_1 b + N_2}{1+b}\right] \dagger.$$

Hence, since we measure N_1, N_2 and N_s we can find, N, provided we know b. If we neglect back-scatter from the support, i.e. $b=0$, we get

$$N = \frac{2N_s(N_s-N_2)}{2N_s-(N_1+N_2)}.$$

This is always larger than when we take back-scatter into account and leads to a lower value for the half-life. This is because back-scattering from the support tends to increase N_1 relative to N_2 and if we ignore it, the absorption of beta rays in the support appears to be worse than it really is, and we over correct.

We have not attempted to measure b at low energies but instead have taken published values for the saturation back-scattering factor of electrons into 2π geometry since, for electrons which are not transmitted, the support appears to be of saturation thickness.

The values taken were $b=0{\cdot}33$ for aluminium (McNair *et al.* 1956) and $b=0{\cdot}5$ for the VYNS plus gold supports. This latter figure is based on the assumed value for aluminium, and on the way in which the saturation back-scattering factor varies with atomic number (Nijgh *et al.* 1959), taking into account the relative thicknesses of gold and plastic. The values assumed for the back-scattering factors do not appear to be critical as a 10% change in back-scattering factor produces less than 0·5% change in the final half-life.

§ 3. Apparatus

The counter is shown in outline sketch in fig. 1 (*b*). It is a copper-lined cylinder, 14 cm in diameter divided along a diametral plane by a brass plate carrying a sliding shelf which can easily be removed to insert the source supporting foils. The effective counting length is 34 cm and the source area is some 50 cm^2 or 60 cm^2, depending on the trays used. The foil area is generally some 30% greater than the source area. The two halves of the counter operate independently. The thin tungsten wire anodes lie parallel to the axis of the cylinder in the diametral plane perpendicular to the plane of the source and some 3 cm away from the source on either side. Initially we were rather concerned with the effect on the counting characteristics of the D-shaped cross section of each counter and placed two more wires in each counter in the corners of the D. These wires could be run above or

† Dr. D. B. Smith of the Wantage Radiation Laboratory informs us that he has deduced a similar expression to allow for absorption in 4π counting.

below cathode potential. However, the characteristics of the counters appeared to be independent of the voltage on these wires over a wide range, and they were removed to keep the counter as simple as possible.

Outputs from each anode pass, as in fig. 1 (*b*), to separate amplifiers which have been modified so that no after-pulsing takes place following severe over-load pulses. By so modifying the amplifier the counter can be run at high gain and the limiting factor becomes counter rather than amplifier noise. Careful earthing and screening arrangements effectively removed external interference and we can now switch off the counter voltage and run the apparatus at its most sensitive setting for several days at a time and detect no counts at all from external effects or amplifier noise.

After amplification the outputs are passed through discriminators to scaling units. The two amplifier outputs are also added together in a separate channel and passed to a third discriminator and scaler to give the sum count N_s. In later experiments the discriminators and scalers were replaced by three 100-channel kicksorters. These give equivalent information but permit better counting statistics to be obtained more quickly by counting at all discriminator levels simultaneously.

A geiger anti-coincidence ring placed round the proportional counter operates an over-riding gate on the system, blocking all three pulse channels each time a cosmic ray particle triggers the geiger array. The counter and anti-coincidence ring are shielded by 8 in. of steel. Backgrounds of around 36 c.p.m. are obtained in each counter with about 55 c.p.m. in the sum channel. The additional count rate obtained in the sum channel from a typical 5 μg/cm^2 layer of ^{87}RbCl is of the order of 20 c.p.m.

§ 4. Manufacture of Source Mounts and Sources

In the main experiment the source supporting foils were made from VYNS by the flotation technique (Pate and Jaffe 1955) and coated on both sides with about 15 μg/cm^2 of gold, by vacuum distillation. The thickness of the foils was found to be fairly constant and averaged about 42 μg/cm^2. We tried to reduce the foil thickness by coating with half the amount of gold, but found that we could not get consistent count rates from one run to the next, possibly due to poor conduction in the gold layer. We could produce conducting layers of aluminium down to about 2 μg/cm^2 but the VYNS invariably became too brittle to use in the counter.

The source layer was also deposited by vacuum distillation in order to obtain uniform thin layers. Only vacuum distillation can give the uniform sources with minimum absorption which are essential to an experiment of this kind. This has been amply demonstrated by Merritt *et al.* (1959) and confirmed by preliminary work of our own. In these preliminary experiments, layers of RbCl of 50 μg/cm^2 and 80 μg/cm^2 were distilled *in vacuo* onto the foil and counted. The layers were then dissolved in distilled water *in situ* and allowed to dry in as uniform a layer as possible. The count rate was then some 30 to 40% less than before. On re-dissolving the

layers in distilled water, to which a little wetting agent had been added, the count rate rose again but was still 15 to 20% below the original.

Pure natural rubidium chloride was used for the sources thicker than $12\,\mu g/cm^2$ and enriched rubidium (99·3% ^{87}Rb) for sources thinner than $12\,\mu g/cm^2$.

§ 5. Estimation of the Source

The amount of ^{87}Rb in the source was estimated by the mass spectrometer isotope dilution technique. The entire source and its supporting film were carefully removed from the counter shelf and placed in a crucible containing, in solution, an accurately measured quantity of rubidium of different but known isotopic ratio. The change in isotopic ratio gave the number of atoms of ^{87}Rb in the source.

§ 6. Procedure

The procedure, then, is to make a series of VYNS films, coat them with gold, and measure the background of the counter with the films in position. In the earlier experiments counts were taken at five bias points in each pulse channel from an energy corresponding to about 3 kev down to about 300 ev. The integral bias curve was then extrapolated to zero energy. The extrapolation generally amounted to between one and two per cent of the count rate. In the later kicksorter experiments the extrapolation was between 3 and 4%, but both counting methods were shown to give the same results within statistical error. The same films are then coated with source, and the counts repeated. The difference counts in the three channels give N_1, N_2 and N_s, and the number of electrons emitted from the source can be calculated according to the formula already derived. Thereafter the amount of ^{87}Rb in the source is measured by the isotope dilution technique, and the half-life calculated in the normal way.

§ 7. Results

7.1. *Source Absorption*

We have corrected for self absorption in the source by making half-life measurements on a series of sources of different thicknesses up to about $70\,\mu g/cm^2$. The half-lives so obtained are plotted against source thickness as in fig. 2. We find that, within experimental error, the apparent half-life is a linear function of source thickness up to $70\,\mu g/cm^2$. Extrapolation to zero source thickness is therefore simple, and yields a half-life for infinitesimal source thicknesses and hence, presumably, zero source absorption.

7.2. *Source Support Absorption and Back-scattering*

We correct for this in fig. 2 by applying the formula for N already derived. However, to test the effectiveness of this correction, we made a series of measurements using a supporting foil of different material (thus with a different back-scattering factor b) and different thickness (hence different

electron absorption). The most convenient material was commercial aluminium leaf of mean thickness 180 μg/cm^2. The half-lives measured with this support, and corrected by the previous formula, are also shown in fig. 2 and prove to be collinear with those obtained using the thin support. The best straight line through these points, then yields our value of the half life of ^{87}Rb corrected for source and supporting foil absorption and foil back-scattering. This turns out to be $(5{\cdot}37 \pm 0{\cdot}02) \times 10^{10}$ years.

Fig. 2

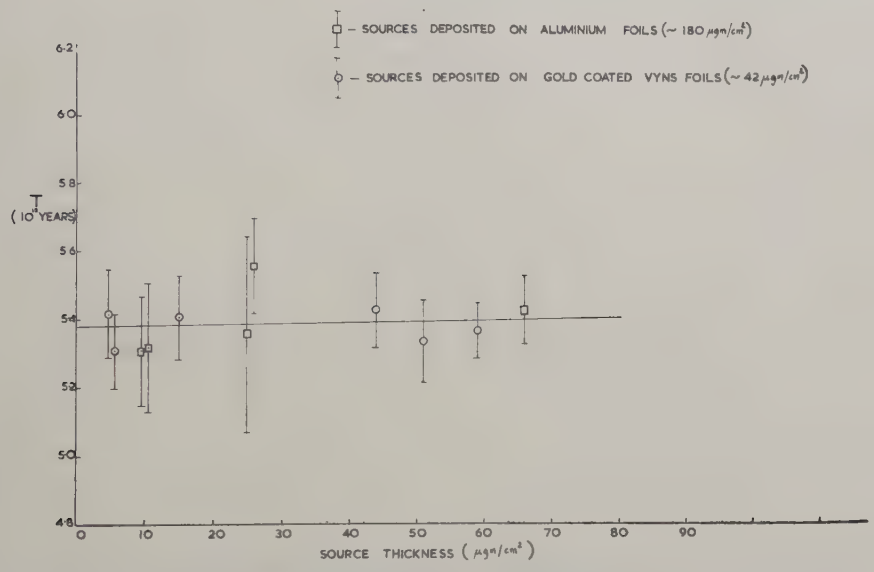

Apparent half-lives of ^{87}Rb corrected for back-scattering and absorption of electrons in the source support.

7.3. *Maximum Possible Half-life*

If we calculate half-lives directly from the apparent 4π count rate we shall obviously get a maximum possible half-life, since we are ignoring support absorption. These half-lives are shown in fig. 3, once more plotted against source thickness. Once again the relationship is a linear one, and by extrapolating to zero we remove the effects of source self-absorption. In this case, however, we get two separate parallel lines and the values measured from sources deposited on aluminium supports show the expected extra absorption over those mounted on thin VYNS plus gold supports.

We find

$$T_{\max} = (5{\cdot}79 \pm 0{\cdot}03) \times 10^{10} \text{ years (aluminium support)},$$
$$T_{\max} = (5{\cdot}53 \pm 0{\cdot}01) \times 10^{10} \text{ years (VYNS + gold support)}.$$

We now have an interesting new possibility for arriving at the half-life of ^{87}Rb without making any assumptions other than that the maximum possible half-life is a linear function of support thickness up to 180 μg/cm^2. This does not appear to be too sweeping an assumption since we know from fig. 2 that the half-life is a linear function of source thickness up to 70 μg/cm If we make this assumption, and extrapolate linearly to zero support thickness, we arrive at a figure for the half-life which should be the true value. We get $5{\cdot}45 \times 10^{10}$ years, which is in reasonable agreement with the value derived from fig. 2, especially as the aluminium leaf was very non-uniform, 180 μg/cm^2 being only an average value for the thickness.

Fig. 3

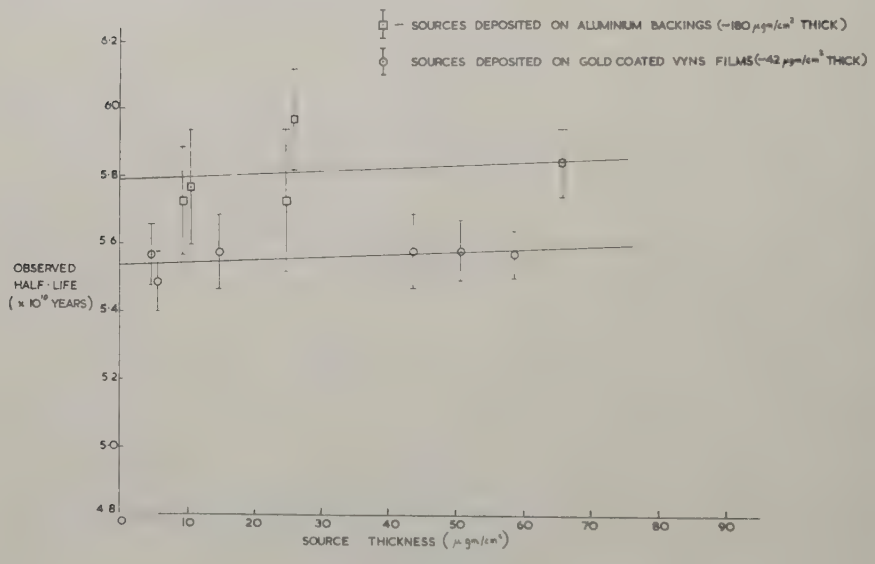

Maximum half-lives calculated from N_s without corrections.

To the measured value of $5{\cdot}37 \times 10^{10}$ years corrections must be made to allow for the effects of dead-time in the registers and for counter geometry, which may be less than the 4π steradians assumed up till now. The geometry factor was estimated in a subsidiary beta–gamma coincidence experiment using ^{203}Hg which has a fairly soft beta spectrum (maximum energy 208 kev, rising steeply at low energies). The corrections for geometry and dead-time amounted to 2% of the experimentally determined half-life.

The error of $\pm 0{\cdot}02 \times 10^{10}$ years which has previously been quoted is calculated on the basis of counting statistics only, but taking into account all possible sources of uncertainty we believe that an error of $\pm 0{\cdot}10 \times 10^{10}$ years is more realistic. We therefore conclude that the half-life of ^{87}Rb is

$$(5{\cdot}25 \pm 0{\cdot}10) \times 10^{10} \text{ years.}$$

§ 8. Discussion

Our value for the half-life of ^{87}Rb is rather higher than the most recent published figures (Flynn and Glendenin 1959, Huster and Rausch 1956, Huster 1957). We believe our value to be genuine but, if it is not, then about the only possible explanation would appear to be losses in the proportional counter caused by quenching of the discharge by gaseous impurities from the counter itself. However, we believe this to be a negligible effect because a plot of total counts against time is strictly linear for periods up to 24 hours, after which slight deviations from linearity become just perceptible. Any one counting period was limited, therefore, to 15 or 16 hours and the counter was refilled before the next run. Secondly,

Fig. 4

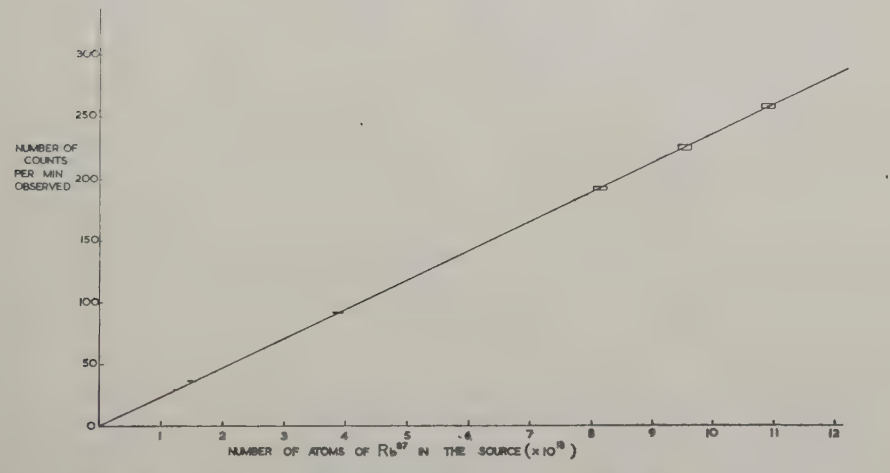

Plot of number of counts observed in sum channel against number of atoms of ^{87}Rb in the source. (i) The experimental values have been adjusted to what would have been obtained had all the rubidium in the source been ^{87}Rb. (ii) The size of the rectangle represents the statistical error in the measurements.

the counter was operated as a continuous flow counter for about half the measurements with complete agreement in the results. Losses in the external pulse registers appear unlikely, because of the correspondence between results from a discriminator and scaler and those from a 100-channel kicksorter. Nor can our high value for the half-life be caused by inactive impurities in the source, since the method of estimating the source measures only the ^{85}Rb and the ^{87}Rb content. We also find complete agreement between values obtained from sources of enriched $^{87}RbCl$ and those from sources of the natural material.

In some of our earlier experiments we found an appreciably higher count rate (and hence lower half-life), than in others. This effect was traced to thorium impurity in the tantalum metal used for the evaporating boats. On

heating the boat, a small quantity of ThB (^{212}Pb), rather less than 10^4 atoms, was deposited on to our source holders. We got round this difficulty by heating the boat to a high temperature before using it to evaporate gold or RbCl, and we checked for freedom from short-lived impurities by counting background and background + source over at least four separate periods of 15 hours each.

An attempt was made to see if there was likely to be any zero point error in the experiment, i.e. a sudden increase in count rate for very thin sources, below our thinnest of just under 5 μg/cm^2. To do so, we have plotted, in fig. 4, the sum count rate obtained (using the VYNS supports) as a function of number of atoms of ^{87}Rb in the source. In order to allow for source thickness, when natural RbCl was used we have scaled up the measured sum count to what would have been obtained if the source had been 100% ^{87}RbCl, and scaled up the number of atoms of ^{87}Rb accordingly. The relationship is linear and extrapolates to pass through the origin as would be expected if there were no zero error.

Acknowledgments

We wish to thank the Director of the Establishment for permission to publish this paper.

We also thank Mrs. R. C. Jeffery for making the isotopic ratio measurements, and Mr. J. P. Franklin for assistance with the experimental work.

Thanks are also due to the Electromagnetic Separation Group, A.E.R.E., Harwell, for the supply of enriched ^{87}Rb.

References

Aldrich, L. T., and Wetherill, G. W., 1958, *Ann. Rev. nucl. Sci.*, **8**, 257.
Curran, S. C., Dixon, D., and Wilson, H. W., 1951, *Phys. Rev.*, **84**, 151.
Flynn, K. F., and Glendenin, L. E., 1959, *Phys. Rev.*, **116**, 744.
Giletti, B. J., 1959, *Nature, Lond.*, **184**, 1793.
Huster, E., and Rausch, W., 1956, reported by Aldrich and Wetherill 1958.
Huster, E., 1957, reported by Aldrich and Wetherill 1958.
Lewis, G. M., 1952, *Phil. Mag.*, **43**, 1070.
MacGregor, M. H., and Wiedenbeck, M. L., 1954, *Phys. Rev.*, **94**, 138.
McNair, A., Glover, R. N., and Wilson, H. W., 1956, *Phil. Mag.*, **1**, 199.
Merritt, J. S., Taylor, J. G. V., and Campion, P. J., 1959, *Canad. J. Chem.*, **37**, 1109.
Nijgh, G. J., Wapstra, A. H., and van Lieshout, R., 1959, *Nuclear Spectroscopy Tables* (Amsterdam : North-Holland Publishing Co.), p. 41.
Pate, B. D., and Yaffe, L., 1955, *Canad. J. Chem.*, **33**, 15.

The Solar Diurnal Variation of Cosmic Rays during 1958 and 1959, at Makerere, Hermanus and Herstmonceux†

By D. M. Thomson
Physics Department, Makerere College, Kampala, Uganda

[Received November 21, 1960]

Abstract

The results of observations of the solar diurnal variation in cosmic radiation at Makerere (East Africa), Hermanus (South Africa), and Herstmonceux (England) are presented for the years 1958 and 1959. The average amplitude and phase of the 24 hr component of the variation were obtained at each station and the relative values were compared with the values predicted by two types of modulation of the primary spectrum. In the first case a modulation of the type $\Delta n(P)/n(P)=a\,.\,P^{-1}$ was considered where P is the magnetic rigidity of the primary particle. The best account of the main features of the observations was given if the modulation was effective for rigidities in excess of a cut-off value which averaged 15 GV, the value of a being 0·236, and if the direction of maximum modulation was 79°, to the east of the sun–earth line.

In the second case the primary spectrum was considered to be modulated in the manner suggested on theoretical grounds by Elliot (1960).

Neither model gives complete agreement with observation.

§ 1. Introduction

In recent years a number of workers (e.g. Dorman 1957) have attempted to explain the diurnal variation in cosmic rays, which is observed by monitors at ground level, in terms of an anisotropy produced by some means in the region outside the earth's magnetic field. In this paper an attempt is made to find out to what extent two simple types of modulation of the primary cosmic ray spectrum can account for the solar diurnal variations in cosmic-ray intensities observed at Makerere, Hermanus and Herstmonceux during 1958 and 1959.

These stations were chosen for comparison because they differ so widely in latitude but lie in a comparatively narrow band of longitude. Also the equipment used at Makerere is closely similar to that at Herstmonceux.

§ 2. Observations

2.1. *Meteorological Effects on Cosmic-ray Intensities at Makerere*

A standard neutron monitor and standard cubical meson telescopes have been in operation at Makerere College (geographical coordinates 0°20·2′ N, 32° 33·8′ E, conventional geomagnetic coordinates −2° lat., 101·4° long.) since the beginning of 1958. The neutron monitor has been calibrated from time to time with a Ra–Be neutron source and has shown a long-term

† Communicated by the Author.

stability in sensitivity within 0·5%. The data from both monitors have been corrected in the usual way for variations in barometric pressure. The locally determined pressure coefficient for the neutron monitor is −0·71% per millibar, and for the meson telescope −0·16% per millibar. Some care is needed in deriving the barometric correction to cosmic-ray data at an equatorial station. This is because the atmospheric tides are the predominant cause of pressure variations in the tropics, and the barometric pressure, as a result, has a well-marked diurnal and semi-diurnal rhythm. Changes in the mean daily pressure from day to day are usually less than the range of the diurnal variations in pressure. The barometric coefficients at Makerere were determined by means of a partial correlation between the daily mean pressure at Makerere, the daily total recorded by the cosmic-ray monitor at Makerere, and the daily total, corrected for barometric effects, recorded by the Herstmonceux neutron monitor. The use of the Herstmonceux data in the analysis enabled us to take most of the primary variations into account. Data for a period of over one year were used.

A spurious component of diurnal variation can remain in the pressure corrected data if a barograph is used for measuring the pressure. This is because there may be a systematic time-lag in the pressure measurements due to pen friction. During 1958 pressure data from a local meteorological station were employed at Makerere and these, being derived from readings of a mercury barometer, should be free from this error.

Another meteorological factor whose diurnal variation is greater, as a rule, than the variation in daily mean at Makerere, is the local temperature. In the analysis of the daily variation of the pressure-corrected neutron component at Makerere in 1958 it was found that the amplitude (0·43%) seemed to be greater than that found at other equatorial stations such as Huancayo (0·22%), and also rather anomalously larger than the amplitude of the variation of the meson component at Makerere. Though Simpson (1953) has shown that a standard neutron monitor has only a very small local temperature coefficient, it was suspected that the Makerere neutron monitor may have been affected by a temperature coefficient possibly mainly due to effects on the electronic recording equipment. The range of local temperature in the cosmic-ray laboratory could be as high as 6°C on an exceptional day and on the average the daily range was between 3 and 4°C. Careful tests using a standard neutron source and artificially increasing the temperature range in the laboratory showed that the temperature effect on counting rate was of the order of ($-0{\cdot}02 \pm 0{\cdot}01$% per °C). This effect was such as to reduce the observed diurnal variation below its true value but no correction has been made for this. The geiger-counter trays were enclosed in thermostatically controlled enclosures, and the efficiencies of the geiger counters for meson detection should be close to 100% over their sensitive volume, so long as the supply voltage remains in the middle of the counter plateau. There should not, therefore, be any instrumental temperature effect on the meson counting rate.

Fig. 1

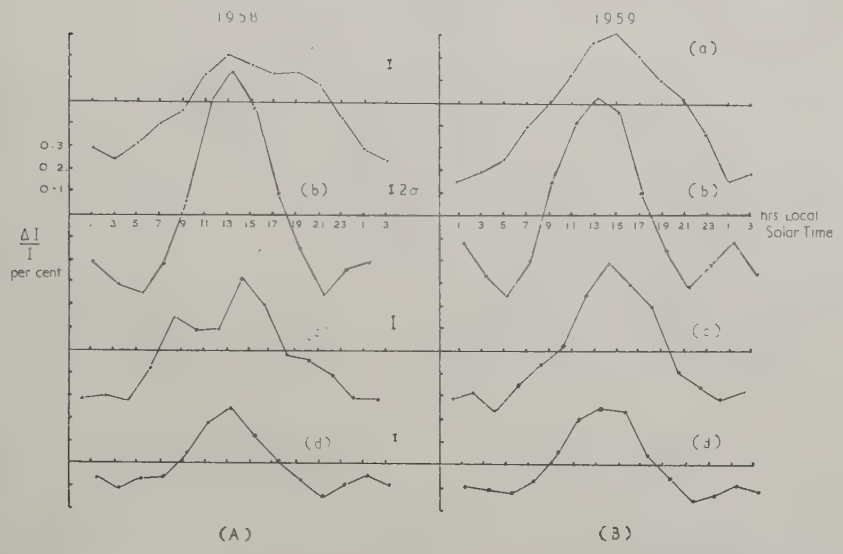

Annual mean solar diurnal variations in cosmic-ray intensities 1958 and 1959. (*a*) Herstmonceux neutrons, (*b*) Makerere neutrons, (*c*) Hermanus neutrons, (*d*) Makerere mesons.

Fig. 2

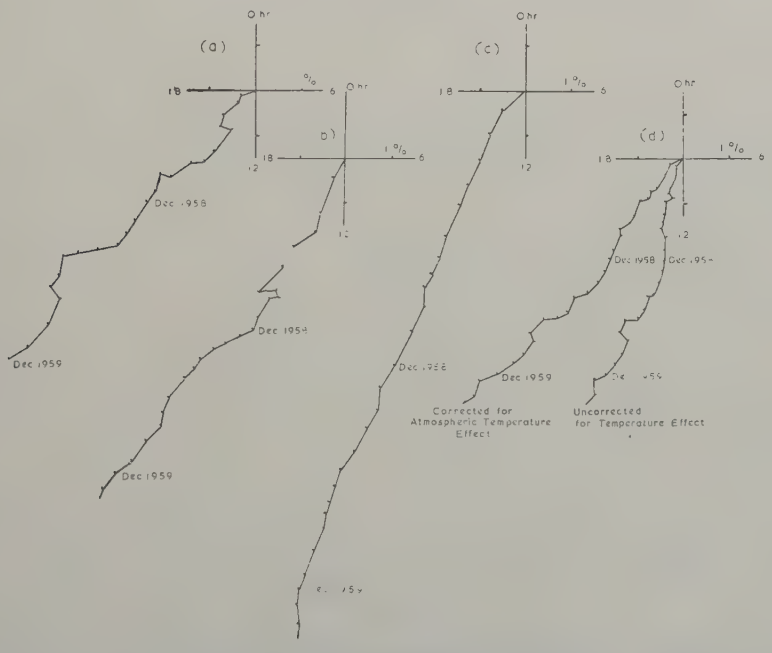

Harmonic dial vector-sums of the monthly mean 24 hr component of the solar diurnal variations 1958 and 1959. (*a*) Herstmonceux neutrons, (*b*) Hermanus neutrons, (*c*) Makerere neutrons, (*d*) Makerere mesons.

Dorman (1957, 1959) has explained how the diurnal variation of the meson component of the cosmic radiation should be affected by diurnal temperature changes in the atmosphere. He has shown how corrections may be worked out from a knowledge of the heights of the isobaric levels. During most of the period of this work the only place where atmospheric soundings were undertaken in East Africa was at Nairobi, over 350 miles from the cosmic-ray station. As a rule flights were made only once every 24 hrs at night. On selected days two flights were made but always at the same times. It is therefore not possible to know in detail how the heights of the isobaric layers vary during the 24 hrs.

Quenby and Thambyahpillai (1960) have worked out the temperature effect at Huancayo. It has a maximum at about 05·30 hrs local time and amplitude 0·11%. This has been used in correcting the Makerere data, in tables 1 and 2.

2.2. *Corrected Diurnal Variations and Harmonic Analysis*

The annual mean diurnal variations, corrected for barometric effects, in the neutron and meson components at Makerere and the neutron components at Herstmonceux and Hermanus are shown in fig. 1. Figure 2 shows vector sums of the monthly averages of the 24 hr waves for the same components. In both diagrams the times are local solar times. In computing the data for these diagrams some days, including those at the beginning of Forbush-type decreases, or showing pronounced magnetic activity have been omitted. Sandström (1959) has shown that this does not in general greatly affect the long-term average amplitude and phase of the 24 hr wave.

Table 1 summarizes the results of harmonic analysis for the 24 hr and 12 hr wave for the components considered. The errors given after the amplitudes of the variations have, for the neutron component, been taken as $1{\cdot}3\sigma$ where σ is the standard deviation calculated from the counting statistics (McCracken 1958).

The Makerere meson data are shown in table 1 both with and without the correction for the temperature effect. The errors shown are standard deviations calculated from counting statistics only.

The following features of the results may be noted:

1. There appears to be a greater variability in the amplitude and phase of the 24 hr component at the middle latitudes (Herstmonceux and Hermanus) than at the equatorial station (Makerere). This is revealed by fig. 2.

2. The semi-diurnal component is larger and more significant at Makerere than at the other stations. It does not appear to be significant at all equatorial stations; Huancayo shows a much smaller effect (0·06%). Katzman and Venkatesan (1960) have argued that the entire semi-diurnal variation of neutrons observed at some equatorial stations is due to residual barometric effects. This conclusion is disputed here for two reasons. Firstly, a significant semi-diurnal component in the

Table 1. Results of harmonic analysis of diurnal variations in cosmic-ray intensity. (All times given in local solar time.)

Monitor	24 hr component		12 hr component	
	Amplitude (%)	Time of max. (hr)	Amplitude (%)	Time of max. (hr)
1958				
Makerere neutron	$0{\cdot}43 \pm 0{\cdot}02$	$13{\cdot}5 \pm 0{\cdot}1$	$0{\cdot}21 \pm 0{\cdot}02$	$1{\cdot}2 \pm 0{\cdot}3$
Hermanus neutron	$0{\cdot}25 \pm 0{\cdot}01$	$12{\cdot}7 \pm 0{\cdot}2$	$0{\cdot}00 \pm 0{\cdot}01$	
Herstmonceux neutron	$0{\cdot}21 \pm 0{\cdot}01$	$15{\cdot}3 \pm 0{\cdot}2$	$0{\cdot}03 \pm 0{\cdot}01$	$9{\cdot}6 \pm 1{\cdot}2$
Makerere meson (no temperature correction)	$0{\cdot}15 \pm 0{\cdot}01$	$12{\cdot}7 \pm 0{\cdot}2$	$0{\cdot}08 \pm 0{\cdot}01$	$1{\cdot}3 \pm 0{\cdot}3$
Makerere meson (temperature corrected)	$0{\cdot}21 \pm 0{\cdot}01$	$14{\cdot}7 \pm 0{\cdot}2$	$0{\cdot}08 \pm 0{\cdot}01$	$1{\cdot}3 \pm 0{\cdot}3$
1959				
Makerere neutron	$0{\cdot}40 \pm 0{\cdot}02$	$13{\cdot}6 \pm 0{\cdot}1$	$0{\cdot}18 \pm 0{\cdot}02$	$1{\cdot}1 \pm 0{\cdot}3$
Hermanus neutron	$0{\cdot}28 \pm 0{\cdot}01$	$14{\cdot}6 \pm 0{\cdot}2$	$0{\cdot}08 \pm 0{\cdot}01$	$2{\cdot}8 \pm 0{\cdot}5$
Herstmonceux neutron	$0{\cdot}30 \pm 0{\cdot}01$	$14{\cdot}8 \pm 0{\cdot}1$	$0{\cdot}01 \pm 0{\cdot}01$	
Makerere meson (no temperature correction)	$0{\cdot}18 \pm 0{\cdot}01$	$13{\cdot}5 \pm 0{\cdot}2$	$0{\cdot}09 \pm 0{\cdot}01$	$1{\cdot}7 \pm 0{\cdot}3$
Makerere meson (temperature corrected)	$0{\cdot}25 \pm 0{\cdot}01$	$14{\cdot}5 \pm 0{\cdot}2$	$0{\cdot}09 \pm 0{\cdot}01$	$1{\cdot}7 \pm 0{\cdot}3$

Makerere barometric pressure			
24 hr component		12 hr component	
Amplitude (mb)	Time of min.	Amplitude (mb)	Time of min.
1·07	21·52	0·99	4·17

cosmic-ray intensity is found at Makerere for both neutron and meson components, and the ratio between the amplitudes of the semi-diurnal and diurnal variations is similar for the two components despite the difference in pressure coefficients. Secondly, the phase of the maximum of the residual semi-diurnal variations in the neutrons at Makerere differs from that of the minimum of the semi-diurnal pressure wave by almost 90°. This corresponds to a time interval of 3 hrs, which is more than could be accounted for by possible barograph errors.

3. The amplitude of the 24 hr wave at Herstmonceux was larger during 1959 than in 1958. The change in amplitude at Makerere was smaller but in the opposite sense. This indicates a change in the rigidity or energy dependence of the modulating mechanism responsible for the variation.

4. The time of maximum of the 24 hr wave at Makerere is more than 1 hr earlier than the time of maximum at Herstmonceux. The time of maximum of the 24 hr wave at an equatorial station produced by a modulating field system at a fixed orientation with respect to the sun–earth line is sensitive to the rigidity or energy dependence of the modulation. At latitudes above 50° the dependence is much less, owing to the focusing effect of the earth's magnetic field for particles of rigidities between 10 and 30 GV which arrive at these latitudes. This has already been pointed out by a number of observers including Dorman (1957).

§ 3. Calculation of the Effect of Primary Modulations

3.1. *Effective Aperture of Cosmic-ray Monitors*

In attempting to see how far the daily variations in cosmic-ray intensities recorded at different stations can be related to a common mechanism it is necessary to investigate the effect of the angular aperture over which a particular type of monitor accepts the incoming particles, and also to consider the effect of the earth's magnetic field on the trajectories of the particles.

The angular apertures of the monitors were considered first. In the case of the neutron monitor it was assumed that the angular aperture of a monitor deep in the atmosphere is determined only by the atmospheric absorption, and that the secondary particles detected by the monitor retain the direction of motion of the incoming primary as they pass through the atmosphere. Exponential absorption of the nucleonic component was assumed, and the characteristic thickness in which the intensity is reduced by a factor $1/e$ was taken as 140 g/sq. cm. The resultant sensitivity per unit angular range at the top of the atmosphere of a neutron monitor at sea level is shown in fig. 3 (A). It is clear that this is only a first approximation to the correct angular aperture, since there must be appreciable scattering of the particles which form the nuclear cascade. One would expect this to be more important for particles arising from the interactions of the low energy primaries since at high energies relativistic effects limit scattering angles in the laboratory frame

of reference. It will appear later that the diurnal variation appears to affect mainly those primaries whose magnetic rigidities exceed 15 GV. For such particles half the nucleons emitted from elastic nucleon–nucleon collisions must lie within a cone of half-angle of about 20° about the direction of the incident particle. Particles emitted from inelastic collisions, and which are sufficiently energetic to propagate the cascade, are likely to be emitted in a narrower cone.

Fig. 3

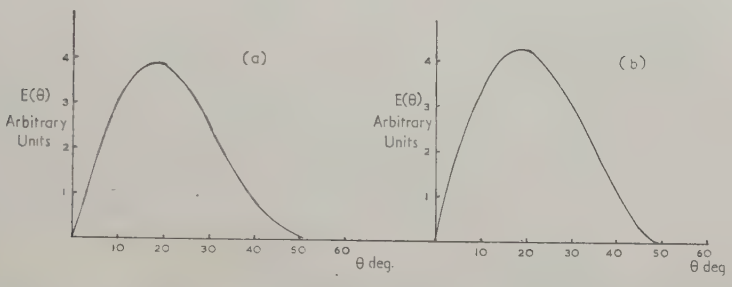

Acceptance apertures of cosmic-ray monitors at sea level. (*a*) Neutron monitor, (*b*) Meson monitor. For an isotropic distribution of particles at the top of the atmosphere the number of counts due to particles incident at angles between θ and $\theta+d\theta$ to the zenith, is proportional to $E(\theta)\,d\theta$.

It is reasonable to expect that it will be the first few interactions of obliquely incident primaries near the top of the atmosphere which will contribute most to widening the effective aperture of a monitor at sea level. Secondary particles from such interactions which travel in directions nearer the vertical than the incident primary will contribute more to the monitor counting rate than those preserving the original direction, because of their reduced absorption. A change of direction late in the nuclear cascade will be less effective because of the greater atmospheric absorption before the scattering occurs. As a rough estimate one might expect angles of up to 40° between the primary and secondary trajectories. Simple arguments show that the amplitude of the diurnal variation should be multiplied by a factor of the order of $\sin\phi/\phi$ where ϕ is a typical angle between primary and secondary trajectories. When $\phi=40°$ this factor is $\sim 0{\cdot}9$ and the observed amplitude will be 10% less than if there were no atmospheric scattering.

This estimate shows that the recorded diurnal variation is in any case comparatively insensitive to the exact form of the effective aperture of the monitor until it becomes comparable with 2π.

In the case of cubical meson telescopes it was assumed that the angular aperture was as described by Parsons (1957) and shown in fig. 3(b).

In the following calculations these acceptance curves were approximated by dividing the solid angle over which particles are accepted into sections centred at 0°, 16°, 32°, and 48° to the vertical (zenith), and an average

sensitivity was taken for each section. The geomagnetic effect on the particle trajectories varies not only with the angle the incident particle makes with the zenith, but also with the azimuthal angle. A rather crude allowance has been made for this by dividing each section of the acceptance cone centred round one of the standard zenith angles into four parts, centred on the azimuth directions N, S, E and W and taking the central trajectories as typical.

3.2. *Geomagnetic Effects*

The complicated problem of transforming the distribution of particle trajectories which affect a monitor deep in the atmosphere was thus approximated and simplified to the problem of tracing a few standard trajectories to infinity, through the earth's magnetic field. This was done with the aid of the curves presented by Brunberg and Dattner (1953) and set out in a review article by Singer (1958). These curves give the two coordinates of the asymptotic velocity vector; the north latitude ϕ_N, and ψ_E the longitude angle measured towards the east from the observer's meridian plane.

The yield functions worked out by Webber and Quenby (1959) were used in calculating the contributions to the counting rates due to particles of different rigidities.

Hence it was possible to calculate the contribution to the counting rate of a particular monitor made by one primary particle of magnetic rigidity P incident on the earth's magnetic field from an asymptotic direction determined by ϕ_N and ψ_E. In order to proceed further and attempt to locate the asymptotic direction of the source of the modulation of intensity of the primary cosmic rays which produces the daily variation observed by the monitors at sea level, it is necessary to make some assumption about the rigidity dependence of the modulation.

3.3. *Choice of Primary Modulation Spectrum*

Dorman (1957) following Alfven (1950) suggested that the main contribution to the modulation arises from streams of ionized matter proceeding outward from the sun and carrying frozen-in magnetic fields. If it be assumed that the undisturbed primary cosmic-ray differential rigidity spectrum is of the form

$$n(P)\,dP = AP^{-\nu}\,dP \text{ per unit solid angle} \quad . \quad . \quad . \quad . \quad (1)$$

and supposed that for particles of particular magnetic rigidity P the rigidity increases by ΔP on crossing the stream, then it can be shown that the effects due to deflection of the trajectories, and the change in rigidity on crossing the stream, combine to increase the intensity in the range of rigidity P to $P+dP$ in such a way that

$$\frac{\Delta n(P)}{n(P)} = \text{const.}\,\frac{(\Delta P)}{P} \quad . \quad . \quad . \quad . \quad . \quad (2)$$

If further, as in the simplest model, the electric field in the stream increases

the energy of all the particles by the same amount ΔE, a simple transformation shows that the change in rigidity ΔP will also be almost constant.

Over most of the relevant part of the cosmic-ray primary spectrum the relative change in intensity is therefore approximately given by

$$\frac{\Delta n(P)}{n(P)} = \frac{a}{P}. \qquad (3)$$

There is some empirical evidence in favour of this modulation spectrum in that it seems to be of the right type to explain long-term changes in average cosmic-ray intensities, though the long-term changes do not seem to need the low rigidity cut-off found necessary in attempting to account for the diurnal effect (McDonald and Webber 1959).

Additional calculations were made using the modulation spectrum worked out by Elliot (1960). Elliot assumed that the diurnal variation arises from the action of a solar dipole field.

3.4. *Comparisons with Observations*

Relative total undisturbed average intensities for the various monitors were calculated using the modified primary spectrum at solar maximum given by McDonald (1959) and geomagnetic cut-offs based on those given by Quenby and Webber (1959) for vertical incidence. At the equator the cut-off varies markedly with angle of incidence and this was allowed for. The primary spectrum was combined with the yield functions and angular acceptance factors mentioned above to determine the relative counting rates of the monitors.

Dorman (1957) has shown that, in order to account for the amplitudes and phases of the 24 hr component of the diurnal variation of cosmic rays seen by monitors at different latitudes, using the P^{-1} modulations, it is necessary to apply to the modulation spectrum $\Delta n(P)$ a low rigidity cut-off higher than that determined by the earth's magnetic field at middle or high latitudes. He attributes this cut-off to the finite thickness of the corpuscular streams which produce the modulation. Particles with less than a certain minimum rigidity will be reflected from the streams with unchanged rigidity. Invoking Liouville's theorem for such particles he predicted that their intensity at the upper boundary of the atmosphere and their isotropy will not be affected by this process. The required cut-off rigidity is determined empirically so that the predicted ratio of the amplitudes of the 24 hr variation in intensity of cosmic radiation at different stations is as near as possible to that found experimentally. The same cut-off is then applied at other stations and predictions compared with observations.

In the present work the amplitude and phase of the 24 hr wave in neutron intensity at Herstmonceux in 1959 were taken as standard. It was found that the other data could best be accounted for by assuming a low-rigidity cut-off of 15 GV for the modulation. The results are rather insensitive to the value of this cut-off within 2 or 3 GV.

It was supposed that the field system giving rise to the 24 hr component applies to the intensity of particles arising from asymptotic directions whose longitude measured to the east from local zenith is ψ_E, a modulation of the form:

$$\Delta n(P,t,\psi_E)=(A/P)[\cos(15(t-12)+\psi_E-\alpha)n(P,\psi_E)] \quad (4)$$

where t is the local solar time in hours and α is the angle between the sun–earth line and the effective centre of the modulating field system (see fig. 4). When expression (4) is multiplied by solid angle and yield functions, and integrated over all values of P above cut-off, and over ψ_E the result is of the form

$$\Delta N/N=\text{const.}\cos[15(t-12)+\bar{\psi}_E-\alpha] \quad . \quad . \quad . \quad (5)$$

where $\bar{\psi}_E$ is an effective average value of ψ_E for the particular monitor and the particular type of modulation spectrum chosen. The maximum

Fig. 4

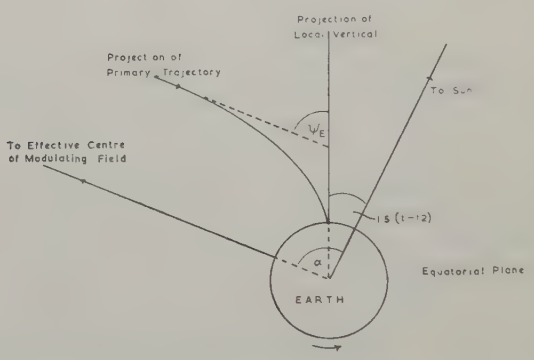

Diagram showing the relation of the direction of maximum modulation to the sun–earth line and local vertical.

amplitude of the variation will be achieved when the argument of the cosine is zero, i.e. when

$$t=t_{\max}=12+\frac{\alpha-\bar{\psi}_E}{15}\text{ hrs.} \quad . \quad . \quad . \quad . \quad . \quad . \quad (6)$$

$\bar{\psi}_E$ was found for each monitor as follows.

The counting rate, in arbitrary units, produced by the modulating spectrum of primaries was worked out for the primaries arising from each ten degree longitude belt in ψ_E.

The totals in each longitude belt were then multiplied by a factor $\cos(\psi_E+\theta)$ where θ was arbitrarily chosen, and the results summed. This is a numerical approximation to an integration. The summation was done for several different values of θ. From the results the value of θ which makes the sum a maximum was found by interpolation. This value of θ equals $\bar{\psi}_E$. The constant was found from the maximum amplitude of the variation at Herstmonceux.

Table 2

Monitor	ψ_E		Amplitude of 24 hr wave (%)				Time of maximum (hrs, local time)			
			Predicted		Observed		Predicted		Observed	
	A	B	A	B	1958	1959	A	B	1958	1959
Herstmonceux neutron	39°	42°	0·30*	0·59	0·21	0·30	14·8*	15·2	15·3	14·8
Hermanus neutron	47·5°	68°	0·29	0·54	0·23	0·28	14·2	13·5	12·7	14·6
Makerere neutron	75·5°	84°	0·33	0·41	0·43	0·40	12·4	12·4	13·5	13·6
Makerere meson	67·5°	79°	0·20	0·24	0·15	0·18	12·9	12·8	12·7	13·5
Makerere meson (temperature corrected)					0·21	0·25			14·7	14·5

Columns labelled A: $\Delta n(P)/n(P) = 0{\cdot}236/P$, $P > 15$ GV
$= 0$ $P < 15$ GV.

Columns labelled B: Spectrum modulated in the manner suggested by Elliot (1960).
Values shown with an asterisk were used in fitting the parameters.

The value of $\bar{\psi}_E$ thus found was substituted in eqn. (6) together with the value of t_{max} for the Herstmonceux neutron monitor, found experimentally, in order to find α.

Using eqn. (6) for the other monitors, with the appropriate value of $\bar{\psi}_E$, and the value of α found as stated above, expected times of maximum at the other monitors were calculated. In these calculations no account was taken of the possible variation of the modulation with celestial latitude. Dorman (1957) gives an estimate of this which shows that there may be a significant reduction in amplitude at angles greater than 20° to the ecliptic.

The inclination of the earth's axis of rotation and the axis of its magnetic dipole to the ecliptic was also neglected. If this is taken into account, and if the modulation amplitude varies as the cosine of the celestial latitude, the calculated values of the mean diurnal amplitudes over a solar year should be reduced by some 7%.

In table 2 the predicted values of amplitude and times of maximum predicted by both types of modulation of the primary spectrum are given.

§ 4. Discussion

It is difficult to assign standard errors to the predicted values of amplitude and time of maximum contained in table 2. The estimation of these values involves a number of stages and a number of approximations whose accuracy is not easy to determine. In particular the earth's magnetic field has been assumed to be that of a simple dipole when working out the deflections of cosmic-ray trajectories. It is certain that this is not a good approximation, particularly in the neighbourhood of Hermanus (Quenby and Webber 1959). Errors in the times of maximum can also arise through the grouping of trajectories at an average ψ_E which in fact must be spread over a finite range. Dorman (1957) estimated the accuracy of his predictions of the time of maximum of the daily variation by a similar method at $\pm 0{\cdot}5$ hr. If we assume that the error can be approximated by a variation of random phase superimposed on the calculated value, the error in the predicted amplitude corresponding to a phase error of 0·5 hr would be in the region of 10%.

Another difficulty, in comparing the Hermanus data with those from the other stations, arises from the fact that the average latitude of origin ϕ_N for particles affecting a monitor is different at Hermanus from what it is at Herstmonceux and Makerere. The majority of particles responsible for the daily variation at Makerere and Herstmonceux, according to our assumptions, arise within a few degrees north and south of the plane of the magnetic equator. Particles incident at Hermanus arise, on the average, some 20° north of the equatorial plane, and cross the equatorial plane on their path to the earth. The average modulating amplitude for these particles will therefore be some 6% less than that which is effective for Herstmonceux and Makerere, if the amplitude falls off as $\cos\phi$. This has not been allowed for in the tabulated values.

With these considerations in mind it is possible to make a critical examination of table 2.

Agreement between the observations and the amplitudes calculated from the P^{-1} modulation spectrum is better for 1958 than for 1959. However, the calculated amplitude at Makerere is smaller, as compared with that at Herstmonceux, than is observed. Only relative amplitudes are significant in this case.

In the case of the spectrum proposed by Elliot (1960) absolute values of the variation are predicted. The previous discussion of the effect of atmospheric scattering and of the inclination of the axis of the magnetic dipole of the earth to the ecliptic shows that the tabulated amplitudes should perhaps be reduced by between 15 and 20%. This still leaves a significant discrepancy with the Herstmonceux data and with the relative amplitudes at the three stations.

It may be that both the modulation spectra which have been considered are weighted too strongly in favour of low rigidities. Below about 30 GV a monitor at 50° N is sensitive predominantly to primaries arising within 10° of the geomagnetic equator and scans a latitude belt very similar to that scanned by an equatorial monitor. Above about 30 GV this similarity ceases, and the relative amplitudes of the variations at the two stations become more dependent on the ϕ-dependence of the primary modulation, which could well reduce the relative amplitude at 50° N as required by the data.

On the other hand the fact that the average times of maximum for neutrons differ by over one hour indicates that the mean rigidity cannot be greatly in excess of 30 GV.

Evidence from underground experiments (Sandor 1960) confirms that primaries of 30 GV or more are subject to diurnal variations to an appreciable extent.

Since the period surveyed in this study, the diurnal variation at Makerere has decreased in amplitude and the maximum has moved to an earlier time. The average amplitude between April 1959 and April 1960 was 0·35% and the time of maximum was 13·1 hrs. This is consistent with a reduction in the mean rigidity of the modulated particles, as solar activity declined.

Any adequate account of the daily variation must of course take account of the great variability of the effect from day to day. In discussing average values over periods of one year, one makes the assumption that the disturbances which produce the variability average out, but this is almost certainly an oversimplification.

Acknowledgments

I am grateful to Mr. A. M. van Wijk of Hermanus and Mr. D. R. Palmer of Herstmonceux for supplying cosmic-ray data from their respective observatories, also the East African Meteorological Department for the supply of radio-sonde and other data. The Makerere cosmic-ray observatory was set up as part of the British contribution to the

International Geophysical Year, and was supported financially by the British National Committee for the IGY, through the agency of the Royal Society.

During 1959 the Royal Society made a further generous grant from its Warren Research Fund, which made possible the employment of Mr. Kazibure, who assisted with the maintenance of the Makerere Cosmic-ray Observatory and with some of the computations.

Mr. J. Coggins gave valuable assistance with the construction of the equipment at Makerere.

References

Alfven, H., 1950, *Cosmical Electrodynamics* (Oxford).
Brunberg, E. A., and Dattner, A., 1953, *Tellus*, **5,** 135.
Dorman, L. I., 1957, *Cosmic Ray Variations* (Moscow: State Publishing House for Technical and Theoretical Literature).
Dorman, L. I., 1959, *Trudy ya Fan, Physics*, Ser. 3.
Elliot, H., 1960, *Phil. Mag.*, **5,** 601.
Katzman, J., and Venkatesan, D., 1960, *Canad. J. Phys.*, **38,** 1011.
McCracken, K. G., 1958, Thesis, University of Tasmania.
McDonald, F. B., 1959, *Phys. Rev.*, **116,** 462.
McDonald, F. B., and Webber, W. R., 1959, *Phys. Rev.*, **115,** 194.
Parsons, N. R., 1957, *Rev. sci. Instrum.*, **4,** 265.
Quenby, J. J., and Webber, W. R., 1959, *Phil. Mag.*, **4,** 90.
Quenby, J. J., and Thambyahpillai, T., 1960, *Phil. Mag.*, **5,** 585.
Sandor, T., Somogyi, A., and Telbisz, F., 1960, *Nuovo Cim.*, **17,** 1.
Sandstrom, A. E., and Lindgren, S., 1959, *Ark. Fys.*, **16,** No. 12.
Simpson, J. A., Fonger, W., and Treiman, S. B., 1953, *Phys. Rev.*, **80,** 934.
Singer, S. F., 1958, *Progress in Elementary Particle and Cosmic Ray Physics*, Vol. IV (Amsterdam : North Holland Publishing Co.).
Webber, W. R., and Quenby, J. J., 1959, *Phil. Mag.*, **4,** 654.

Helical Dislocations in Crystals of Lead Iodide†

By A. J. Forty
H. H. Wills Physics Laboratory, University of Bristol

[Received October 23, 1960]

Abstract

The appearance of ' zig-zag ' dislocation lines during the decomposition of crystals of lead iodide in the electron microscope can be explained by the climb of existing dislocations into a flattened helical form. The simple zig-zags are often distorted into cusped and looped forms and it is shown how these distortions may be accounted for by the elastic interaction between neighbouring segments of the helices. Such internal re-arrangement within helices is possible only as a result of the marked anisotropy of climb and glide processes in these particular crystals. The climb of arrays of dislocations leads to interactions between neighbouring helices. Some examples of such interaction are described and it is shown how these may lead to the formation of isolated loops of dislocation and double helices. An examination of the nature of loops formed in this way suggests an interesting possibility for the creation of new regenerative sources of glissile dislocations.

§ 1. Introduction

Some preliminary observations on the mode of decomposition of lead iodide crystals under irradiation in an electron microscope have already been described in a previous paper (Forty 1960). As reported there, it is possible to classify the events leading to complete decomposition according to a number of stages in the process, and the first of these is one of structural re-arrangement within the crystal. At this stage the distribution and configuration of arrays of dislocations already existing in the crystals changes in detail and, at the same time, new loops of dislocation begin to appear. The configurational changes can be accounted for by considering that the dislocations are climbing out of their glide planes and this, together with the observations of loop formation, may be taken as evidence that point defects are being created within the crystal during the electron bombardment. The climb of the dislocations appears to proceed along certain preferred planes. The orientation of these planes in the crystal structure suggests very strongly that the point defects involved in the process are molecular vacancies (i.e. PbI_2 vacancies or associated complexes of lead and iodine ion vacancies) which are probably created thermally as a result of the heating of the crystal by the electron beam.

† Communicated by the Author.

One of the most interesting features of the initial phase is the formation of 'zig-zag' dislocation lines. Simple examples of these have already been described and discussed in the previous paper. They are thought to be the projected images of segmented or flat helices whose axes lie in the plane of the crystal, and which have been developed by the climb of dislocations originally lying in this plane and predominantly in the screw orientation. In general, the forms of these helices are more complex than those which might be expected for more isotropic crystals, and it is the main purpose of this paper to describe the various forms which have been observed and to attempt to relate these to the crystallographic features of climb and glide processes in the hexagonal structure of lead iodide.

The basic unit in the lead iodide structure may be described as a sandwich of divalent lead ions between two close-packed layers of iodine ions. The hexagonal structure is built by stacking these sandwiches in the *c*-direction. In this paper, however, we find it most convenient to describe the structure as a hexagonal close-packing of iodine layers with the smaller lead ions filling one-half of the octahedral positions between alternate layers. Thus, all planes and directions in the lattice may be indexed simply in the h.c.p. system, a procedure which will be adopted throughout the following discussion. One feature of the structure which deserves emphasis at this stage, since it relates the observed climb planes with the production of molecular vacancies, is the observation that low-index planes having molecular composition are limited to two kinds. These are the basal planes, which contain PbI_2 sandwiches, and the first order pyramidal planes $\{10\bar{1}1\}$, which are followed closely by slightly corrugated PbI_2 layers. The climb of the dislocations appears to be restricted to follow these planes and this might reflect the ease with which molecular vacancies can be created or moved in them. Moreover, in such a structure easy glide occurs in one plane only, namely the basal plane where glide presumably proceeds most readily between the neighbouring iodide layers which are not separated by the interstitial lead ions. The restrictions on climb and glide of dislocations thus imposed by the crystal structure can account for many of the configurations observed and described in the following section.

§ 2. The Observations

Techniques for preparing the crystals and detecting dislocations in them have been described already in the earlier paper (Forty 1960). It is convenient, however, to give a further brief account here. Crystals thin enough for direct transmission electron microscopy can be grown from a solution of the re-crystallized salt in aqueous alcohol by just saturating the solution at 100°C and allowing this to cool slowly to room temperature. It is found that, whereas the thicker crystals precipitate to the bottom of the container, those which are thin enough for this work remain floating as very thin platelets on the surface of the solution. These can be collected

on a microscope specimen grid for direct observation without further preparation. The observations described here have all been made with specimens prepared in this way and examined in the standard Philips electron microscope operating at 80 kv.

It is found that, although a few of the crystals appear to be free of dislocations, many of them contain extensive arrays which appear to lie in the plane of the platelet and have Burgers vectors lying in this plane (i.e. in the basal plane). These are introduced by deformation during mounting. Clearly the geometrical conditions are ideal for observing any climb out of the basal plane which may occur to modify the shapes of the dislocations. The geometrical conditions are also extremely favourable for observing glide processes in these crystals; a feature which can be exploited and which will be discussed more fully in a later paper.

After a short period of exposure to the electron beam the crystals begin to undergo some structural rearrangement. At this stage the dislocations lose their initially smooth appearance to take up more complex configurations. Figure 1†, for example, shows part of a crystal in which a simple network of dislocations has become distorted in this way. It will be noticed that the basic feature in this pattern is the zig-zag. Similar shapes have been observed by Thomas and Whelan (1959) in their investigation of the climb of dislocations in quenched aluminium/copper alloys. These have been attributed to the formation of helical dislocations by the condensation of vacancies on screw dislocations, and it seems reasonable that a similar interpretation might be applied to our present case. As pointed out by Thomas and Whelan, a simple circular helix viewed at right angles to its axis should be projected as a sine waveform. Variations from sinusoidal form can be expected if the helix is not circular or if it is not viewed at right angles. The extreme sharpness of the zig-zags in lead iodide in fact lead us to the conclusion that, if they represent helices, these must have a flattened cross section with long segments lying in the basal plane and shorter segments lying in some plane, probably one of the $\{10\bar{1}1\}$ planes, inclined to this. Such a form is drawn in perspective in fig. 4 (*a*) where the different thicknesses of line are intended to represent segments at different levels in the crystal. This conclusion is also necessary on geometrical grounds if helices having projected widths equal to those of the zig-zags (i.e. about 5000 Å) are to be accommodated in a platelet whose thickness is only a fraction of this. Evidence that the zig-zags do, in fact, represent flattened helices with segments at different levels in the crystal rather than zig-zag dislocations confined to a single plane can be drawn from an inspection of contrast effects in the image. This is discussed later in connection with figs. 5 and 6.

Figure 2 shows further examples of zig-zags. Again, these have the sharpened form which suggests that they represent flattened helices. There are, however, some additional features of interest in this photograph.

† Figures 1, 2, 3, 5, 7, 8, 10, 11 and 12 are shown as plates.

In the areas marked A, for instance, the simple zig-zag form is replaced by a cusped shape. Other examples of this cusped form are to be found in the photographs illustrating this paper. In particular, a number of good examples can be seen in the helices within region A in fig. 3. The appearance

Fig. 4

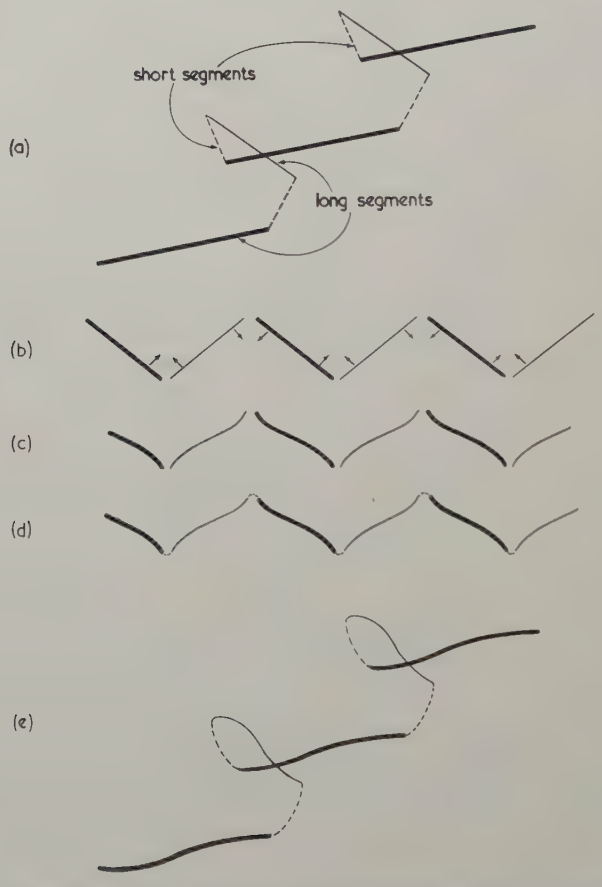

Illustrating the distortion of a flattened helix to produce a cusped zig-zag in projection. (*a*) Perspective view of flattened helix. (*b*) Projection of flattened helix into simple zig-zag. (*c*) Cusped zig-zag produced by attraction between neighbouring long segments of the helix. (*d*) More accurate description of cusped zig-zag, showing the projected portions of the short segments. (*e*) Perspective view of cusped helix.

of cusps on one side of a zig-zag can be expected if the helix is viewed at an angle, and many examples of this kind have been published by Thomas and Whelan. Cusps on both sides, however, cannot be accounted for in this way and a different explanation providing some real distortion of the helix must be sought. Figure 4 illustrates one possible mechanism. A flattened

helix has its long segments lying in the basal plane of easy glide whilst its short segments lie in inclined pyramidal planes in which glide is not possible. Thus, although the long segments are free, the helix is effectively pinned against translation along its axis by the short segments. Therefore only internal rearrangement is possible. Adjacent long segments of the helix have opposite Burgers vectors and since they lie in parallel glide planes they tend to glide by mutual attraction into a more stable relationship to lie closer together. This leads to a distortion of the long segments, giving rise to the cusped appearance in the projected image.

It is difficult to calculate the final shape of the helix resulting from this kind of internal interaction or even to estimate the magnitude of the forces experienced by the long segments. An approximate description might be found by considering a pair of neighbouring segments as a pair of edge dislocations lying in parallel glide planes and having opposite Burgers vectors. If the dislocation lines were continuous and the structure was isotropic then a position of stability against further glide would be reached when their separation in projection equalled that between their glide planes (see, for example, a discussion of this kind of situation by Read (1953)). This conclusion must, of course, be modified by taking into account the presence of the short segment terminating the long segments, the fact that the long segments are not continuous and are not pure edge dislocation but have a mixed character, and also the crystal anisotropy. However, refinements of this kind are not likely to have a significant effect on the final shape.

A closer inspection of the cusped zig-zags shows that the tips are not perfectly sharp but that the segments are separated here by a distance of a few hundred angstrom units, where the dislocation line becomes less visible. According to the present discussion this should represent the portion occupied by the short segment and gives an order of magnitude for the separation between the basal planes containing the long segments. A value of a few hundred A is consistent with the geometrical restriction imposed by the crystal thickness. It appears, therefore, that a more accurate description of the cusped helix should be represented by fig. 4 (*e*), giving a projected zig-zag image as shown in fig. 4 (*d*).

A further interesting feature of fig. 2 is shown in the area marked B. In this region the normal zig-zag has been modified to one in which the tips are terminated by chains of loops. Similar examples are shown in fig. 5 at the places marked A and C. This feature has been reproduced in fig. 6 where the different thicknesses of line are intended to represent the different depths at which the dislocations lie in the crystal. The variation in depth is indicated by the variation in contrast of the dislocation image in the photograph; since the zig-zag must be a continuous dislocation having the same Burgers vector everywhere, and there is only one set of reflecting planes contributing to the dislocation contrast, variation in depth is the only factor which can change the contrast in this way. The extent of this variation in contrast depends on the particular diffracting

conditions, on the positions of the dislocations, and on the thickness of the crystal. This explains why the variation is more pronounced in some of the photographs shown here than in others.

A number of mechanisms leading to the formation of chains of loops have been examined, but none of these is completely satisfactory. The most attractive is illustrated in stages by fig. 6. It is first necessary to consider the formation of single loops at the tips of the normal zig-zag. This stage

Fig. 6

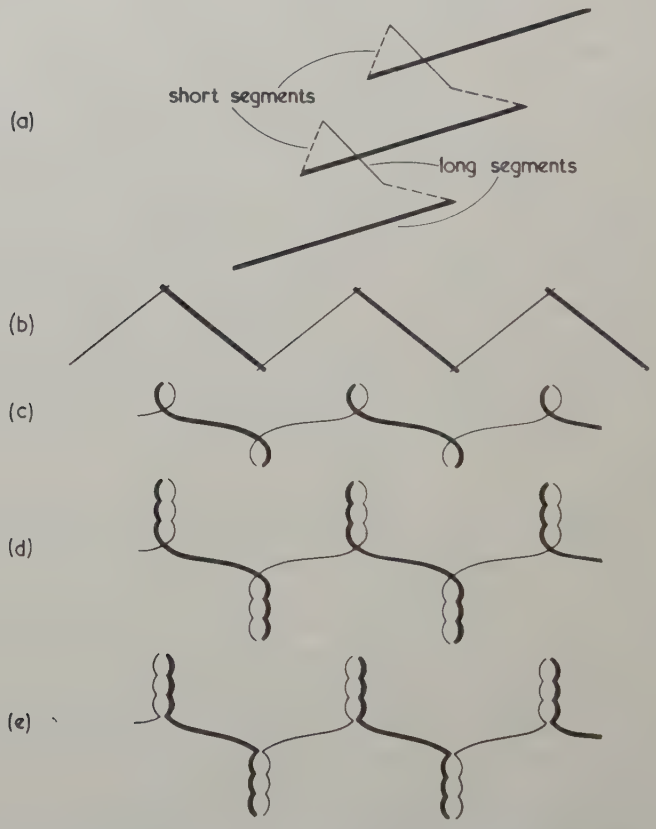

Illustrating the mechanism by which chains of loops may be formed in helices. (*a*) Perspective view of flattened helix in which the short segments lean backward. (*b*) Projection of flattened helix. (*c*) Interaction between neighbouring long segments, leading to loop formation. (*d*) Growth of chains of loops from looped helix after the outward climb of the short segments. (*e*) Growth of chains of loops from cusped helix after the outward climb of the short segments.

in the process is frequently observed and examples are visible in the area marked B in fig. 5. Clearly both loops and cusps are possible in helices in these crystals and it is thought that the choice is determined by the orientation of the climb plane in which the short segments lie. If the short

segments lean forward along the helix cusps are formed (as in fig. 4); if they lean backward (as in fig. 6) loop formation is favoured since neighbouring long segments must always overlap to some extent. The length and apparent width of the loops in fig. 5 is surprising in view of the strong attraction which must exist between neighbouring long segments and which has already been used to explain the cusping in some of the helices. It would appear that some additional shear stress must operate in a systematic manner in the vicinity of the loops in order to hold them further apart. It is considered that such a stress might be accounted for by the observation that the turns of the helix are not pure edge dislocation but have some screw character. Our elementary model of a pair of edge dislocations lying in parallel glide planes must therefore be modified by the addition of a screw dislocation orthogonal to these and lying in a parallel glide plane between them. An inspection of such a model with the appropriate choice of Burgers vectors suggests that the equilibrium separation of the edge components can be increased by the addition of the screw dislocation. Thus the representation of a looped helix given in fig. 6 (*c*) appears to be a permissible form of distortion produced by elastic interaction between neighbouring turns. It is interesting to note that the crossing over of the segments to develop the loops is of the symmetrical form expected for a pair of long dislocations of this kind, and which has been discussed previously by Read (1953) and Amelinckx (1956).

The last stage in the process is indicated in fig. 6 (*d*) which shows how the final appearance of a chain of loops in the projected image can be produced by the glide of the two segments of the loop towards each other to link at a few isolated points. This leads to a stable situation but there is no obvious reason why the attraction should exist to initiate this localized glide. A more satisfactory explanation of the final stage follows if the short segments of the helix climb further outwards in the allowed $\{10\bar{1}1\}$ planes to extend the loops. The segments of the loops then separate to the equilibrium spacing except at a few places where they remain pinned together by some isolated attractive force. Pinning might well result from localized precipitation of lead on the dislocations during the later stage of climb. Some further observations which will be described in a later paper show that precipitation of lead formed by the final decomposition of the crystal often occurs preferentially along helical dislocations. This explanation accounts for the observation that the chains of loops extend preferentially along close-packed directions in the basal plane (see also Forty 1960). The $\{10\bar{1}1\}$ planes in which the short segments of the helices can climb to extend the loops intersect the basal plane along these directions.

Chains of loops can also be formed in a similar manner from cusped helices if the short segments of these climb further outward. It is important though to note that this form does not involve a crossover in the long segments and therefore the alternative linkage of the chains shown in fig. 6 (*e*) must be developed. If the interpretation of contrast variations for the dislocation line in fig. 5 in terms of variation in level in the crystal is

reliable, then the chains at A are developed from looped helices (giving the form of fig. 6 (*d*)) whilst those at C are grown from cusped helices (form 6 (*e*)). Some indication that loops may be formed from cusped helices may also be found in the enclosed area B in fig. 3.

The dislocation in fig. 5 appears to be broken in the region D. This must be a place where the line has climbed completely out of the crystal, presumably in an attempt to overcome an obstacle surrounded by the strongly diffracting patch. It is difficult to interpret the cusping and apparent reversal of the dislocation at the break, although this appears to be a fairly common mode of termination since several other examples can be seen in fig. 2. No satisfactory explanation is available at present.

The climb of arrays and networks of dislocations leads to even more complicated configurations. These are of special interest when the helices produced are sufficiently close to allow interactions to occur. Some examples of this kind have been given by Thomas and Whelan in their discussion of helical dislocations in the aluminium copper alloys. They show how interactions between turns of neighbouring helices in the arrays can lead to tangled networks of helices and isolated loops. Similar observations have been made on the climb of arrays of dislocations in lead iodide and some of these will now be described in the following paragraphs.

Figure 7 shows a fairly simple example of the climb of an array. This appears to be a crossed grid of screw dislocations, each of which has become helical. Such a configuration represents the climb of a twist boundary. It is interesting to note from this that if a twist boundary undergoes climb it loses its planar character as its component helical dislocations occupy a finite slab of the crystal. This is not true for a tilt boundary since the component edge dislocations here simply climb in the same plane.

A more complex array of helices is shown in fig. 8. This includes a family of closely spaced parallel helices crossed by two other independent dislocations. In the region marked A neighbouring helices have interacted to form a tangled network. It is difficult in this case to analyse the details of the interaction although the general form of the individual helices is still detectable. The area B, however, provides a particularly interesting example of interaction which can be followed in detail. In this region two helices have attracted each other and at one point some overlap and annihilation has occurred to produce a pair of double helices and a single closed loop. This kind of interaction is represented in detail in fig. 9. Further interaction between segments of the double helices can lead to the formation of more closed loops, and a simple example of this kind of event is provided by fig. 10. This shows part of a hairpin dislocation, one side of which has become helical whilst the other side has remained undistorted. At the bend in the hairpin segments of the helix have touched the other side, and, after some annihilation, a closed loop has become detached.

Interactions of this kind lead to complex distributions of loops such as those shown in figs. 11 and 12. In fig. 11 segments of the original helices are still recognizable, but in fig. 12 the annihilation has proceeded so far

that their identity has been destroyed completely. There is some indication of lining-up of loops, however, and this probably occurs along the lines of the original dislocations. It might be noted that the loops thus formed by climb have Burgers vectors lying in the basal plane and can therefore be expected to glide or regenerate other glissile dislocations to contribute to the plastic flow of the crystal under suitable applied stress. This is in marked contrast to loops which are formed directly by the collapse of condensed aggregates of vacancies. The Burgers vectors of these loops do not lie in the basal plane and they are therefore sessile. Loops of this kind have been observed in lead iodide (see Forty 1960) and, in fact, some are visible in

Fig. 9

Representing the interaction at B in fig. 8.

the photographs illustrating this paper (for example, see fig. 1, areas A and B, fig. 5, area E and the numerous small loops in the background of fig. 11). It is interesting to observe the marked difference in contrast for the two kinds of loops. This is clearly associated with the different orientations of their Burgers vectors relative to those strongly diffracting planes of the crystal lattice which are contributing to the microscope image in these regions.

§ 3. Conclusion

These observations on the formation of helices in lead iodide are useful in that they draw attention to the marked anisotropy of glide and climb processes in crystals of this kind. As we have seen from the foregoing discussion, the shapes and interactions of helices are largely dependent on the crystallographic details of the processes involved in their formation. This provides a marked distinction between the observations reported here

and those of Thomas and Whelan on helices formed in aluminium/copper alloys, where climb and glide may proceed in a much more isotropic manner and where, in fact, the helices are generally rounded and lack crystallographic detail. The peculiarities of the features reported in the present paper clearly result from the anisotropy of the hexagonal structure. It should be noted, however, that the anisotropy of the particular crystals with which we are dealing here is almost certainly enhanced by the molecular composition, and it does not necessarily follow that similar features might be observed in other hexagonal structures. In the present case, the structure and the composition of the crystals restricts the glide motion of dislocations to follow the basal (0001) plane and the climb motion to this and the $\{10\bar{1}1\}$ planes.

One of the most interesting features of helices, both in lead iodide and in aluminium/copper, is the extreme stability of these dislocations against further glide. No overall movement which might be described as glide has been observed, although some internal re-arrangement of helices in lead iodide occurs. In the case of the aluminium/copper alloys, this stability has been attributed to the possibility that the helices are favoured sites for the separation of θ' precipitates during the ageing of these alloys, and that these pin the dislocations against further movement. This might account also for the lack of any distortion of the helices from their original rounded shape. There is also some evidence that precipitation of metallic lead formed during the later stages of decomposition occurs preferentially along helical dislocations in lead iodide. It is not necessary, however, to seek an explanation of this kind for stability in this case; indeed, the distortions inside the helices indicate that some segments remain free to move. Stability is provided by the short segments of the helices which appear to lie in pyramidal planes and are therefore unable to glide. Thus the dislocations in lead iodide are pinned only at isolated points. Moreover, this pinning is effective only against glide since some further movement can take place by the climb of the short segments. The distortions of the helices from the elementary form are possible only as a result of this greater freedom of movement.

Some explanation is required for the extreme flatness of the helices in these crystals. A flattened cross section clearly indicates that climb proceeds more readily along directions in the basal plane; that is, the climb of the short segments in these directions proceeds faster than that of the long segments out of the basal plane. This anisotropy in the rate of climb might be associated with a greater flux of vacancies through the basal planes or it might be determined simply by the relative capacities of the long and short segments for accepting vacancies. The former possibility is perhaps the controlling factor as it is thought that the vacancies are being created near the centre of decomposition in the crystal, where the electron beam is most intense, and flow outwards into the surrounding good crystal to create the supersaturation required to promote climb. This flow can be expected to proceed more readily in the basal planes.

The formation of loops by the interaction of neighbouring or overlapping helices during the climb of an array of dislocations suggests an interesting means of creating regenerative sources for further plastic flow in these crystals. For loops created by such a process have Burgers vectors lying in the glide plane and are therefore able to move during further stressing. Moreover, as they are formed from helices, many of these loops must be jogged out of the basal plane in the way shown in fig. 13. The jogs, like the short segments of the helices, lie out of the glide plane and might therefore act as pinning points against the translation of the long segments. In this way the long segments might well become sources of new dislocation loops by the regenerative mechanism suggested by Frank

Fig. 13

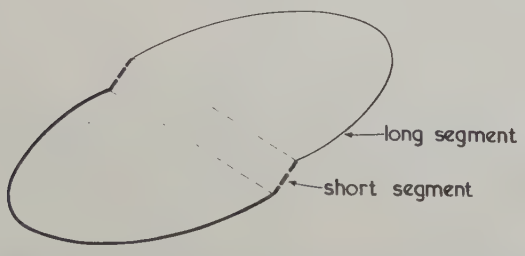

Illustrating one possible form of jogged loop created by intersection of flattened helices. This particular loop could be that formed by the interaction shown in fig. 10.

and Read (1950) and developed further in a recent paper by Kuhlman-Wilsdorf (1958). Evidence for the generation of new loops of dislocation from existing arrays has been found in some of the crystals, but it has not yet been possible to resolve the details of the operative mechanism.

Acknowledgment

I wish to thank Professor F. C. Frank, F.R.S., for some useful discussions and suggestions during the course of the work, and particularly during the preparation of this paper.

References

Amelinckx, S., 1956, *Phil. Mag.*, **1**, 269.
Forty, A. J., 1960, *Phil. Mag.*, **5**, 787.
Frank, F. C., and Read, W. T., 1950, *Phys. Rev.*, **79**, 722.
Kuhlmann-Wilsdorf, D., 1958, *Phil. Mag.*, **3**, 125.
Read, W. T., 1953, *Dislocations in Crystals* (New York : McGraw-Hill).
Thomas, G., and Whelan, M. J., 1959, *Phil. Mag.*, **4**, 511.

NOTICE

X-ray Evidence for Segregation of Solute to Stacking Faults in a Copper–Aluminium Alloy, R. W. Cahn and R. G. Davies, 1960, *Phil. Mag.*, **5**, 1119.

It has been brought to our attention that K. Nakajima has observed an enhanced small angle scattering from cold worked and heat treated copper–aluminium alloy (Nakajima, *Sci. Rep. Res. Insts Tôhoku Univ.*, A, 1960, **12**, 39), and not from copper–nickel alloy as we had deduced from a brief note published by him earlier (*J. Phys. Soc. Japan*, 1959, **14**, 1825).

REVIEWS OF BOOKS

Reports on Progress in Physics. Vol. XXIII. By The Physical Society. (John Wright & Sons Ltd., 1960.) [Pp. 629.] Price £3 3*s.* 0*d.*

This volume contains ten stiff doses of contemporary physics—doses that will cure the malady of ignorance about any of the specialties covered. However, the volume is no panacea; the ailing physicist who cannot keep himself informed about annual progress along the whole front of physics cannot look to this volume for a cure. No one could reconstruct what happened in physics during 1959–1960 by reading the book and no one will be expected to read it from page 1 through page 629, except a reviewer.

There was a time when the *Reports on Progress in Physics* informed you about the year's progress in many active parts of the subject ; the spectroscopist could keep informed about crystallography, the nuclear physicist about molecular physics. This age has passed and the *Reports* have changed; they are no longer—as they once were—the ' Annual Reports ' of the company of physicists. They no longer show signs of a consistent, comprehensive plan to deal with the year's physics in a single volume. The twenty-third volume leaps from one corner of physics to another, boring in with vigour and virtuosity wherever it lights, but the volume could as easily have been ripped into ten separate little tracts. The contents of the volumes are as unplanned as the content of an issue of *The Physical Review*; it is a collection of miscellaneous review papers disguised as progress reports.

On every side one hears physicists complaining more and more frequently that keeping up with the literature is a job that has become impossible. The Reports do little to solve the problem behind this complaint; perhaps in the face of the enormous variety and complexity of physics there is no longer a way to meet the complaint, but I wonder if the editors of the Reports did not abandon their early efforts too soon. The turning point seems to have been in the early years of World War II. Did war pressures cause an expedient course to be taken, a course that has not been changed back because it has been an easier course to follow ? Or has physics really become so much more complex than in the 1930's that the editorial policies of that decade would be impossible in the 1960's ?

The quality of each separate article is good—each is thorough, reasonably well written, and competent. There are three articles on subjects of solid state physics. One of these, on ' Group Theory in Solid State Physics ', is really a short text-book on the subject. It, like each of the other nine articles, is available separately and I would guess that it may often be used separately by solid state theoreticians. Another article, ' Experimental Analysis of the Electronic Structure of Metals ', uses 30 pages to review—with a novel touch, to be sure—the traditional independent particle model of electrons in metals. The remaining two-thirds of the article develops a physical understanding of the four principal experimental techniques that have been used with remarkable success to map the Fermi surfaces of several real metals. The third article, ' Band Structure Calculations in Solids ', covers an active corner of theoretical physics, and this article goes over each of the principal methods of calculating band structures that theorists have been exploiting.

Three articles in the field of optics are included: ' Optical Properties of Thin Films ', ' Photoelectric Photometry ', and ' New Developments in Interference Spectroscopy '. These three articles treat the theory and practice of experimental techniques in optics. The second article is short and almost completely oriented to experiment; the other two are long and carry along developments of the theory of the experimental techniques and apparatus.

One article, ' Planetary Nebulae ', treats a problem in theoretical astrophysics: how can the characteristics of these nebulae be deduced from the observational data ? Planetary nebulae are mentioned in almost every elementary astronomy text, a distinction not shared in elementary physics texts by many of the nine companion topics; however, this article is definitely for the specialist, being filled with detailed calculations based on known physical principles.

The last three articles deal with topics in nuclear physics. In ' Orbital Electron Capture by the Nucleus ', the authors review the theory of this process, show how the transition probabilities are to be calculated and then run through experimental results for each type of transition. The article, ' Precision Measurement in Gamma-Ray Spectroscopy ', is another contribution on the theory and practice of an experimental technique; this article should guide one to almost anything he wants to know about precision gamma-ray spectrometers, including details of the leading instruments in various laboratories. The final report on ' ^{3}He Induced Reactions ' covers the use of ^{3}He as a nuclear projectile and the nuclear reactions induced by it, surveys experimental results, and ends with a section on ' Suggested Experiments '.

I am sure that some of these articles may become the ' Bible ' for workers in the specialized fields just as have the famous articles by Bleaney and Stevens and by Bowers and Owen which nurtured a scientific generation of workers on electron paramagnetic resonance in crystals. However, I see no reason why a high quality annual review journal should be camouflaged by the green covers of a Progress Report. Nor do I see why the early purposes of this series should have been permanently abandoned. The Report of the Council of the Physical Society for the year ending February 28, 1934, has this to say: " Some time ago the Council sought the opinion of the Fellows of the Society on the desirability of initiating a series of annual reports on the progress of physical science. The unequivocal approval expressed by the Fellows . . . have encouraged the Council to proceed with this project." These words, inaugurating the series, and the early volumes of the series show that the intent was to cover the important new developments in physics as they occurred and were recognized. Lest my account of the contents of this volume still leave any reader believing this coverage has been achieved, I will add that nowhere in this volume did I find reference to the work of Mössbauer. R. W. S.

Modern Physics. By M. S. Smith. (London: Longmans, Green & Co., 1960.) [Pp. 254.] Price 15*s*.

This is a brave and, on the whole, successful attempt to introduce the ideas of modern physics to the intelligent but uninstructed reader. It is perhaps not surprising that the treatment is least satisfactory for the more highly developed branches of classical physics, such as statistical mechanics, which are not susceptible to abbreviated presentation. But the author's accounts of relativity and wave mechanics are excellent, and form a good, though rather stiff, introduction to more detailed study. On the descriptive side the writing is clear; perhaps there is occasionally too much emphasis on historical experiments and outworn ideas, but this is a matter where differences of opinion need not be construed as adverse criticism. The book may be highly recommended to the sixth-former who really wants to now about physics, and to the undergraduate scientist whose speciality is not physics. Physics specialists will soon outgrow it, but there is very little in it which they will have to unlearn, and this is most creditable. A. B. P.

[*The Editors do not hold themselves responsible for the views expressed by their correspondents.*]

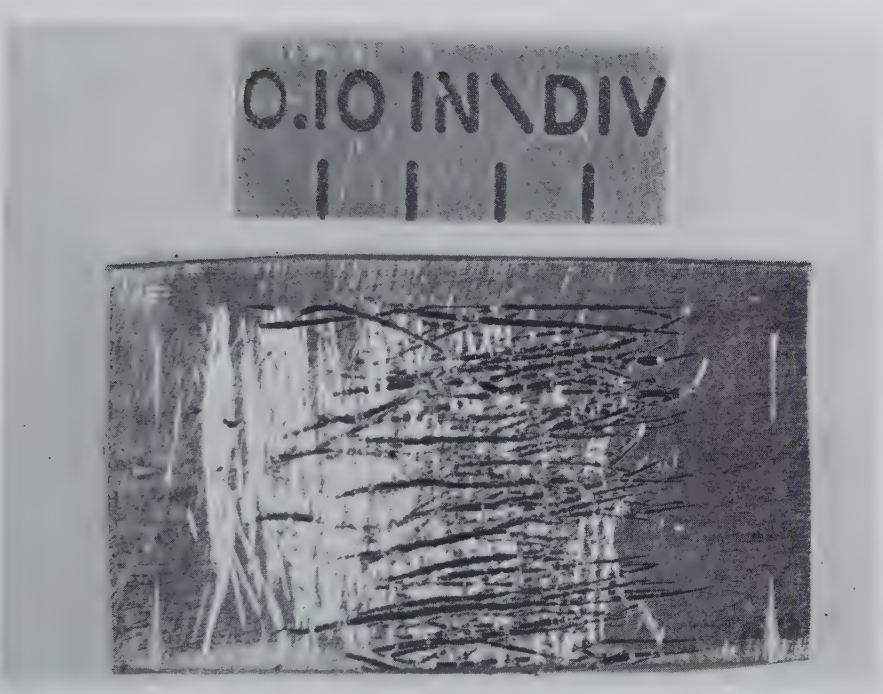

An enlarged view of a zone-refined lead specimen exhibiting the surface condition produced by cold-work.

Fig. 1

Replica from (100) face of alloy annealed at 450°C for 45 min. Not shadowed. Approximate size of precipitate particles : 400 Å. The macroscopic etch pits are believed to be a secondary etching effect arising from the lining up of the precipitate particles.

Fig. 2

Replica from (110) face of alloy annealed at 450°C for 30 min. Shadowed. Approximate size of precipitate particles : 400 Å.

Fig. 3

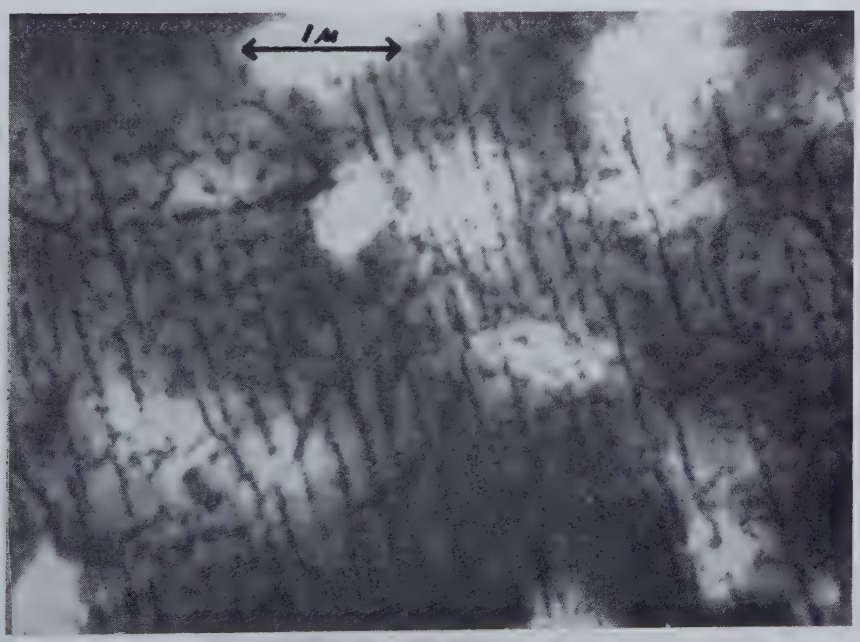

Transmission electron micrograph of alloy annealed at 450°C for 200 min. The dark streaks are the cobalt precipitate. These dark regions became empty when the foil was preferentially cobalt etched.

Fig. 1

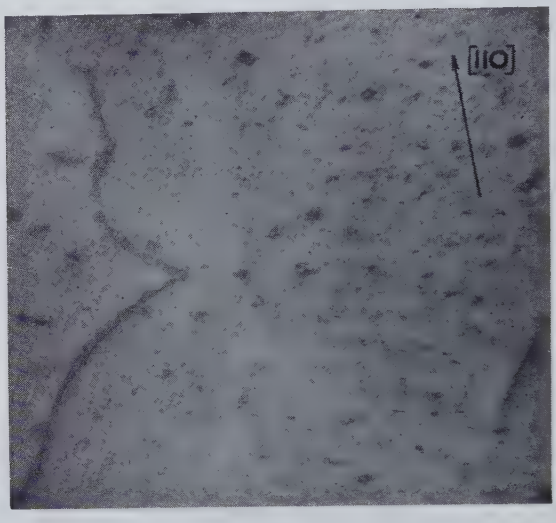

Specimen irradiated for 12 hours, fine precipitation and decorated dislocation line. Plane of the foil is close to (111). ×30 000.

Fig. 2

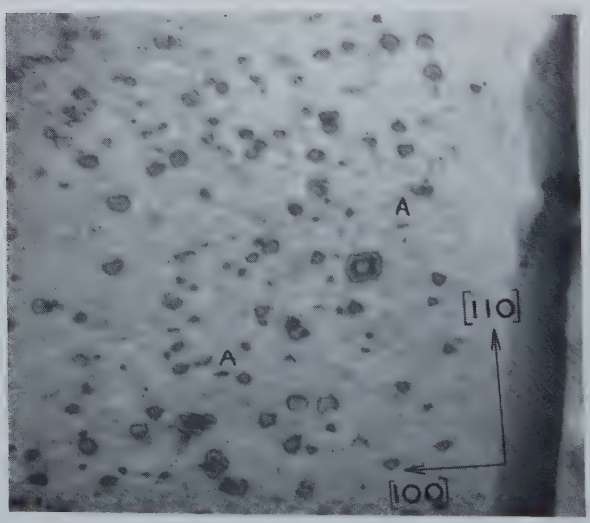

Specimen irradiated for 72 hours, irregular loop shaped particles some of which appear edge-on lying parallel to ⟨110⟩. Note denuded zone around low angle boundary. Plane of foil close to (110). ×30 000.

Fig. 3

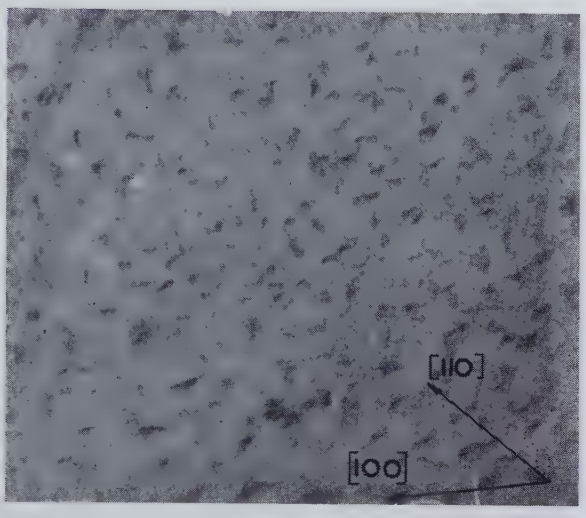

Specimen irradiated for 72 hours, edge on loops at right angles. Plane of the foil is close to (100). ×30 000.

Fig. 4

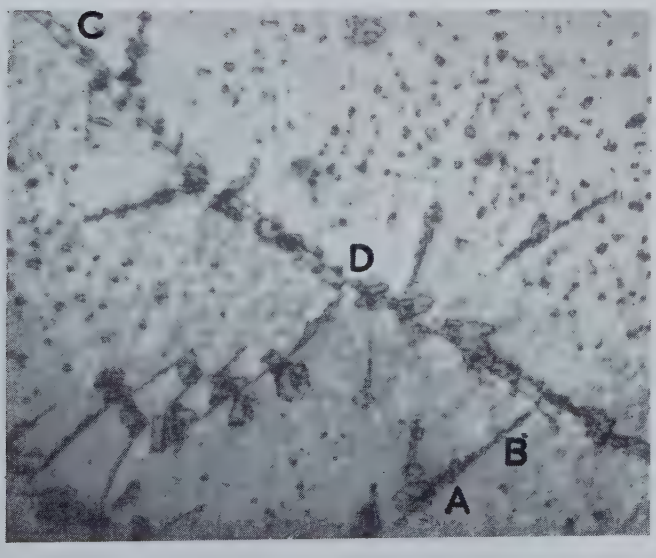

Specimen irradiated for 72 hours, network of dislocations decorated with precipitates. ×30 000.

Fig. 5

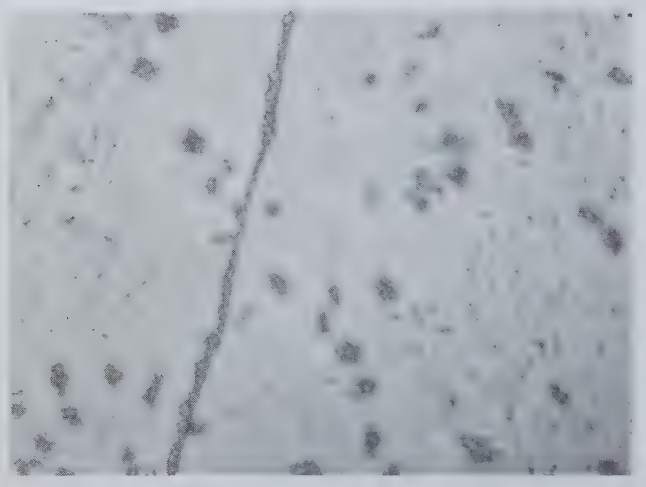

Specimen aged for 72 hours at 60°c, then irradiated for a further 72 hours, coarse irregular precipitate with fine precipitates. Plane of foil is close to (111). ×30 000.

Fig. 6

Specimen aged for 72 hours at 100°c. Clustered precipitates with 6-fold symmetry. Plane of the foil is close to (111). ×30 000.

Fig. 7

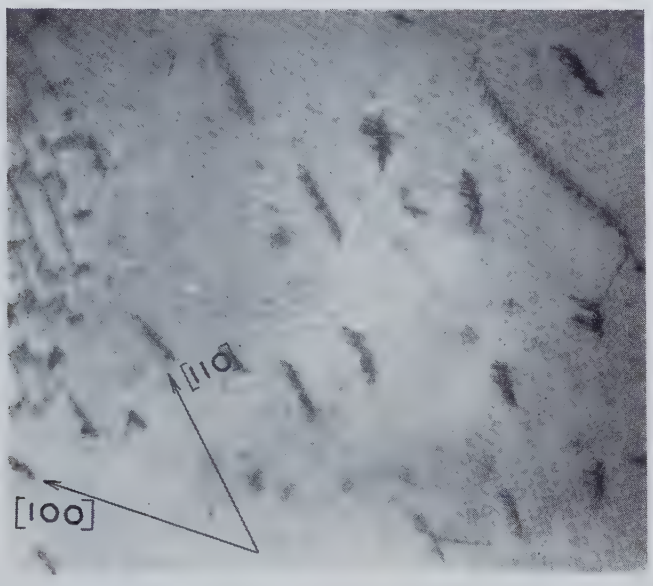

Specimen aged for 72 hours at 100°c, edge-on precipitates at right angles along dislocation lines. Plane of the foil is close to (100). ×30 000.

Fig. 8

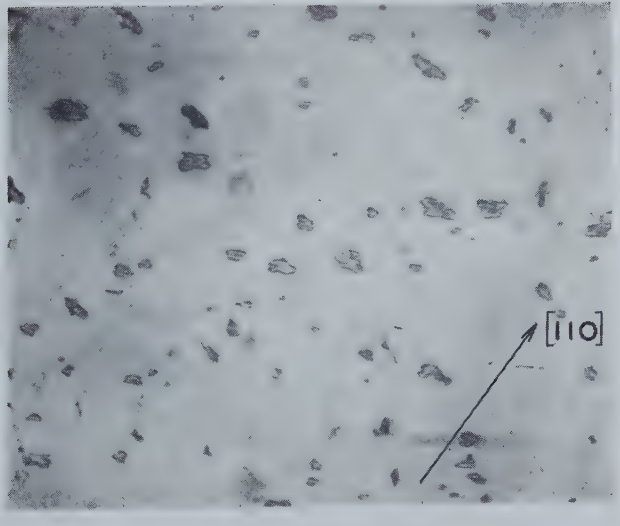

(*a*)

Fig. 8 (*continued*)

(*b*)

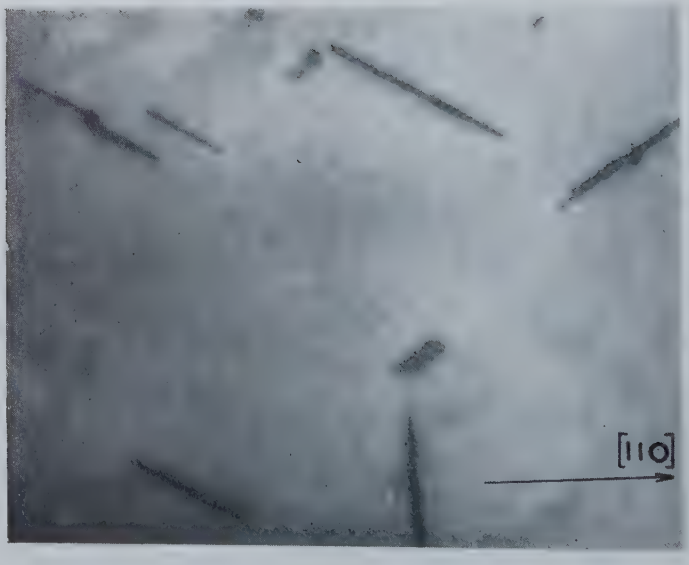

(*c*)

Specimen irradiated for three days followed by 1 hour at (*a*) 175°, (*b*) 200°, and (*c*) 250°c. Plane of the foil is close to (111). ×30 000.

Fig. 9

(*a*)

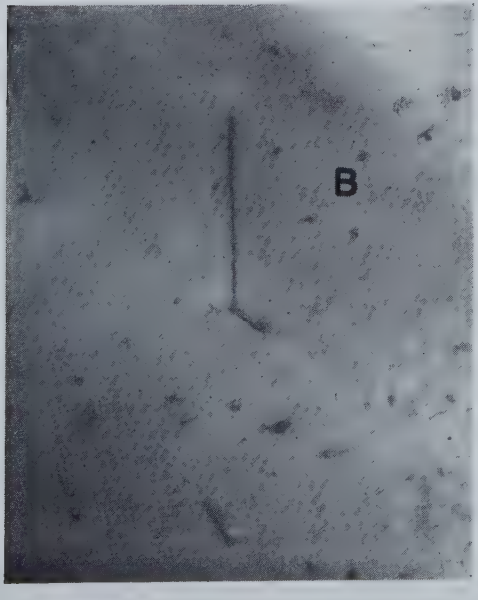

(*b*)

Specimen irradiated for three days (*a*) before heating on the hot stage in the microscope, (*b*) after heating for 3 minutes at 180°C. Plane of the foil is close to (110). ×30 000.

Fig. 1

(*a*)

(*b*)

Detail of Debye–Scherrer ring structure (Fe radiation; line 16) from: (*a*) original rolled 99·8% aluminium sheet; and (*b*) fracture surface formed by slow fatigue crack growth in the sheet.

Fig. 2

Transmission photographs (unfiltered Fe radiation) divergence $d\theta = 10^{-2}$ from (*a*) annealed 99·8% aluminium crystal ; (*b*) crystal deformed 20% in tension; and (*c*) crystal deformed in tension as for (*b*) and then subjected to 30 000 cycles at $\epsilon_{pl} = 7 \times 10^{-3}$.

Fig. 3

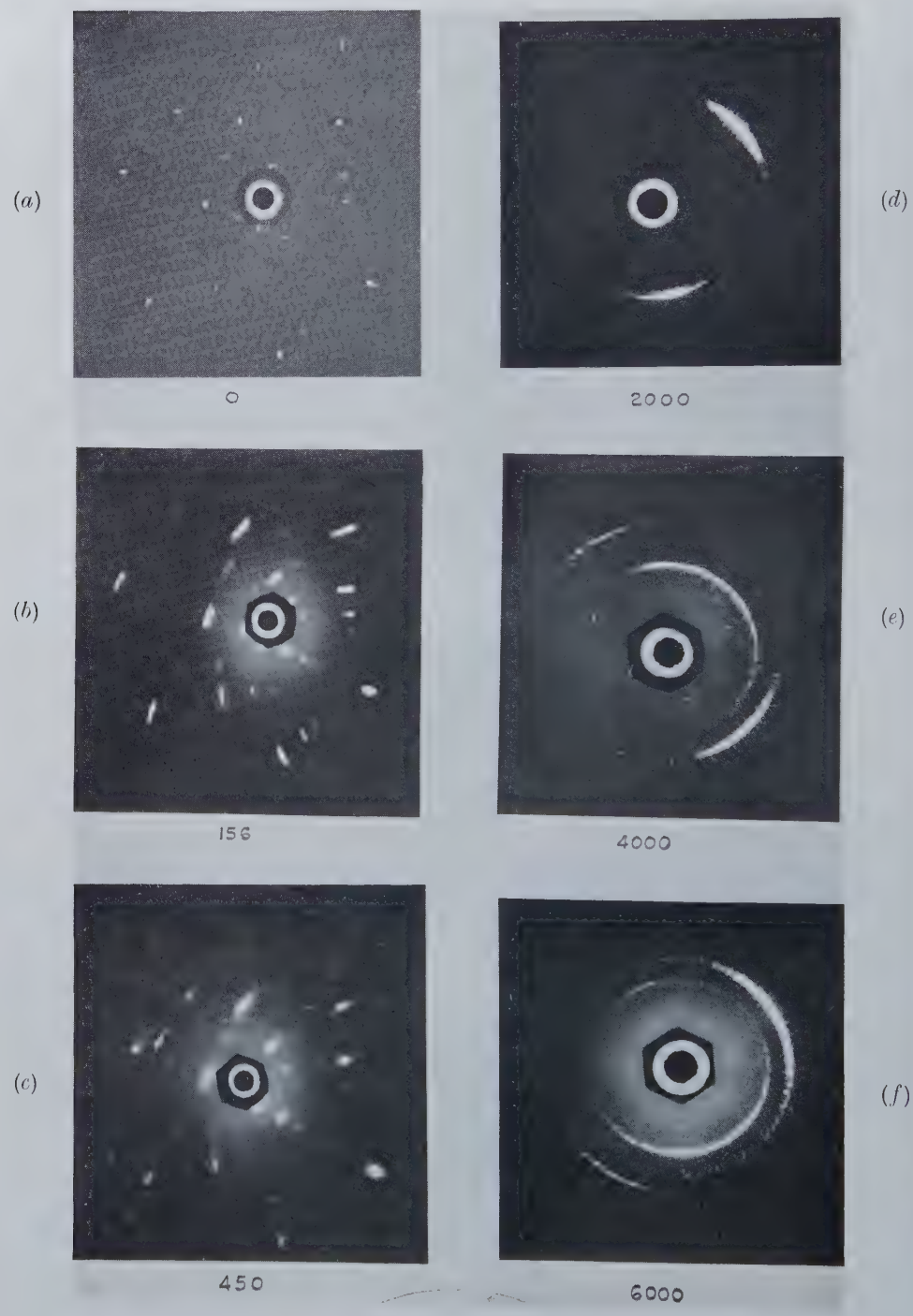

Development of cyclic sub-grain structure in a crystal subjected to increasing numbers of cycles of torsion at $\epsilon_{pl}=5\times10^{-3}$. Unfiltered Fe radiation. (*a*) 0 cycles, (*b*) 156 cycles, (*c*) 450 cycles, (*d*) 2000 cycles, (*e*) 4000 cycles, (*f*) 6000 cycles.

Fig. 4

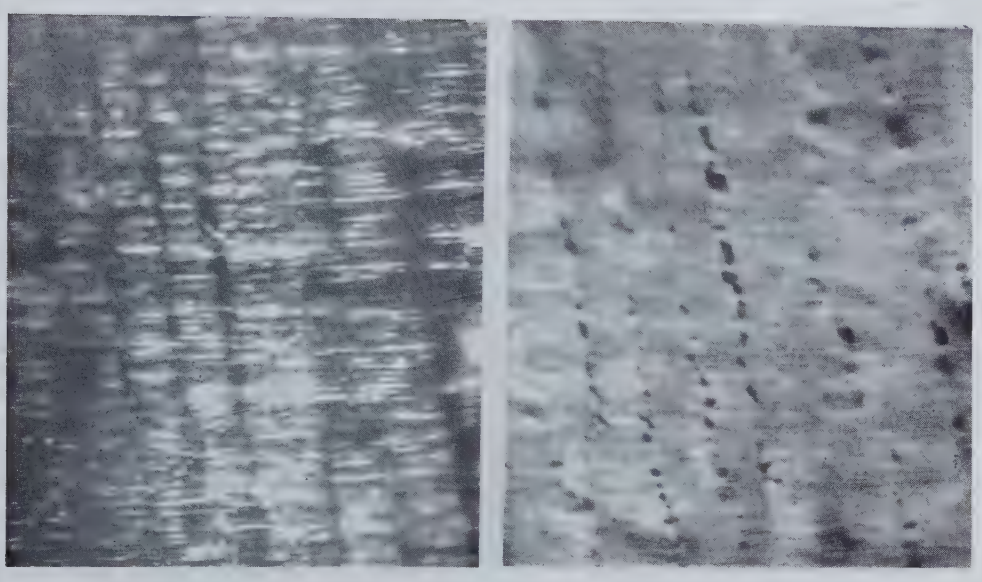

(*a*) (*b*)

Development of cyclic sub-grain structure: (*a*) dark ground; and (*b*) same field polarized light (×500).

Fig. 5

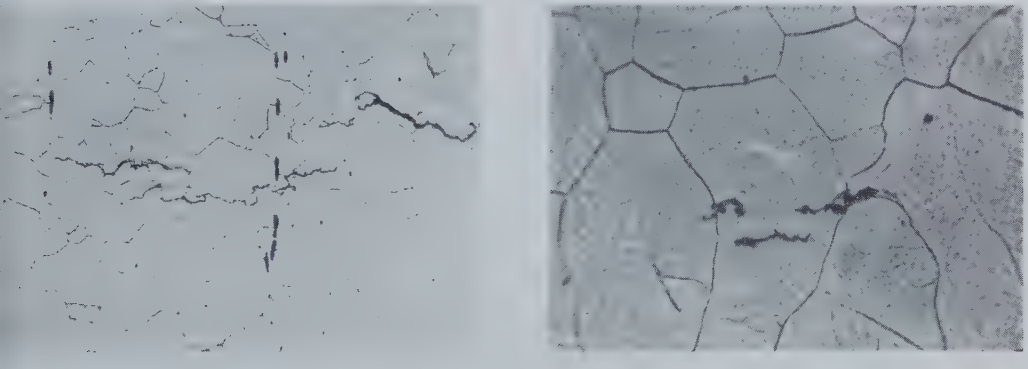

(*a*) (*b*)

(*a*) Section of part of crack front in mild steel sheet specimen showing joining of numerous small cracks (×350); and (*b*) leading cracks at centre of mild steel sheet specimen (×900).

Fig. 1

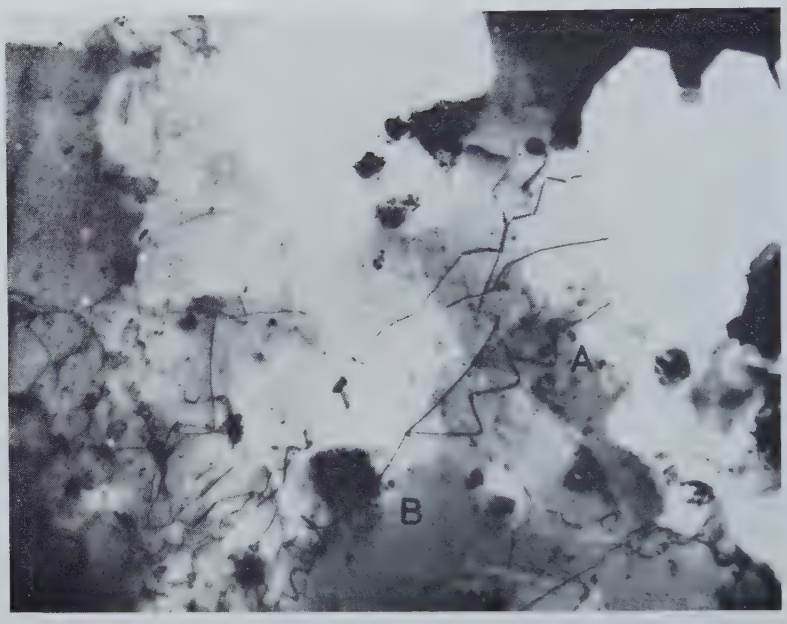

The distortion of an array of dislocations during the initial stage of decomposition. $\times 16\,000$.

Fig. 2

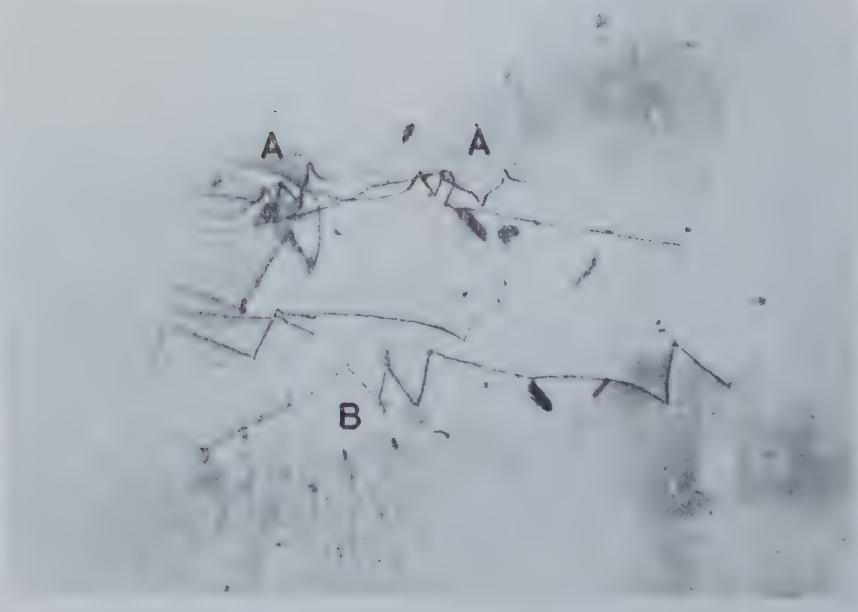

The climb of dislocations into flattened helices. Showing simple zig-zags, cusped zig-zags (A) and looped zig-zags (B). $\times 20\,000$.

Fig. 3

The climb of a family of dislocations. Note the cusped zig-zags in region A, and the creation of loops at the tips of cusped zig-zags in area B. $\times 7000$.

Fig. 5

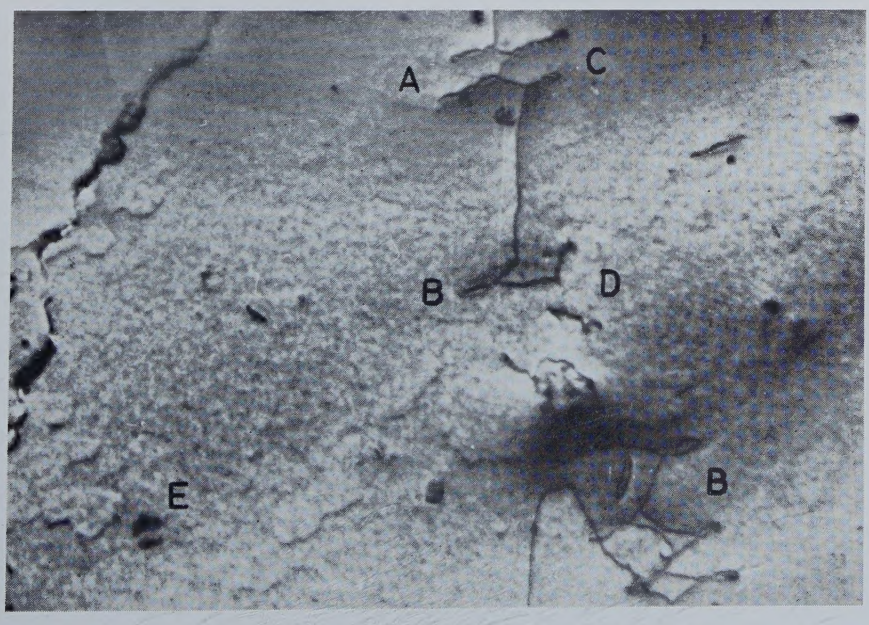

Illustrating the formation of loops in zig-zag dislocations. Note the single loops in region B and the multiple loops in regions A and C. $\times 27\,000$.

Fig. 7

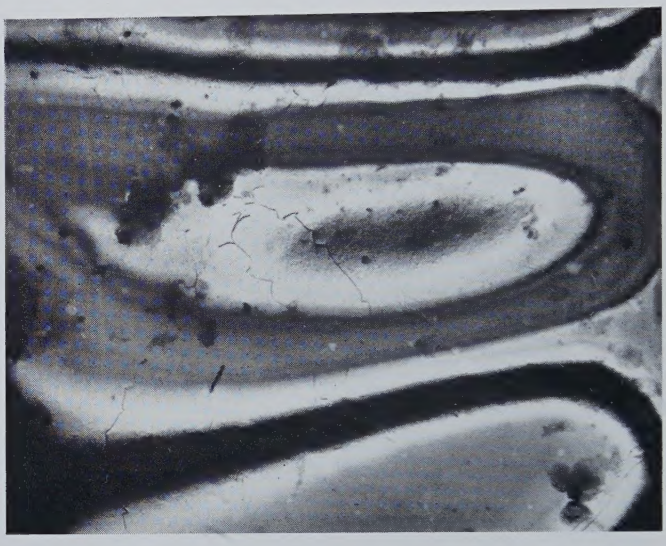

The climb of a crossed grid of screw dislocations. × 7000.

Fig. 8

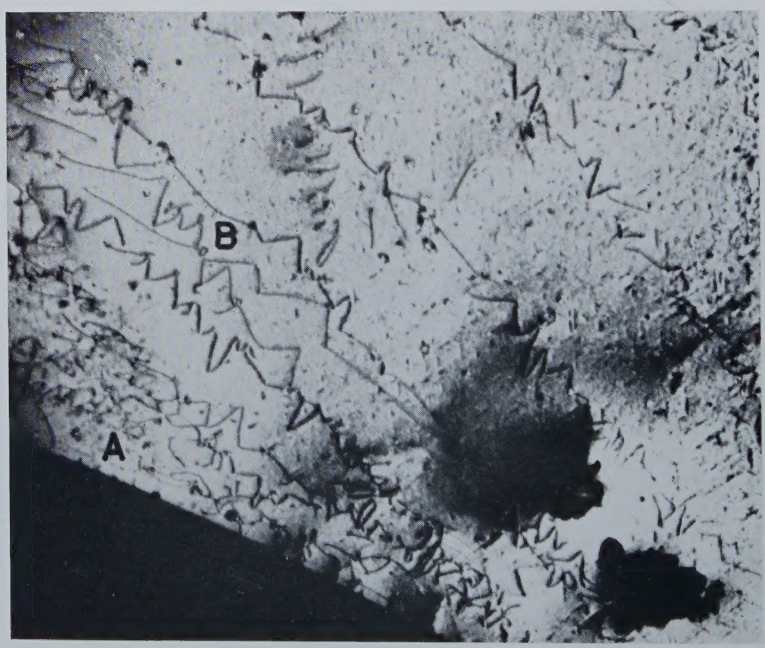

The climb of an array of dislocations, leading to interactions between neighbouring helices. Note the tangled network at A and the interaction between a pair of helices at B. × 8000.

Fig. 10

The formation of an isolated loop from a helical dislocation. ×20 000

Fig. 11

Distribution of elongated loops formed by the interaction of looped zig-zags. The long segments of the helices are still recognizable. ×14 000.

Fig. 12

Distribution of loops formed by the interaction of helices. The helices are no longer recognizable but there is some alignment of the loops along the original dislocations. $\times 10\,000$